Gregor Maria Schöpf, BSc.

Assessment of Grid Forming Algorithms with Hardware-in-the-Loop Tests

Master thesis

to achieve the university degree of

Master of Science

submitted to

Graz University of Technology

1. Supervisor: Dipl.-Ing. Dr.techn. Ziqian Zhang
2. Supervisor: Dipl.-Ing. Philipp Hackl

Institute of Electrical Power Systems

Graz, October 2024

Affidavit

I declare that I have authored this thesis independently, that I have not used other than the declared sources/resources, and that I have explicitly indicated all material which has been quoted either literally or by content from the sources used. The text document uploaded to TUGRAZonline is identical to the present master's thesis.

Graz, 31.10.2024

Gregor Schöpf

Danksagung

Ein besonderer Dank gilt Philipp Hackl, dessen fachliche Kompetenz nur von seiner außerordentlichen Hilfsbereitschaft übertroffen wird. Die Tatsache, dass das Thema meiner Arbeit fast schon eine Symbiose mit seiner Dissertation bildet, ist dabei eine sehr glückliche Fügung. Besonders dankbar bin ich ihm auch, für die Motivation, ein Paper aus meiner Masterarbeit zu entwickeln.

Meinen Eltern danke ich von Herzen nicht nur für die finanzielle Unterstützung, sondern auch für die stetige Versorgung mit Schokolade und aufmunternden Worten. Ihr unermüdlicher Beistand und das ehrliche Interesse an meiner Arbeit haben mich stets motiviert.

Mein Bruder verdient eine besondere Erwähnung, da er mich stets unterstützt hat und immer Interesse zeigte. Besonders wertvoll war seine Fähigkeit, sich meine Erklärungen anzuhören und Rückfragen zu stellen, sodass ich die Themen auch für einen Nicht-Fachexperten verständlich formulieren konnte.

Ein großes Dankeschön gilt auch meinen Freunden, für die kontinuierliche Unterstützung während der gesamten Zeit. Ohne euch wäre der Weg um einiges schwieriger gewesen.

Ein weiterer Dank geht an meine Kommilitonen, die nicht nur akademische Wegbegleiter, sondern auch gute Freunde geworden sind. Euer Zusammenhalt und die herzliche Aufnahme in die Gruppe haben den Studienalltag und meine Zeit in Graz deutlich verschönert.

Abstract

The increasing integration of renewable energy sources into modern power grids has introduced significant challenges. Particularly in terms of grid stability and reliability. Traditionally, these aspects were ensured by synchronous machines, which provided mechanical inertia and high short-circuit current capabilities. However with the shift towards power-electronics based generation, there are less and less synchronous machines connected to the grid. The task of assuring grid stability, will therefore have to be taken over by converters. Grid-following converters, which are predominantly used today, use the grid as a reference and consequently face issues with small signal stability in weak grids. Therefore, taking over this task, are a new type of converter called grid-forming. They are designed to actively regulate voltage and frequency with a internal voltage reference. Although grid-forming is promising, as a new concept and product, it has yet to undergo widespread testing in power systems. Therefore, comprehensive testing, including simulations, Hardware-in-the-Loop and Power Hardware-in-the-Loop are necessary. New grid codes are also addressing these emerging challenges. With a comparison of a select few carried out, to highlight key differences.

This thesis investigates the performance of grid-forming converters, focusing on different control implementations and a basic comparison to grid-following technologies. The grid-forming control strategies are designed to mimic the inertia characteristics of traditional synchronous machines and achieve synchronisation. To evaluate the effectiveness of these controls under realistic conditions, Power Hardware-in-the-Loop testing is employed. This enables the simulation of grid disturbances, such as voltage and frequency variations, without the need to connect to the real grid in the field. It also allows for a comprehensive analysis of converter responses under various scenarios. Finally the influence of grid conditions and control settings on converter performance are quantified.

Mathematical analysis reveals that two grid-forming controls namely the virtual synchronous machine and the droop control with low-pass filter can be tuned to achieve equivalent performance. This analysis is further validated through simulations. The Simulation setup is compared to the Power Hardware-in-the-Loop results and a fairly major deviation of results is detected. The reason is a inadequate modelling of he frequency dependence of certain components. To aid testing a emulated grid impedance using Power-Hardware in the Loop is introduced. It can be shown that the results with a emulated grid impedance closely align with those obtained using real grid impedance. Confirming PHIL as a reliable method, then used in further testing. The analysis of converters and their disturbance management capabilities reveals a key distinction between grid-following and grid-forming converters. Grid-forming converters inherently possess the ability to respond actively to the test disturbances, while grid-following converters lack this intrinsic capability. The experiments, also show that stronger grids lead to more pronounced disturbance responses from grid-forming converters. It is observed that the low-pass filter cut-off frequency of the grid-forming control inversely affects inertia and the proportional gain has an inverse relationship with both inertia and damping.

Kurzzusammenfassung

Die steigende Integration von erneuerbaren Energiequellen in moderne Stromnetze hat zu erheblichen Herausforderungen geführt. Dies gilt insbesondere für die Netzstabilität und Zuverlässigkeit. Traditionell wurden diese Aspekte durch Synchronmaschinen gewährleistet, die eine mechanische Trägheit und hohe Kurzschlussstromfähigkeiten aufwiesen. Mit dem Übergang zur leistungselektronischen Erzeugung sind jedoch immer weniger Synchronmaschinen an das Netz angeschlossen. Die Aufgabe, die Netzstabilität zu gewährleisten, wird daher von Umrichtern übernommen werden müssen. Netzfolgende Umrichter, die heute überwiegend eingesetzt werden, nutzen das Netz als Referenz und haben daher Probleme mit der Kleinsignalstabilität in schwachen Netzen. Daher übernimmt ein neuer Typ von Umrichtern, der sogenannte netzbildende Umrichter, diese Aufgabe. Diese sind so konzipiert, dass sie Spannung und Frequenz mit einer internen Spannungsreferenz aktiv regeln. Obwohl die netzformenden Umrichter als neues Konzept und Produkt vielversprechend sind, müssen sie in Energiesystemen noch umfassend getestet werden. Daher sind umfassende Tests, einschließlich Simulationen, Hardware-in-the-Loop und Power Hardware-in-the-Loop, erforderlich. Neue Netz- und Systemregeln befassen sich ebenfalls mit diesen neuen Herausforderungen. Dazu wurde auch ein Vergleich einiger ausgewählter Netz- und Systemregeln durchgeführt, um die wichtigsten Unterschiede hervorzuheben.

In dieser Arbeit wird die Leistung von netzbildenden Umrichtern untersucht, wobei der Schwerpunkt auf verschiedenen Steuerungsimplementierungen und einem grundlegenden Vergleich von netzbildenden Technologien liegt. Die netzbildenden Regelungsstrategien sind so konzipiert, dass sie die Trägheitseigenschaften herkömmlicher Synchronmaschinen nachahmen und eine Synchronisierung erreichen. Um die Wirksamkeit dieser Steuerungen unter realistischen Bedingungen zu bewerten, werden Hardware-in-the-Loop-Tests durchgeführt. Dies ermöglicht die Simulation von Netzstörungen wie Spannungs- und Frequenzschwankungen, ohne dass eine Verbindung mit dem realen Netz im Feld erforderlich ist. Es ermöglicht auch eine umfassende Analyse der Reaktionen der Umrichter unter verschiedenen Szenarien. Schließlich wird der Einfluss der Netzbedingungen und der Regelungseinstellungen auf das Verhalten der Umrichter quantifiziert.

Die mathematische Analyse zeigt, dass zwei netzbildende Regelungen, nämlich die virtuelle Synchronmaschine und die Droop mit Tiefpassfilter, so abgestimmt werden können, dass sie ein gleichwertiges Verhalten erzielen. Diese Analyse wird durch Simulationen weiter validiert. Der Simulationsaufbau wird mit den Power Hardware-in-the-Loop Ergebnissen verglichen und es wird eine ziemlich große Abweichung der Ergebnisse festgestellt. Der Grund dafür ist eine unzureichende Modellierung der Frequenzabhängigkeit bestimmter Komponenten. Zur Unterstützung der Prüfung wird eine emulierte Netzimpedanz mit Power-Hardware-in-the-Loop eingeführt. Es kann gezeigt werden, dass die Ergebnisse mit einer emulierten Netzimpedanz eng mit denen übereinstimmen, die mit einer realen Netzimpedanz erzielt wurden. Dies bestätigt, dass Power-Hardware-in-the-Loop eine zuverlässige Methode ist, die bei weiteren Tests eingesetzt wird. Die Analyse der Umrichter und ihrer Fähigkeiten zum Störungsmanagement zeigt einen wichtigen Unterschied zwischen netzfolgenden

und netzbildenden Umrichtern. Netzbildende Umrichter besitzen von Natur aus die Fähigkeit, aktiv auf die Teststörungen zu reagieren, während netzfolgende Umrichter diese Fähigkeit nicht besitzen. Die Experimente zeigen auch, dass stärkere Netze zu ausgeprägteren Störungsreaktionen von netzbildenden Stromrichtern führen. Es wird beobachtet, dass die Grenzfrequenz des Tiefpassfilters der netzbildenden Regelung die Trägheit indirekt proportional beeinflusst und die Verstärkung eine umgekehrte Beziehung sowohl zur Trägheit als auch zur Dämpfung hat.

List of Symbols

$\mathbf{u}_{\mathrm{abc}}$	Voltage in abc Coordinate System
$\mathbf{u}_{\alpha\beta}$	Voltage in $\alpha\beta$ Coordinate System
$\mathbf{u}_{dq}$	Voltage in dq Coordinate System
θ	Angle of the rotating voltage system
$K_{\mathrm{p,PLL}}$	Proportional gain of PLL
$K_{\mathrm{i,PLL}}$	Integral gain of PLL
$f_{\mathrm{cut,PLL}}$	Cut off frequency of the PLL
T_{s}	Control period of converter controller
U_{Base}	Base voltage amplitude in p.u.
S_{Base}	Base apparent power in p.u.
I_{Base}	Base current amplitude in p.u.
Z_{Base}	Base impedance in p.u.
$K_{\mathrm{p,CC}}$	Proportional gain of the current control
$K_{\mathrm{i,CC}}$	Integral gain of the current control
$f_{\mathrm{cut,CC}}$	Cut off frequency of the current control
L_{f}	Filter inductance
R_{Lf}	Inductance filter resistance
R_{Cf}	Capacitive filter resistance
a	placeholder for interim formulas
b	placeholder for interim formulas
$K_{\mathrm{p,VC}}$	Proportional gain of the voltage control
$K_{\mathrm{i,VC}}$	Integral gain of the voltage control
$f_{\mathrm{cut,VC}}$	Cut off frequency of the voltage control
φ_{PM}	expected phase margin of the voltage control
h	intermediate frequency bandwidth of the voltage control
C_{f}	filter capacitance
τ_{c}	Time constant of current control
P^*	Active power set point
Q^*	Reactive power set point
P_{POC}	Active power at the POC
Q_{POC}	Reactive power at the POC
P_0	Nominal active power
Q_0	Nominal reactive power
ω_0	Nominal angular frequency
U_0	Nominal voltage
K_{P}	Active power gain factor for GFM with droop control
K_{Q}	Reactive power gain factor for GFM with droop control
f_{p}	Active power cut off frequency for GFM with droop control

f_{q}	Reactive power cut off frequency for GFM with droop control
ω_{p}	Active power cut off frequency for GFM with droop control
ω_{q}	Rective power cut off frequency for GFM with droop control
H	Normalised inertia constant of VSM
τ	Reaction time constant for reactive power of VSM
D_{P}	Damping factor of VSM active power
D_{Q}	Damping factor of VSM reactive power
ω	Output angular frequency of converter controller
U	Output voltage of converter controller
U_{Filter}	Voltage across inductive part of the converter filter
U_{Conv}	Output voltage of the converter
U_{POC}	Voltage at the POC
U_{g}	Nominal grid voltage
S_{r}	Nominal apparent power
R_{g}	Grid resistance
L_{g}	Grid inductance
t	Time
f	Internal frequency of controller
p	Active power at the POC in p.u.
q	Reactive power at the POC in p.u.
u_{d}	Controller voltage d component in p.u.
u_{q}	Controller voltage q component in p.u.
i_{d}	Controller current d component in p.u.
i_{q}	Controller current q component in p.u.
i_{q}	Rated frequency of converter
U_{DC}	Voltage of DC circuit
P_{DC}	Maximum DC power available to converter

List of Acronyms/Abbreviations

DUT	device under test
FRT	fault ride through
GBGF	Great Britain Grid Forming
GFL	grid-following
GFM	grid-forming
HIL	Hardware-in-the-Loop
HVDC	high-voltage direct current
IGBTs	insulated gate bipolar transistors
IGCTs	integrated gate-commutated thyristors
LCC	line commuted converter
LPF	low pass filter
MOSFETs	Metal-Oxide-Semiconductor Field-Effect Transistors
PHIL	Power Hardware-in-the-Loop
PI	proportional-integral
PLL	phase-locked loop
POC	point-of-connection
PWM	pulse width modulation
p.u.	per unit
RMS	root mean square
RoCoF	rate of change of frequency
SCR	short-circuit ratio
THD	total harmonic distortion
TSOs	transmission system operators
VSC	voltage source converter
VSM	virtual synchronous machines

Contents

1 Introduction

1.1 Motivation

With the rising share of power electronics in our electrical grids, which enable the integration of renewable generation [1], new challenges arise, especially regarding reliability and stability of power grids [2]. Historically, these aspects were ensured by synchronous machines with their high short-circuit current capability and mechanical inertia. Today grid-following (GFL) converters, are predominantly used for renewable integration, although they lack essential attributes required for grid stability in weak grids [3]. As a result, grid-forming (GFM) converters have become crucial for maintaining stability in modern power grids [4]. Because their voltage source characteristics allow them to maintain small-signal stability in weak grids and provide inertia to support frequency stability. GFM converters therefore offer a promising solution for effectively stabilising grid frequency and voltage, allowing them to assume the role traditionally held by synchronous machines.

The requirements for GFM generation are also represented in new grid codes which are introduced in the upcoming years and define the grid-forming capabilities [5] in the EU [6] and in Great Britain [7]. They include voltage and frequency regulation capabilities, especially during grid disturbances. Grid codes also specify how GFMs should interact with other grid components and the standards they must fulfil.

There are various approaches to implement GFM converters or synchronisation methods [4], [8], including droop control and virtual virtual synchronous machines (VSM). Droop control mimics the behaviour of the control of synchronous machines by adjusting the internal frequency based on the output power, while VSMs emulate the dynamic performance of synchronous generators [9]. Although GFM is promising, as a new concept and product, it has yet to undergo widespread testing in power systems. Therefore, comprehensive testing, including simulations, Hardware-in-the-Loop (HIL) and Power Hardware-in-the-Loop (PHIL) are necessary.

The power grid strength, which can be defined by the short-circuit ratio (SCR) has a high influence on the converter behaviour and its stability [10], [11]. Additionally disturbances and faults like voltage phase- and amplitude-jumps or short circuit events and their impact on these generation units have to be tested. Also a change in frequency characterized by the rate of change of frequency (RoCoF) with its impact on the dynamic system, as shown in [12] have to be analysed. Methods like PHIL [13] testing allow the evaluation of converters under realistic conditions without the need to be connected to an operational grid. It also allows a variation of parameters such as the grid impedance [14] or disturbance magnitudes with ease.

The power grid strength, which can be defined by the SCR has a high influence on the converter behaviour and its stability [10], [11]. Also disturbances and faults like voltage phase- and amplitude-jumps or short circuit events and their impact on generation units have to be tested. Additionally a changes in frequency, characterized by the RoCoF, with their impact on the dynamic system, as shown in [12] have to be analysed. Methods like PHIL [13] testing allow the evaluation of converters under these varying conditions without the need to be connected to an operational grid. While enabling testing with a complete converter unit as the device under test (DUT). It also allows a variation of parameters such as the grid impedance [14] or disturbance magnitudes with ease.

This thesis combines approaches regarding PHIL testing and GFM control testing. It leverages PHIL [15] to analyse and categorize converter controls based on their grid interaction and functional principles, such as GFL or GFM control. Along with more detailed analysis of specific parameter configurations and their influence on the converter behaviour. Additionally a commercially available converter will be tested and used for comparisons. Building on the research in this thesis, key findings have been published in the paper *Evaluating Grid-forming Converter Performance: Insights from Power Hardware-in-the-Loop Testing* in [16].

1.2 Objectives

The overarching aim of this thesis is to enhance the understanding and validation of grid-forming converter control strategies in the context of modern power systems. With a additional comparison to grid-following controls. The specific research goals are defined as follows:

- Comparison of Grid Codes:
  Compare different grid codes according to their different requirements and select one grid code as a basis for testing procedures.
- Development of Assessment Tools:
  Create converter models to test compliance with GFM grid codes. With the use of simulations and hardware implementations.
- Simulation:
  Perform detailed simulations comparing different levels of simulation detail and validating the simulations against the PHIL testing.
- PHIL Methodology:
  Investigate and validate the suitability of a Power Hardware-in-the-Loop (PHIL) approach to accurately emulate various power grid conditions through hardware validation.
- Comparative Analysis of Control Structures:
  Conduct a comparison of GFM and GFL control structures, focusing on their capability to meet grid code requirements, specifically for active phase jump power, reactive magnitude jump power and RoCoF events.
- Examine Grid Strength Influence:
  Analyse the relationship between grid strength and the converter's behaviour, during disturbances.
- Examine Disturbance Strength Influence:
  Observe the impact of disturbance strength on the converter's behaviour.

- Sensitivity Analysis of Control Parameters:
  Perform a sensitivity analysis of the GFM control parameters to assess their impacts on the overall performance and stability of the system.

1.3 Structure

The thesis is structured into six main chapters. They are organized to progressively build from theoretical foundations to a hardware implementation for testing with conclusions in the end.

1. Introduction:
   The motivation for the thesis and the research objectives are stated. A structural overview is given.
2. Grid-Forming Control: Applications, Standards, and Testing:
   This chapter reviews the necessity of grid-forming applications, compares grid-forming standards and introduces a testing methodologies for disturbances in power systems.
3. Converter-Interfaced Generation:
   A theoretical basis for converter-interfaced generation, focusing on hardware as well as grid-following and grid-forming controls is given in this section.
4. Modelling and Simulation:
   The chapter details the implementation of the control models for the previous chapter using MATLAB Simulink®. Key simulation results are analysed, providing insights into system behaviour.
5. Power Hardware-in-the-Loop (PHIL) Implementation:
   PHIL testing enables real-time evaluation of grid-forming controls with a practical test setup that includes a commercial converter. This chapter outlines the PHIL setup and presents test results, analysing the performance and different parameters of the setup.
6. Conclusion:
   This final chapter synthesizes the findings from theoretical analyses, simulations and PHIL testing. Aiming to address the research questions outlined in the objectives.

2 Grid-forming Control: Applications, Standards and Testing

2.1 Applications and Necessity of Grid-Forming Controls

Numerous emerging technologies, particularly renewable energy generation systems, depend on converters to integrate their generation into AC grids [2]. At the present, grid-following converters are predominantly used for this purpose, as defined by current grid codes [17].

The challenges associated with grid-following control have already resulted in negative impacts during fault events, as demonstrated by the incident in the UK on the 9th August 2019 [18]. A lightning-induced trip of two power stations a (N-2) event, led to a loss of distributed generation. A following rapid frequency decline triggered load shedding, eventually restoring the power balance. While the system initially functioned as intended, the incident highlighted significant issues. Specifically the integration of new technologies, such as converters, which reduced system inertia and increased the likelihood of hidden failures. It is suggested that the current (N-1) security standard may need re-evaluation to incorporate additional reserves and innovative frequency controls, such as "virtual inertia" and remedial action schemes. Furthermore, the high penetration of distributed generation (DG) complicates load shedding processes, necessitating real-time assessment of feeder loads for more selective interventions. Here a grid forming-technology could have been able to stabilise the grid and prevent load shedding

Grid-forming technologies now represent a significant advancement over traditional grid-following converters, addressing many of their limitations and enhancing overall grid stability, including [8]:

- Independence from Grid Stability:
  Grid-forming technologies create their own stable voltage and frequency references, independent of the grid. This allows them to operate reliably even in unstable or weak grid conditions.
- Strong Performance During Grid Faults:
  Grid-forming technologies are designed to handle grid faults effectively by mimicking the behaviour of synchronous machines. Unlike other technologies that require additional fault ride-through routines, grid-forming systems inherently exhibit the desired response to grid disturbances.
- Fast Response to Grid Changes:
  Grid-forming technologies respond rapidly to changes in grid conditions, such as frequency fluctuations, due to their inherent control mechanisms. These technologies maintain stability by relying on an internal reference that adjusts slowly, making them independent of the external grid's immediate variations. This characteristic allows them to contribute to grid stability and reliability more effectively.

- Low Sensitivity to Harmonics:
  These technologies are designed to handle harmonics more effectively and can include built-in filtering to mitigate harmonic distortion. This improves power quality and reduces the need for external filtering systems. In turn improving small-signal stability.

In summary, while grid-following converters, are the current standard for integrating renewable energy into power systems. They face significant challenges. This stems mainly from their dependence on the grid voltage for their phase information, resulting in poor small-signal stability during disturbances or faults in the grid system. Although they have certain fault ride through (FRT) behaviours they have to be triggered first, resulting in a delayed reaction. Grid-forming technologies, on the other hand, offer a robust solution by having a internal voltage reference and therefore maintaining stability and inherently providing synthetic inertia, without any FRT routines. This marks the benefit of grid forming control, trying to aid in the next era of power grids, with less and less inertia from synchronous generators.

2.2 Comparison of Grid Codes

As the penetration of renewable energy continues to grow, grid-forming generation is becoming a critical focus for transmission system operators (TSOs) around the world. This is represented in the next generation of grid codes, which are being updated to reflect these evolving requirements. While these grid codes share the common goal of maintaining grid stability and reliability, with the absence of rotating machines in mind. Their specific requirements vary across different TSOs.

2.2.1 Requirements of different Grid Codes

Although the various documents may use different terminology, they often describe similar metrics and aim to achieve a common objective. To now better understand these metrics, [19] introduces a useful framework for categorising these requirements, shown in Figure 2.1. The requirements as a whole are split up into the frequency response, voltage, other technical requirements and the non technical requirements.

For the frequency response four different sub categories are identified.

- Frequency deviation:
  Defines the range of steady-state frequency deviations from the nominal frequency, for which the system has to stay operational. Along with the system's ability to handle transient conditions like phase-angle jumps and RoCoF.
- Primary frequency control:
  Measures the system's ability to control active power around nominal frequency with a proportional gain.
- Fast frequency response:
  Evaluates the converter's ability to quickly adjust active power output to stabilise the grid in response to frequency changes.

- Inertial response:
  Assesses how well converters are able to emulate inertia. By modulating active power to counteract frequency or phase angle changes at the point-of-connection (POC).

The voltage requirements are split into three different groups.

- Voltage deviation:
  Describes the allowable discrepancy form the nominal voltage, typically occurring during transient events such as faults, over specific time intervals. During these periods, the converter has to remain operational, employing different FRT strategies if the deviation becomes too large for normal operation to continue.
- Voltage support:
  Regulates the exchange of reactive power at the POC to keep the voltage magnitude between desirable levels.
- Unbalanced operation:
  Involves the response to non symmetrical voltages or currents. Mostly during asymmetric faults.

Other technical requirements are split into four subsets.

- Harmonic behaviour specifies:
  The maximum values for total harmonic distortion (THD) and the magnitude of each relevant harmonic for the voltage at the POC.
- Damping:
  Lays out requirements for damping the of power oscillations and sub-synchronous resonances. This has long been a consideration, but the rising penetration of converters, has expanded the frequency range for potential interactions, now reaching up to several kilohertz.
- Islanding and black start capability:
  Refer to the system's ability to start and operate independently without relying on an external grid as a reference.

Under non-technical requirements two varieties are defined.

- Testing Specifications:
  The documents included on how the compliance to all the above mentioned requirements can be tested.
- Grid-Forming Capability:
  Publications which provide an explicit definition of grid-forming capability.

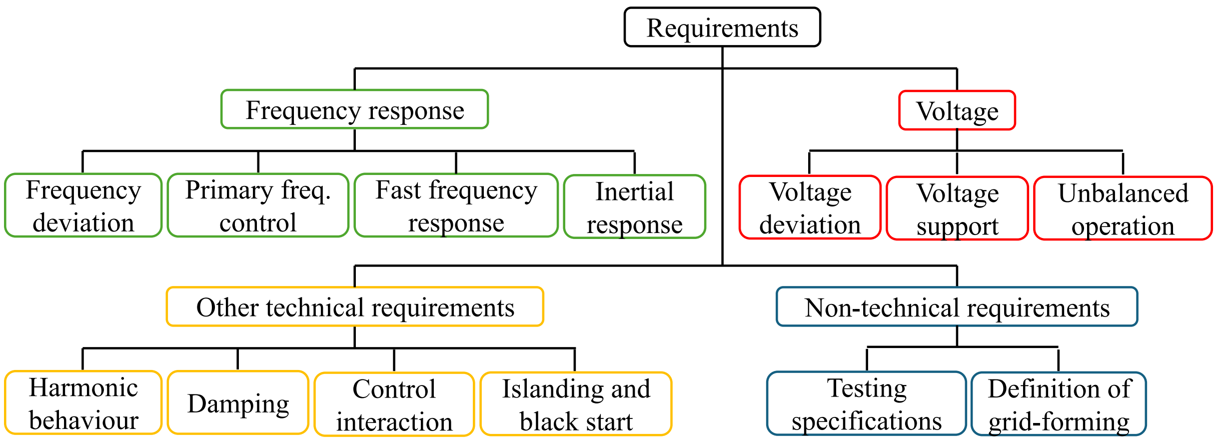

Figure 2.1: Categorisation of grid forming requirements [19]

2.2.2 Selected grid codes

The following section provides an overview of the selected grid codes and standards. They are designed to address the technical challenges posed by the growing integration of renewable energy sources and converter-based technologies into power grids. But with their different settings and categories each offers a unique approach also depending on the purpose they are meant to fulfil.

Great Britain Grid Forming (GBGF) [7] (GBGF in Table 2.1) specifically the requirements laid out in NG GC0137, is a proposed modification to the United Kingdom's Grid Code aimed at addressing the challenges posed by the increasing integration of non-synchronous renewable energy sources like wind and solar. The GC0137 modification proposes a minimum non-mandatory specification for grid-forming technologies, to replicate stability features and support grid reliability. With the idea of grid forming as a service.

The **ENTSO-E** report [6] (ENTSO-E in Table 2.1) examines the increasing penetration of power electronic interfaced power sources, such as renewable energy sources in the European grid and the technical challenges associated with managing a power system increasingly dominated by these sources. It offers solutions like GFM which are supposed to maintain system stability, provide inertia and manage faults under conditions of high renewable penetration (60-100%).

VDE-AR-N 4131 [20] (VDE-AR-N in Table 2.1) establishes standardised requirements for the connection of high-voltage direct current (HVDC) systems and power generation facilities connected through HVDC systems to the grid.

The **IEEE P2800/D6.2** [21] (IEEE in Table 2.1) standard establishes technical minimum requirements for the interconnection, performance and capability of converter-based resources connecting to transmission systems. It covers voltage and frequency ride-through, active and reactive power control, dynamic power support during abnormal conditions, power quality and system protection. Additionally, the standard applies HVDC transmission facilities.

2.2.3 Overview of Grid Code Requirements

Table 2.1 now depicts these four different grid codes, along with the specific requirements they outline as described in Figure 2.1. A check mark (✓) indicates that the requirement is explicitly stated. A circle (○) denotes an implicit or unspecific specification. With a cross (×) indicating that the requirement is not mentioned at all.

Table 2.1: Comparison of requirements for GFM generation from different TSOs [19]

Requirement	Grid Codes			
	GBGF	ENTSO-E	VDE-AR-N	IEEE
Frequency response				
Frequency deviation	○	○	✓	✓
Primary frequency control	×	×	✓	✓
Fast frequency response	×	×	✓	✓
Inertial response	✓	✓	✓	×
Voltage response				
Voltage deviation	○	○	✓	✓
Voltage support	○	○	✓	✓
Unbalanced Operation	×	✓	✓	○
Other technical requirements				
Harmonic behaviour	○	✓	✓	✓
Damping	✓	✓	✓	○
Control interaction	✓	✓	✓	○
Islanding and black start	×	○	✓	×
Non-technical requirements				
Testing specifications	✓	○	✓	✓
Definition of grid-froming	✓	✓	×	○

2.2.4 Detailed comparison

A more detailed comparison between the GBGF [7] and the ENTSO-E report [6] reveals both common goals and significant differences in their approaches to grid-forming requirements. Listed here are the key differences and focus areas for each framework:

- Focus and Scope:
  - The GBGF specifically targets individual generating units, providing detailed requirements with the characteristics of synchronous machines and how to replicate them in converter-interfaced generation. The aim is on a immediate implementation of its specifications, focusing on existing technologies to adapt quickly.
  - On the other hand the ENTSO-E takes a system-wide perspective addressing the challenges of a grid with high penetration of renewable energy sources. For this purpose it is emphasiz-

ing overall grid stability rather than individual generating units, with a very high renewable penetration (60-100%) in mind.

- Requirements and Specifications:
  - GBGF provides a non-mandatory minimum specification for grid-forming capabilities, with precise performance benchmarks and testing strategies. It identifies key attributes such as inertia, active power injection during faults and maintaining of voltage profiles.
  - While the ENTSO-E outlines broader requirements for grid-forming sources. It highlights system needs like voltage maintenance, fault level contributions and avoiding adverse control interactions. Also lists of outstanding questions that remain unanswered, indicating a need for further research are included.
- Implementation and Timeline:
  - Focused on practical implementation the GBGF will be implemented in the short term and has firm requirements.
  - ENTSO-E in contrast focuses on future-proofing the grid against evolving challenges related to high renewable penetration and does not provide immediate timelines or firm requirements.
- Commercial and Market Aspects:
  - GBGF aims to create a new commercial framework to enable gird-forming as a service with converters as well as synchronous machines. Additionally regional distribution network issues, with distributed generation and its impacts on the grid are adressed.
  - The ENTSO-E discusses high-level market aspects but remains vague about commercial implications. It focuses more on system stability, rather than specific market strategies for participants.
- Testing and Benchmarking:
  - The GBGF provides clear and actionable guidelines for testing. Including detailed compliance testing guidelines and modelling requirements, ensuring that specific technical targets are met.
  - While the ENTSO-E only recommends establishing shared benchmark systems without specifying detailed tests or performance measures. It therefore lacks the specificity found in the GBGF.

In summary the GBGF offers a more immediate and detailed framework for individual generating units, while ENTSO-E takes a holistic, long-term view of grid challenges, emphasizing broader system stability and future-proofing without providing specific benchmarks or requirements. For this thesis, the focus will be on individual generating units rather than broader system stability. Additionally the GBGF requirements offer guidelines for testing. Therefore, the GBGF will serve as the primary reference for the requirements and as a basis for the testing of grid-forming converters in this thesis.

2.3 Test Methodology

Figure 2.2 illustrates the converter (blue dashed box) with its filter (purple dashed box) connected to the grid at the POC. The grid is represented by a combination of grid impedance, including inductance and resistance, connected in series to a voltage source. The voltage source is the location where the simulated disturbance will occur. This thesis focuses on three distinct types of distrubances, which are used decoupled, but will occur together during fault events in real power grids. Phase jumps, amplitude jumps and RoCoF. The converter's response at the POC will be measured and analysed to assess its performance and test compliance with the GBGF code.

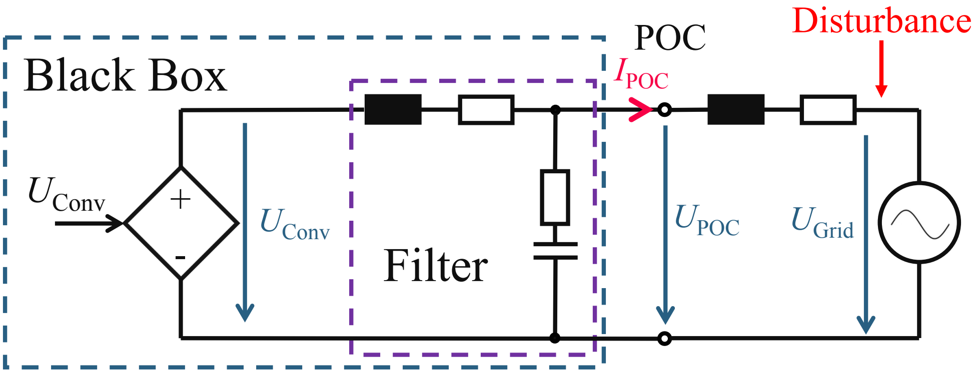

Figure 2.2: Overview Test Methodology

In the tests, as defined in GBGF [7] there are withstand limits where, the converter must remain connected to the grid, while the characteristics may vary from a voltage source due to current limits. This paper considers scenarios where the converter maintains its voltage source behaviour and remains within specified current thresholds as described in [22].

2.3.1 Disturbances in Power Systems

By modelling the grid with a voltage source roughly three distinct types of disturbances can occur. In practice these effects generally do not occur explicitly, but together. As an example, during a fault-ride through event which occurs because of a short-circuit, generally the voltage drop is combined with a phase jump. For simplicity these effects are investigated separately in the grid codes. The different grid codes specify similar responses to those disturbances as described in section 2.2, in this thesis, the grid-forming specifications of the UK are used [7] as basis for comparison. With the test methodology as shown in Figure 2.2.

Phase Jump

For a sudden change in the grid voltage phase the delivery of active phase jump power is required. The GBGF [7] also defines a phase jump angle limit at which the response is not allowed to activate current limiting functions, which is the range the tests in this thesis are kept inside of. This results for example in the requirement to deliver additional positive active power within 5 ms for negative phase jump, without changing the behaviour of the converter from a voltage to a current source.

Amplitude Jump

In this scenario, the voltage amplitude experiences a sudden drop. According to GBGF [7], reactive power must be injected within 5 ms following the voltage change. This injection of reactive power serves to stabilise the voltage levels. The amount of reactive power injected depends on the specific conditions of the grid at that moment. Here again the converter cannot change its behaviour from a voltage to a current source.

Frequency deviation

Frequency serves as an indicator of the balance between generation and load in the power grid. Any imbalance results in a frequency increase or decrease. The RoCoF measures these changes in frequency. The UK requires the converter to withstand a RoCoF of 2 Hz/s up to 52 and down to 47Hz [7]. While remaining connected to the grid, the converter is now allowed to limit the current, if it gets to high, effectively transforming the system from a voltage source to a current source.

3 Converter Interfaced Generation

Converter Interfaced Generation refers to the use of power electronic converters to integrate DC energy sources into the AC electrical grid. The basic structure of a converter interfaced generation unit [4] can be seen in Figure 3.1.

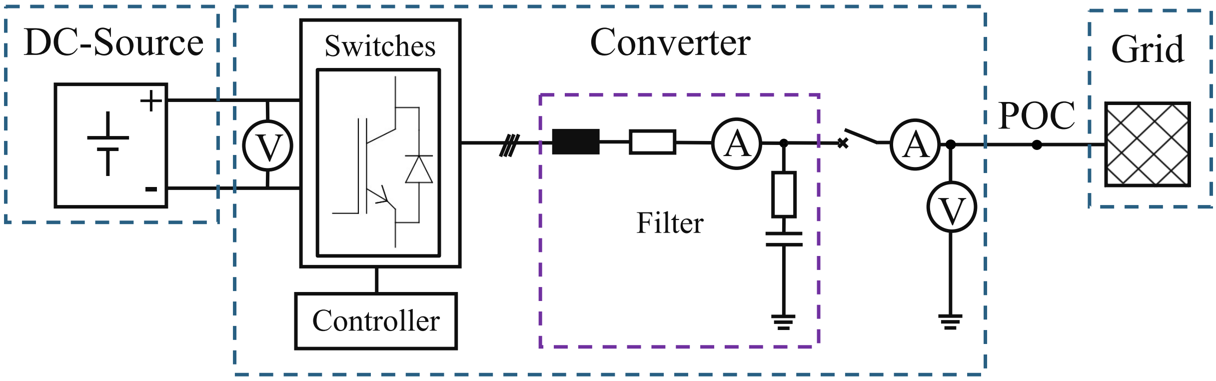

Figure 3.1: Schematic of grid connected converter with Grid

3.1 Converter Interfaced Generation Unit

The converter interfaced generation unit requires both a DC source and an AC grid for operation. The unit features switches to regulate power flow, a filter to smooth the output and a controller to manage overall system functionality.

In this thesis, only voltage source converter (VSC) technology is employed for the converters. VSCs utilize transistors that can be switched on and off independently of external factors. Providing full control over their switching behaviour. As a result, VSCs can independently regulate both active and reactive power. Moreover, VSCs can start operation autonomously without requiring an external power source [23]. In contrast, line commuted converter (LCC) technology relies on thyristors, which depend on the AC system for the commutation process. This reliance limits the independent control of active and reactive power and makes LCCs unsuitable for black start scenarios [23]. As a result, VSC technology is better suited for converters. With the continuous advancements in transistor technology, leading to larger, more efficient and cost-effective transistors, they have become widely adopted today.

3.1.1 Sources

The DC source depicted in Figure 3.1 can represent a wide range of different sources encountered throughout various stages of a modern power grid. These sources are present not only during the power generation but also throughout transmission, storage and even reversible consumption processes. This plays a crucial role in enhancing the efficiency, reliability and flexibility of energy distribution, needed to meet the volatile nature of renewable energy generation.

Generation

On the generation side, DC sources enable efficient integration of renewable energy systems like photovoltaic solar panels, which inherently produce DC electricity. Similarly Type III (double fed asynchronous machine) and Type IV (synchronous machine with a full converter) wind turbines use power electronics to convert the generated variable-frequency AC current partially (Type III) or completely (Type IV) into DC, to improve the efficiency and reduce the susceptibility to maintenance of wind turbines.

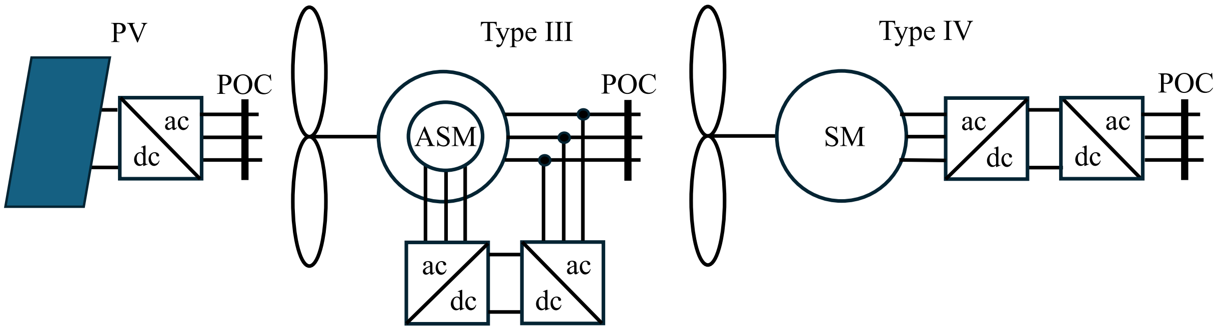

Figure 3.2: Different types of renewable generation

Transmission

In the transmission of electricity, HVDC is often used due to its efficiency in long-distance power transfer. Unlike AC, HVDC systems experience lower energy losses over vast distances, making them ideal for connecting remote power generation sites, for example offshore wind farms. Additionally, HVDC allows for better control over power flow and can link asynchronous grids. In certain cases even improving grid stability and flexibility [24].

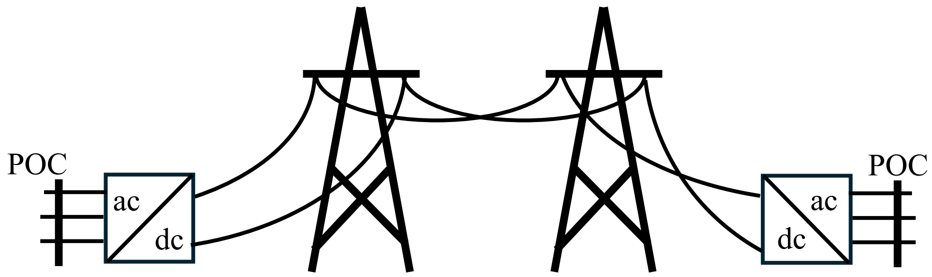

Figure 3.3: HVDC schematic diagram

Storage and Consumption

DC-interfaced energy storage solutions, such as hydrogen electrolysis and batteries, provide efficient methods for storing and retrieving electricity in modern power systems. These technologies enhance the flexibility and resilience of the grid by allowing for better integration and management of renewable energy sources.

Furthermore, DC sources play a pivotal role in advancing technologies such as electric vehicles and micro grids, both of which rely on DC power for efficient charging, operation and optimisation. In these systems, DC power can be stored directly in the batteries of consuming devices, such as electric vehicles. When, these devices are connected not only to the DC system but also to the grid via a converter, their stored energy can be deployed during critical conditions. Using it to stabilise the grid. This seamless integration not only enhances efficiency but also contributes to a more reliable, adaptable and sustainable energy future.

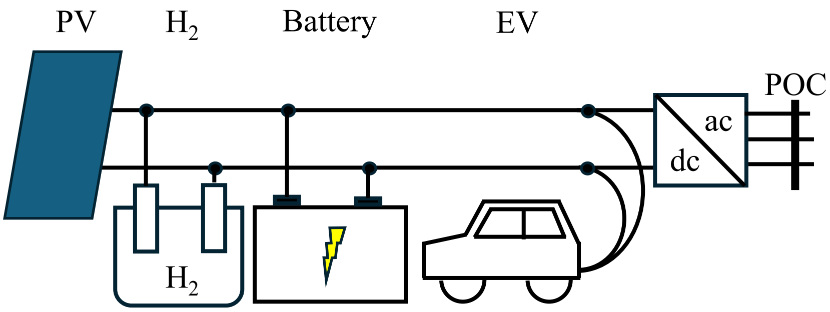

Figure 3.4: Different types of renewable storage and consumption

3.1.2 Switching

Power converters, consist of electronic switches such as integrated gate-commutated thyristors (IGCTs) and insulated gate bipolar transistors (IGBTs). Which are pivotal for converting DC voltage into AC efficiently. A common approach to achieving this, is through configurations such as half-bridge or full-bridge converters. This thesis focuses on three-phase, two-level converters that utilize three half-bridge modules. These modules switch the polarity of the DC input to generate a three-phase AC waveform.

A fundamental technique in this process is pulse width modulation (PWM). PWM is employed to regulate the timing and duration of the switching actions of devices like IGBTs and MOSFETs. By rapidly toggling the switches at a high frequency, PWM adjusts the duty cycle of each pulse. This modulation of pulse width effectively controls the average output voltage, allowing for the synthesis of a smooth AC waveform that approximates a sinusoidal shape. This technique not only enhances the efficiency and precision of the DC-AC conversion but also minimises losses and provides fine-grained control over the output voltage.

3.1.3 Filter

In Converter Interfaced Generation Units, the output waveforms frequently deviate from the desired sinusoidal shapes due to the switching frequency of the power electronic devices. Which are utilized to generate the PWM voltage. To ensure compliance with harmonic distortion and power quality standards, effective filtering is essential. To smooth the output from the semiconductor switches, low-pass filters with resistor-inductor and resistor-capacitor components are commonly employed, as shown in Figure 3.1. These filters are often specifically tuned to effectively eliminate the harmonics generated by afore mentioned the switching frequency. Additionally, magnetic filters are used to remove residual DC components.

3.1.4 Controller

The controller in a power electronic converter is crucial for determining its behaviour and performance, generating PWM signals for the switches to control the amplitude and waveform of the AC output voltage. It relies on feedback from sensors, monitoring parameters such as voltages and currents at the POC. Enabling real-time adjustments to maintain stability and respond to load changes. Advanced controllers incorporate sophisticated algorithms for optimal efficiency and power factor correction, enhancing energy transfer, minimizing losses and improving overall system performance. Additionally, they often include fault detection and protection features. Safeguarding the converter and connected equipment from overloads, short circuits and other anomalies. Thereby ensuring reliable and efficient operation in various applications.

The controllers designed for the converters used in this thesis for comparative testing are structured as illustrated in Figure 3.5. These controllers utilise a dq0 reference frame to transform the three-phase AC quantities into a rotating reference system. The transformation is part of a feedback loop that works in conjunction with the synchronisation method, ensuring the controller can achieve and maintain synchronisation with the external grid. After the synchronisation control, various inner controls can be implemented to enhance system stability and performance. The results of the controls are transformed back into the three-phase AC signals via the inverse Park and Clark conversion. These processed signals are then used to generate PWM signals, which drive the converter switches.

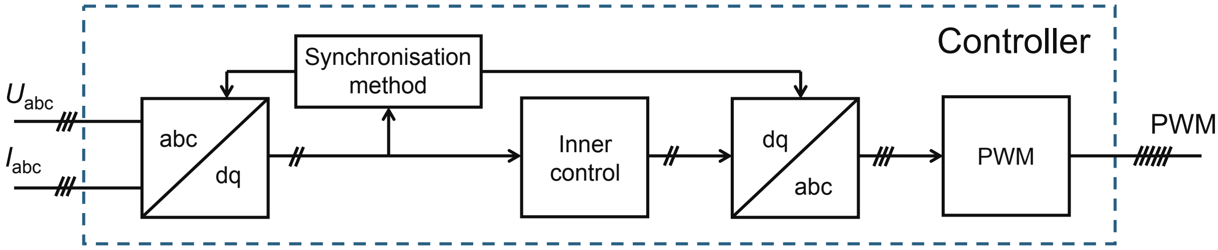

Figure 3.5: Schematic of converter controller

The abc to dq transformation consists of a Clark [25] (Equation 3.1) and Park [26] (Equation 3.2) transformation executed in this order. Mathematically they are represented as follows:

$$\mathbf{u}_{\alpha\beta} = \frac{2}{3}\begin{bmatrix} 1 & -\frac{1}{2} & -\frac{1}{2} \\ 0 & \frac{\sqrt{3}}{2} & -\frac{\sqrt{3}}{2} \end{bmatrix} \cdot \mathbf{u}_{\text{abc}} \tag{3.1}$$

$$\mathbf{u}_{\text{dq}} = \frac{2}{3}\begin{bmatrix} \cos(\theta) & \sin(\theta) \\ -\sin(\theta) & \cos(\theta) \end{bmatrix} \cdot \mathbf{u}_{\alpha\beta} \tag{3.2}$$

The angle θ of the rotating system in the Park transformation (Equation 3.2), which corresponds to the angle of the external grid, is not known in advance. Therefore, a synchronisation method is required to align the Park transformation and consequently the entire control system, with the external grid. There are several approaches to achieve this synchronisation. In this thesis, both grid-following (section 3.3) and grid-forming methods (section 3.4) will be explored and implemented. The dq transformation is typically applied to symmetrical systems. However, when there is a zero-sequence component, a dq0 transformation is required to accurately represent the system in the transformed domain.

The inner controls, explored in detail in subsection 3.4.5, are able to regulate the dynamic response of the converter and aid in maintaining stable operation. Implemented in the dq0 reference frame, these controls efficiently manage critical parameters such as current, voltage, and power flow. By operating within this rotating reference frame, the controls can independently decouple and regulate active and reactive power components. One of the most significant advantages of the dq0 reference system is that it effectively eliminates the 50 Hz components of the signal. This allows for the use of PID controllers, which are more suitable for handling these dynamics, rather than relying on systems designed to additionally manage the 50 Hz components.

After the last control, the signal is transformed back from the dq reference frame to the abc reference frame using the inverse Park and Clarke transformations. Since the angle θ is now known, it can be applied directly.

With the re-transformed abc voltage signal, a PWM signal is created by comparing the sinusoidal reference voltage from the controller of the converter with a high-frequency carrier wave, typically a triangular waveform. The controller uses this comparison to generate switching signals for the converter's transistors. This creates pulses of varying width, which control the converter's output voltage and frequency. Allowing it to reproduce the desired AC waveform.

3.1.5 Power Grid

The grid, while not a component of the generating unit itself, plays a crucial role in the operation of converters, especially in grid-tied systems [10]. When an converter is connected to the grid, it must synchronise its output frequency and voltage with those of the grid. To be able to efficiently and safely transfer power into the grid. Therefore, the dynamic conditions of the grid significantly impact the converter's dynamics. Due to faults and disturbances like short circuits, sudden large loads changes, switching events or fluctuations in power generation, voltage amplitude drops coupled with voltage phase jumps may arise. If the converter cannot ride through such faults, it may disconnect or fail to stabilize, leading to potential further disruptions in connected systems, or damage to the converter itself. Additionally, the grid determines the amount of power the converter can feed back into it.

Since real-life testing on the actual grid is not feasible, simulating or emulating grid conditions is crucial for assessing converter performance [13]. This thesis implements such simulations or emulations to evaluate the converter's performance under various grid conditions.

3.2 Overview of converter controls

Since this thesis includes various converter control types, Figure 3.6 provides an overview of each type, along with the chapters where they are discussed. The two main categories are the GFL and GFM controls, each of which is further subdivided. The GFL controls include the grid-feeding control structure and a commercially available, therefore named commercial off the shelf, GFL converter. In contrast, the GFM controls encompass the droop control, droop control with a low-pass filter and the virtual synchronous machine.

In the context of Figure 3.6, "Theory" indicates that the controls are discussed theoretically in chapter 3. "Simulation" denotes that the control is implemented in chapter 4 for Simulink® simulations, while "PHIL" signifies that the control is applied in chapter 5 for the PHIL implementation in the laboratory.

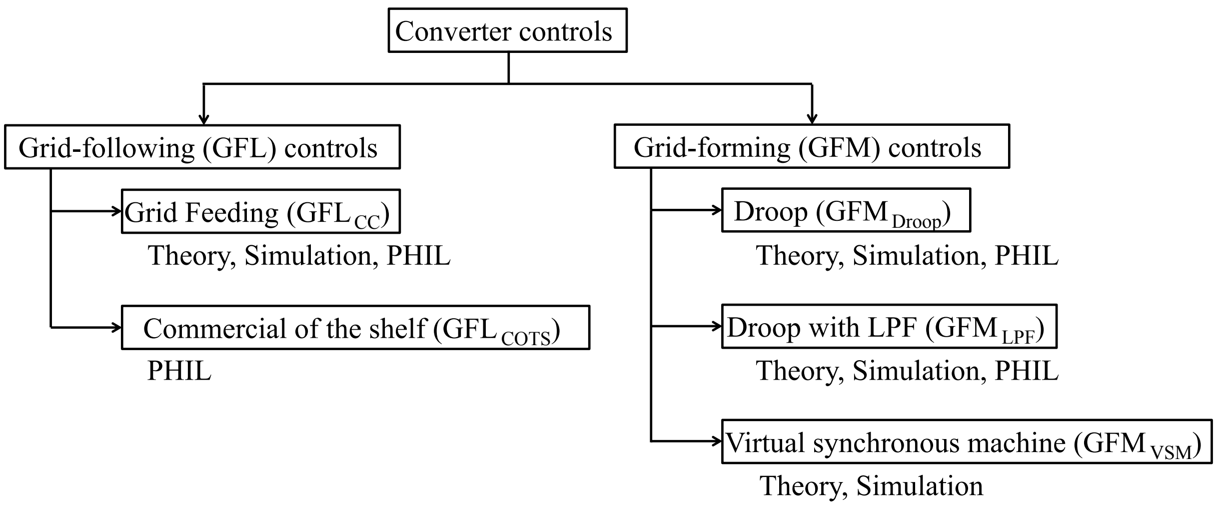

Figure 3.6: Flow chart of different convertertypes in this thesis with the chapters they appear in.

3.3 Grid-Following (GFL)

A GFL device synchronizes with the local grid voltage, injecting an electric current vector aligned with the voltage, effectively functioning as a current source. The majority of installed converter-based resources are GFL converters. GFL devices, by their inherent design, lack stability during significant voltage or frequency disturbances [3]. This occurs because the converter relies on grid voltage to obtain its phase information. If the grid voltage is too distorted or too low, the GFL converter cannot accurately gather this information, preventing it from functioning properly. As a result, they are unable to contribute to grid strength or provide inertia without a delay caused by the phase-locked loop (PLL). This limitation underscores the need for a new control paradigm that allows such devices to enhance grid stability under dynamic conditions.

The most basic GFL strategy, called a grid-feeding control [27] and illustrated in Figure 3.7(a) only injects a reference current I^* into the grid. To enable this it relies on a PLL to achieve synchronisation with the grid voltage, as shown in Figure 3.7(b). The PLL provides a stable reference for the converter. The current is based on a reference based on the DC power source, which could be a battery, photovoltaic system, or another type of energy source [28]. The ability to adjust the reference current is limited, by the maximum power provided from the primary DC energy source. As the AC grid voltage is only allowed to fluctuate minimally, the maximum AC current is limited by the primary source power. This limitation means, the control has less flexibility, simply feeding the available power from the primary source into the system.

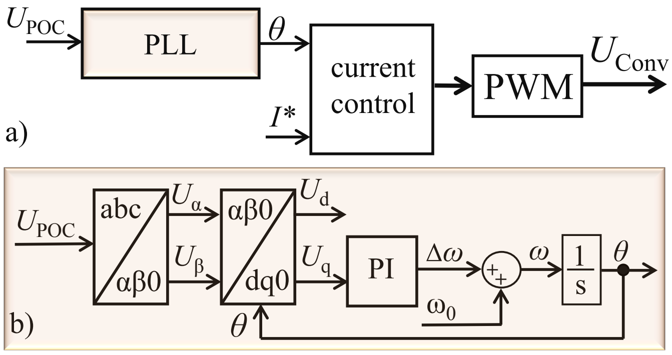

Figure 3.7: Schematic of grid feeding controller (a) control diagram (b) PLL control block diagram

However, this method is contingent on the presence of a stable external grid voltage for proper operation, which has notable limitations. Specifically, in situations where the grid is weak or unstable, the PLL may lose its synchronisation, leading to potential instability in the control system. This instability not only affects the reliability of the current injection but also the implementation of advanced grid support features that are crucial for maintaining grid stability and resilience [29] as they all rely on a PLL for phase information. The grid-feeding control strategy serves as a baseline or reference point in this thesis. Subsequently, a commercially available converter with more advanced features will also be tested in chapter 5.

3.3.1 Phase-Locked Loop (PLL)

The PLL Figure 3.7(b) is used to synchronise the control with the grid frequency and determine the angle of the voltage space vector. The PLL accomplishes this by aligning the d-axis of a rotating reference frame with the voltage phasor. This alignment is achieved by adjusting the q-component of the voltage to zero using a proportional-integral (PI) control scheme. By continuously regulating the q-component to 0, the PLL ensures that the d-axis accurately tracks the voltage vector, which is essential for the Park transformation Equation 3.2 and subsequently the control of the power system.

Tuning of the PI controller is critical to the PLL's performance, for this thesis the guide [30] is used to tune the PLL. Formulas (1-15) from [30] are adapted to calculate the proportional gain $K_{\mathrm{p,PLL}}$ and the integral $K_{\mathrm{i,PLL}}$ gain of the PLL. With chosen cut off frequency of the PLL $f_{\mathrm{cut,PLL}}$, control period T_{s} and known voltage amplitude U_{Base}. The calculation is then implemented as follows:

$$\omega_{\mathrm{cut,PLL}} = 2\pi \cdot f_{\mathrm{cut,PLL}} \tag{3.3}$$

$$K_{\mathrm{p,PLL}} = \frac{\omega_{\mathrm{cut,PLL}}}{U_{\mathrm{Base}}} \tag{3.4}$$

$$K_{\mathrm{i,PLL}} = K_{\mathrm{p,PLL}} \cdot T_{\mathrm{s}} \cdot \omega_{\mathrm{cut,PLL}}^2 \tag{3.5}$$

3.3.2 Current Control (CC)

Similar to the PLL, the current control can also be implemented using a PI controller. This controller then requires tuning. A tuning method outlined in [30] is employed to tune the current control. Two tuning methods are presented in [30]: one based on the open-loop cut off frequency and another based on the natural oscillation frequency. In this thesis, the latter approach is used.

Formulas (2-12) and (2-13) from [30] are adapted to calculate the proportional gain $K_{\mathrm{p,CC}}$ and integral $K_{\mathrm{i,CC}}$ gain of the current control. These gains are calculated based on the cut off frequency of the current control $f_{\mathrm{cut,CC}}$, control period T_{s}, filter inductance L_{f} and inductance filter resistance R_{Lf}. The calculation for the proportional gain $K_{\mathrm{p,CC}}$ is then implemented as a set of equations:

$$a = -\frac{1.5 \cdot K_{\mathrm{p,CC}} \cdot T_{\mathrm{s}}}{(1 + 9 \cdot T_{\mathrm{s}}^2 \cdot \pi^2 \cdot f_{\mathrm{cut,CC}}^2) \cdot L_{\mathrm{f}}} \tag{3.6}$$

$$b = -\frac{0.5 \cdot K_{\mathrm{p,CC}}}{(1 + 9 \cdot T_{\mathrm{s}}^2 \cdot \pi^2 \cdot f_{\mathrm{cut,CC}}^2) \cdot L_{\mathrm{f}} \cdot \pi \cdot f_{\mathrm{cut,CC}}} \tag{3.7}$$

$$a^2 + b^2 - 1 = 0 \tag{3.8}$$

Where Equation 3.8 is solved for $K_{\mathrm{p,CC}}$. With this $K_{\mathrm{i,CC}}$ can then be calculated with:

$$K_{\mathrm{i,CC}} = \frac{R_{\mathrm{Lf}} \cdot K_{\mathrm{p,CC}}}{L_{\mathrm{f}}} \tag{3.9}$$

While this chapter offers a fundamental overview of GFL control methodology, commercially available converters designed around this principle incorporate more sophisticated features to align with current grid codes and regulatory standards. These converters are equipped with advanced functionalities, particularly concerning fault response and resilience. For instance, they must adhere to specific fault ride-through behaviours and demonstrate resilience characteristics to comply with regulatory requirements. Such features ensure that the converters not only meet performance expectations but also enhance grid stability and reliability under fault conditions. Such a commercially available converter is later introduced and tested in chapter 5.

3.4 Grid-Forming (GFM)

Grid-forming (GFM) controls, with a basic outline shown in Figure 3.8 [4], utilise both active and reactive power at the POC to synchronise with the power grid. By maintaining both the frequency and voltage within specified limits, GFM converters contribute to grid stability, especially in grids with high renewable energy and therefore converter penetration.

Internally, GFM converters generate and continuously adjust a reference voltage based on the active (P^*) and reactive power (Q^*) set points. The active power control (P-f control) governs the phase angle of the converter output, directly influencing the frequency, while the reactive power control (Q-U control) adjusts the voltage level. The converter's internal reference voltage is dynamically adjusted to meet these targets, enabling the GFM controls to mimic the behaviour of traditional synchronous generators. This allows the converter to not only synchronise with the grid but also to contribute actively to voltage and frequency regulation, making it a critical component in maintaining grid reliability.

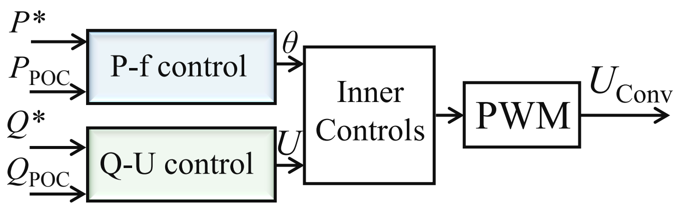

Figure 3.8: Grid-forming control

3.4.1 Droop

The droop control method [4], [8] used for converters is fundamentally derived from the proportional droop control mechanism found in synchronous machines. This approach regulates the output active and reactive power (or frequency and voltage) to ensure stable and balanced load sharing among parallel generating units. The droop control formula for active power is typically represented as:

$$K_{\mathrm{P}} = -\frac{\Delta\omega/\omega_0}{\Delta P/P_0} \tag{3.10}$$

Similarly for the reactive power:

$$K_{\mathrm{Q}} = -\frac{\Delta U/U_0}{\Delta Q/Q_0} \tag{3.11}$$

The control of reactive power offers greater flexibility and proportional control is one viable option used in this case. Alternatively, an integral, derivative, or a combination of these three control strategies (PI control) can also be employed, depending on the system's requirements.

The implementation of the proportional droop control into the control circuit for the active power component is depicted in Figure 3.9 (blue). In this setup, the angular frequency is derived by subtracting the measured active power P_{POC} at the POC from the reference active power P^*, followed by multiplying the result with the gain factor K_{P}. A feed-forward signal, represented by the nominal angular frequency ω_0, is then added to this value to aid on startup. Finally, the reference angle is obtained by integrating the resulting angular frequency.

The reactive power control (Figure 3.9(green)) implementation differs from active power as there is no need for integration at the end because U can be used directly. Again, a proportional controller is utilised, which adjusts the output voltage, directly in response to the discrepancy between the measured reactive power Q_{POC} at the POC and the specified reference reactive power Q^*. This discrepancy, or reactive power error, is multiplied by a proportional gain factor K_{Q}, which determines the extent of the voltage adjustment. The resulting adjustment is applied to the converter's output voltage, thereby modulating it to align the reactive power with the reference value. Both of these represent first-order control systems.

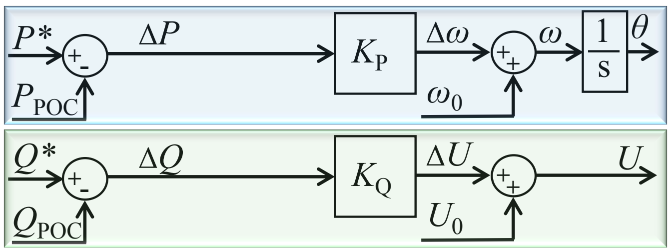

Figure 3.9: Droop control

With the transfer function for the active power:

$$\theta = \frac{1}{\mathrm{s}}(\omega_0 + K_{\mathrm{P}}(P^* - P_{\mathrm{POC}})) \tag{3.12}$$

and for the reactive power:

$$U = U_0 + K_{\mathrm{Q}}(Q^* - Q_{\mathrm{POC}}) \tag{3.13}$$

3.4.2 Droop with LPF

The second type of GFM control incorporates a low pass filter (LPF) within both sections of the droop control mechanism, as depicted in Figure 3.10 [4], [8]. This takes into account that a real synchronous machine has mass and therefore doesn't react instantly to changes at the POC. By introducing an LPF with a defined cut-off frequency ω_p, the droop control's ability to manage high-frequency disturbances and provide smoother operation is enhanced. The LPF integration results in a second-order system.

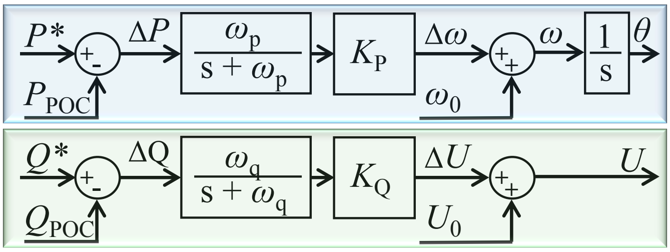

Figure 3.10: Droop control with LPF

With the transfer function for the active power:

$$\theta = \frac{1}{s}(\omega_0 + K_P \cdot \frac{\omega_p}{s+\omega_p} \cdot (P^* - P_{POC})) \tag{3.14}$$

and for the reactive power:

$$U = U_0 + K_Q \cdot \frac{\omega_q}{s+\omega_q} \cdot (Q^* - Q_{POC}) \tag{3.15}$$

3.4.3 VSM

The third type of GFM control scheme Figure 3.11 is the VSM [4], [8]. It is derived from the swing equation of the synchronous machine [31]:

$$\frac{d\Delta\omega}{dt} = \frac{1}{2H}(P_{mech} - P_{el} - \frac{\Delta\omega}{D}) \tag{3.16}$$

Thereby the inertia constant H links the active power with the angular frequency and the damping factor D_P is fed back to the active power difference. For the reactive power again the only difference is the missing integration at the end. The control circuit can be seen in Figure 3.11.

With the transfer function for the active power:

$$\theta = \frac{1}{s}\left\{\frac{1}{2Hs}[D_P(\omega_0 - \omega) + P^* - P_{POC}]\right\} \tag{3.17}$$

and for the reactive power:

$$U = \frac{1}{\tau s}[D_Q(U_0 - U) + Q^* - Q_{POC}] \tag{3.18}$$

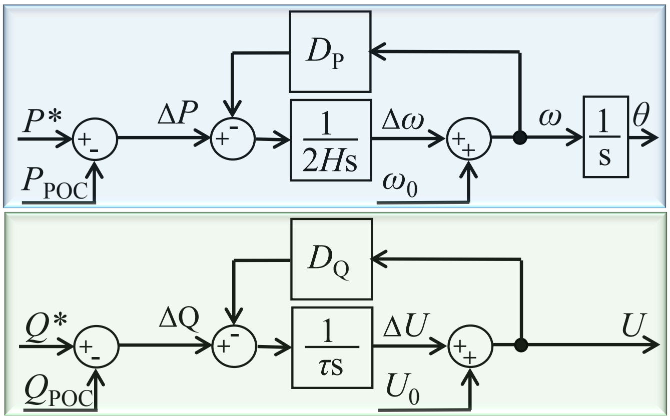

Figure 3.11: Virtual syncronous machine

3.4.4 Equality of VSM and Droop with LPF

The droop control with a LPF and the VSM are both second-order control systems. As a result, it is possible to tune them so that they exhibit equivalent behaviour [9]. This equivalence can be demonstrated mathematically.

To begin, we consider the transfer functions of the active power (P-ω) control for the droop control with LPF Equation 3.14 and the VSM Equation 3.17. The term $1/s$ can be reduced for both for both formulas, with the Equation 3.17 extended by $1/(2Hs + D_P)$ this results in:

$$\omega = \omega_0 + K_P \cdot \frac{\omega_p}{s + \omega_p} \cdot (P^* - P_{POC}) \tag{3.19}$$

$$\omega = \cancel{\frac{D_P}{2Hs + D_P}} \omega_0 + \frac{D_P}{2Hs + D_P} (P^* - P_{POC}) \tag{3.20}$$

Note that Equation 3.20 has been simplified by ignoring the low-pass filtering of the constant term ω_0. Now observing Equation 3.19 and Equation 3.20 it is apparent that the droop control with LPF is the same as the VSM. The equivalence, for the P-ω control, then follows as:

$$D_P = \frac{1}{K_P}, \; H = \frac{1}{2 \cdot K_P \cdot \omega_p} \tag{3.21}$$

For the reactive power (Q-U) control no reduction is needed, the Equation 3.18 is extended by $1/(\tau s + D_Q)$ this now results in:

$$U = \cancel{\frac{1}{\tau s + D_Q}} U_0 + \frac{1}{\tau s + D_Q} (Q^* - Q_{POC}) \tag{3.22}$$

Here Equation 3.22 has been simplified by ignoring the low-pass filtering of the constant term V_0. With Equation 3.15 the equivalence, for the Q-U control, then follows as:

$$D_\mathrm{Q} = \frac{1}{K_\mathrm{Q}}, \; \tau = \frac{1}{K_\mathrm{Q} \cdot \omega_\mathrm{q}} \tag{3.23}$$

The two equations 3.21, 3.23 can now be used to tune the VSM to be equivalent to the droop controller with LPF and vice versa [9].

3.4.5 Inner Controls

The inner controls are after the synchronisation step, as depicted in Figure 3.5. There are several possible ways to implement inner controls [4]. In this thesis, the focus will be on three specific approaches: the direct method, the indirect method and the cascaded control approach.

Direct

The direct approach [4] simplifies the control process by eliminating inner controls, allowing the voltage reference from the Q-U control to feed directly into the dq-conversion stage. This path leads straight to PWM generation and subsequently to the converter's output. As a result, it offers the most straightforward and simplest method.

However, the trade-off lies in the reduced capacity for error correction, as inner controls often enhance efficiency and stability.

Indirect

In indirect control, the converter's filter is taken into account in relation to the desired output at the POC, while the actual controlled output of the converter is located behind the filter [4]. To address this discrepancy, the voltage drop across the filter, denoted as U_Filter (as illustrated in Figure 3.12), is computed and used to adjust the converter voltage U_Conv. This compensation ensures that the voltage at the POC remains as close as possible to the desired value, despite the voltage drop across the filter U_Filter.

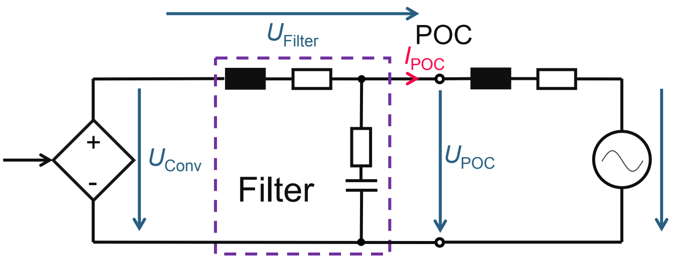

Figure 3.12: Indirect inner control

Cascaded

GFM controls can also use a cascaded control system. This typically consists of two inner controls: voltage control and current control [4]. The voltage control is responsible for regulating the voltage at the POC, ensuring that the voltage levels remain stable and within acceptable limits. Meanwhile, the current control manages the current at the POC, ensuring that the current injected or absorbed from the grid is within operational bounds. This two-tiered structure is applicable to both grid-following and grid-forming control systems.

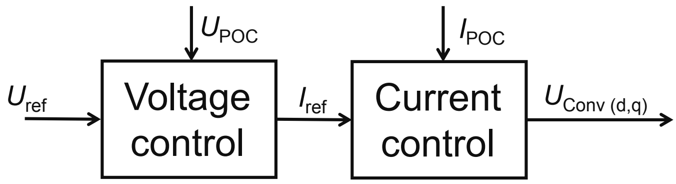

Figure 3.13: Cascaded inner control

3.4.6 Grid Syncronisation

When the GFM converter is connected to the grid, the current across the filter can be measured immediately. However, for an optimal startup process, it is crucial to have an estimate of the current beforehand to avoid overcorrection or incorrect adjustments. The challenge lies in the fact that the grid impedance is typically unknown, making precise calculations difficult. As a result, only an approximation of the current is possible.

To mitigate this uncertainty, a for the GFM converters a PLL is used first to synchronise the converters to the grid and approximately match the voltage of the converter to the voltage at the POC. This means the voltage difference across the filter is only small and when the switch is closed only a small compensating current will occur. After the converter is connected, the power output can then be gradually ramped up to the desired level, allowing for smoother adjustments and better control over the system. This method reduces the likelihood of instability or excessive oscillations during startup.

4 Modelling and Simulation

To develop a functional prototype, the initial step is to model the entire system in software, to validate its performance in a virtual environment. This offers numerous advantages over physical prototyping. It eliminates the need for expensive hardware, reducing costs significantly. Additionally, the setup and modification processes are much faster and easier to implement in software. This allows for rapid iterations and testing. Unlike real-time computing in hardware, software models do not need to run in real time requiring less powerful hardware. Lastly software models also offer the ability to test various scenarios, especially edge cases, without risking damage to physical components.

All the models in this thesis were developed using **MATLAB®/ Simulink® Version 9.2 (R2018b)**, incorporating the specialised power electronics library. For the Simulations closer to the then used (imperix®) Hardware, the **imperix® ACG SDK Development Kit (Version 2024.1)** was used for automated code generation, providing a seamless transition from simulation to real-time execution in embedded systems.

4.1 Physical Model

The Physical Model [4] in Simulink® was created with the Specialised Power Systems library from the Simscape toolbox. The components of the physical model can be seen in Figure 4.1. It includes from left to right the voltage source of the converter. This is a combination of the DC source and the power electronic switches. The filtering components of the converter and lastly the grid modelled as a voltage source with a impedance.

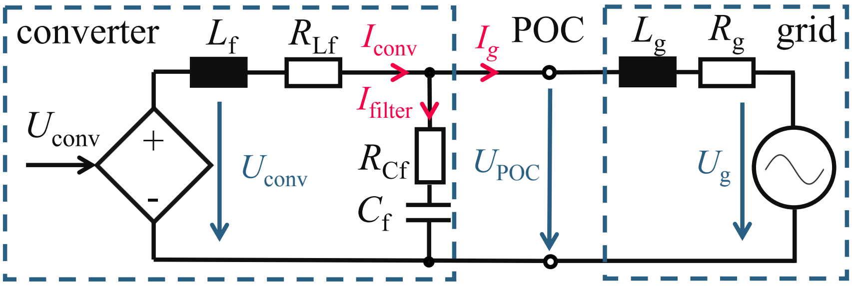

Figure 4.1: Schematic of the physical components of the converter with the grid

All the parameters for the simulated converter can be seen in Table 4.1. The parameters of the simulated model where chosen with the physical model, in the laboratory, in mind. The nominal Voltage U_g was chosen at 100 V to provide sufficient overhead, ensuring a larger safety margin for the hardware tests. The same goes for the nominal apparent power S_r. The grid impedance and the impedance of the converter where represented by the imperix passive filters box in the physical model. For the simulated model the nominal values of the components from the imperix passive filters box where used. The grid resistance R_g is bigger than the nominal value of the filters box. The additional resistance accounts for the physical connections and cables in the system and was measured in the hardware setup.

Table 4.1: Parameters of the Physical Model

Parameters Grid				
U_g	R_g	L_g	SCR	X/R-Ratio
100 V	180 mΩ	2.3 mH	15	4
Parameters Converter				
S_r	R_{Lf}	L_f	C_f	R_{Cf}
1 kVA	40 mΩ	2.3 mH	10 μF	1 Ω

4.1.1 DC-Source

As described in subsection 3.1.1 there is a wide range of different possible DC-Source supplying energy to the converter. The focus in this thesis however is not on the DC-Source but the behaviour of the converter on the AC-side. The behaviour is influenced by the DC voltage sizing, particularly when under-modulation or over-modulation occurs. To eliminate this influence in the simulation the DC-Source was set to double the Voltage of the RMS value of the nominal grid voltage U_g, being 200 V. The model in Simulink® can be seen in Figure 4.2, the model represents a constant DC-Source without any internal parallel resistance or conductance to ground. For the imperix simulations a serious resistance of 1 Ω was added.

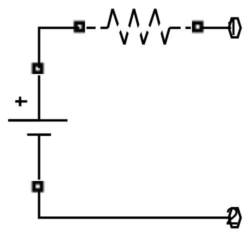

Figure 4.2: Model of DC-Source of the model converter in Simulink®

4.1.2 Grid

Modelling a electrical grid and its behaviour at a certain point is a non trivial problem with a broad variety of approximations depending on the desired outcome, proximity to reality and complexity. In this thesis a single converter is connected to a grid at the POC. The grid is then represented as a voltage source with a series impedance with the values from Table 4.1.

The implementation of this grid model, in Simulink®, can be seen in Figure 4.3. The impedance is represented with a three phase symmetrical impedance. There are three controlled voltage sources connected in a star configuration with a grounded neutral point.

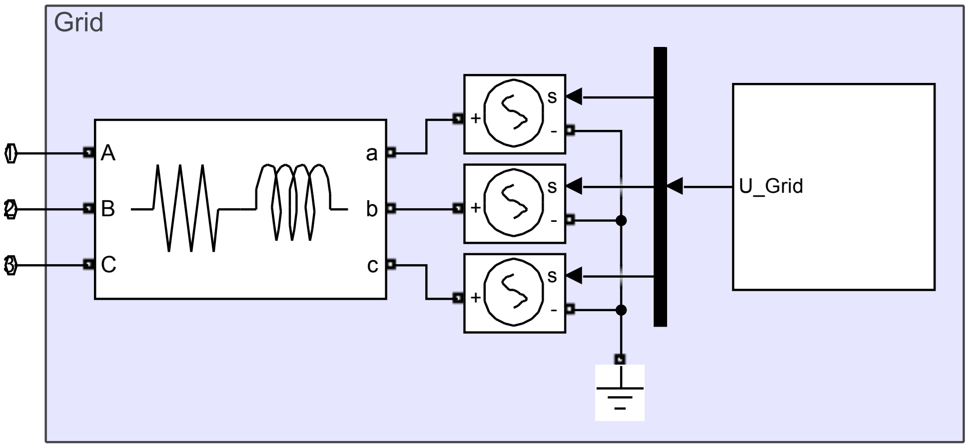

Figure 4.3: Model of the Grid for the model converter in Simulink®

The control signal for these voltage sources is generated in a separate Subsystem which can be seen in Figure 4.4. The basic system is a reference voltage and a reference angular frequency, which is integrated and modulo checked over two pi to circumvent overflows. The angular frequency is then used as the frequency for a dq0 to abc conversion. The d-axis component of the conversion is set to the desired output voltage in p.u., while the q and 0-axis are set to zero. When simulating the three different types of disturbances at the voltage source, dedicated mechanisms are integrated, to efficiently trigger each disturbance scenario. The amplitude jump, when triggered instantly reduces the amplitude of the voltage source to 90%. The phase jump instantly shifts the phase by -5°. For the RoCoF a frequency ramp has to be provided this is implemented with a dynamic rate limiter. Which limits the rate of change to 2 Hz/s while the total drop in frequency is 1 Hz down to 49 Hz.

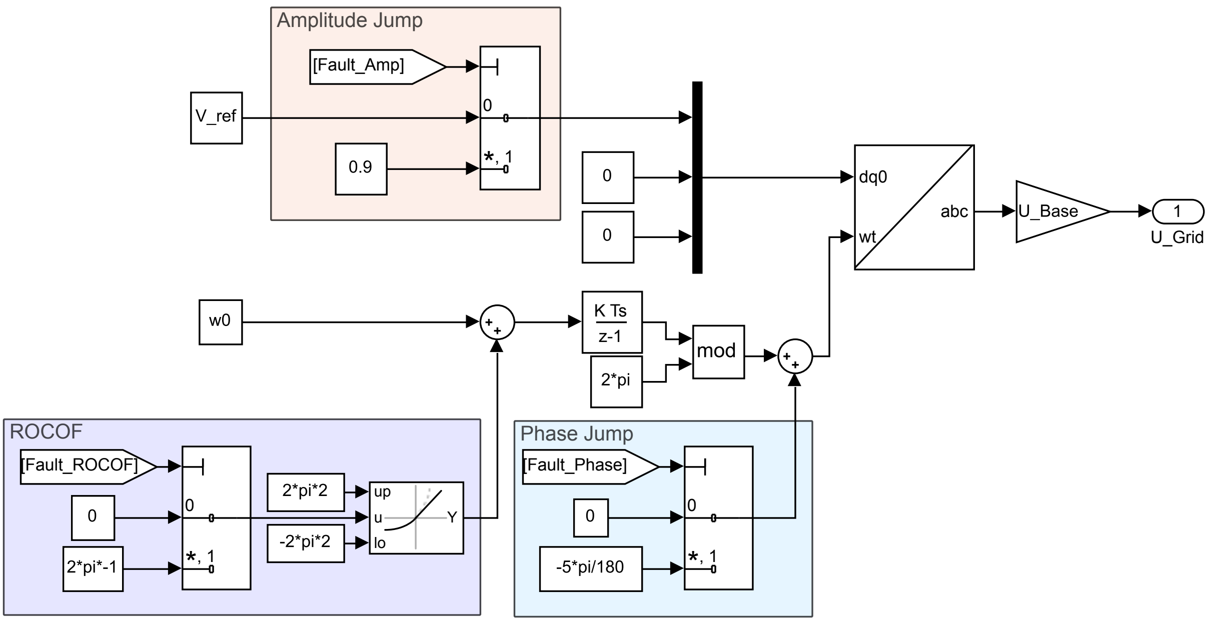

Figure 4.4: Generation and synchronisation of error triggering in the grid

To make the tests as repeatable as possible the need for the synchronisation of the disturbance occurrence arises. As it makes a big difference for the reaction of the converter at which time the disturbance occurs. To get a repeatable point, the voltage was used as a reference to trigger the disturbances. A benefit of this approach is that the voltage signal is crated inside of the grid controller and therefore does not have to be measured but can be taken from the internal digital source eliminating noise. This should insure that the disturbance occurs at the same voltage phase. The setup to measure these maxima and to apply the disturbances for a specified time can be seen in Figure 4.5.

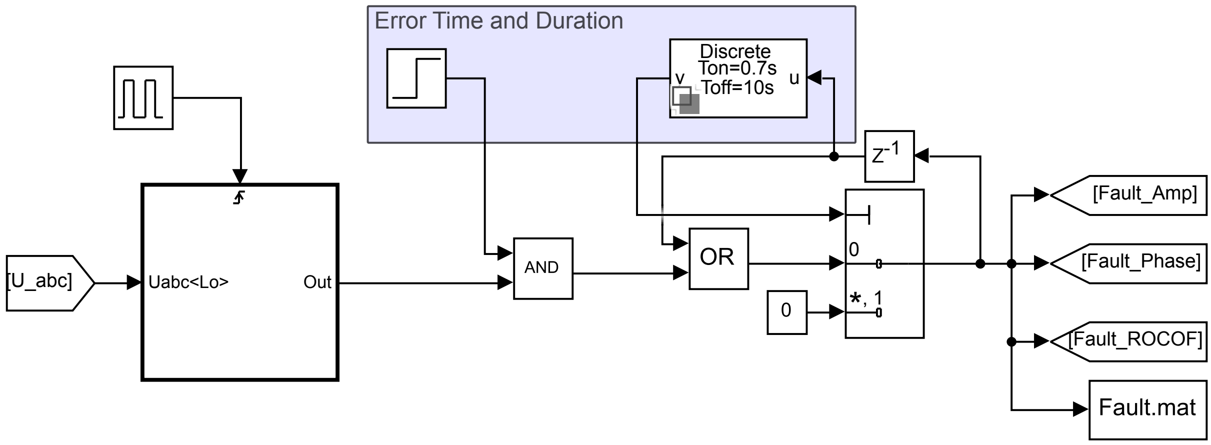

Figure 4.5: Subsystem, generation grid voltage control in Simulink®

4.1.3 Semiconductor Switch Model

In the simulation of the converter hardware, the first component to consider is the switching mechanism. The switches are controlled by a reference signal, which is crucial for regulating their operation. The process of generating this reference signal will be elaborated upon in section 4.2.

Averaged Model

The model in Figure 4.6 is a universal bridge with a average model based VSC selected. The input to this converter is the DC-Source. This is a very basic model of the switching mechanism and outputs a sinusoidal waveform instead of the PWM output of the real hardware. This reduces complexity which speeds up simulation times but reduces the accuracy of the model.

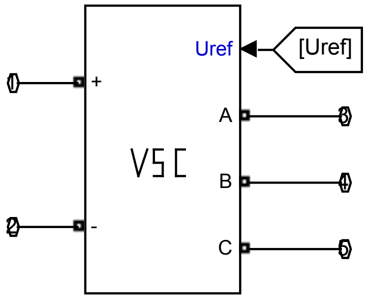

Figure 4.6: Averaged model of the semiconductor switches in Simulink®

Detailed Model

Figure 4.7 now shows a more detailed model of the half bridges. The rest of the hardware (DC-source as Input, filter and measuring points) stays the same. The model is from the imperix library and depicts their PEB 8024 half bridges. These are now controlled by three PWM signals, one for each phase.

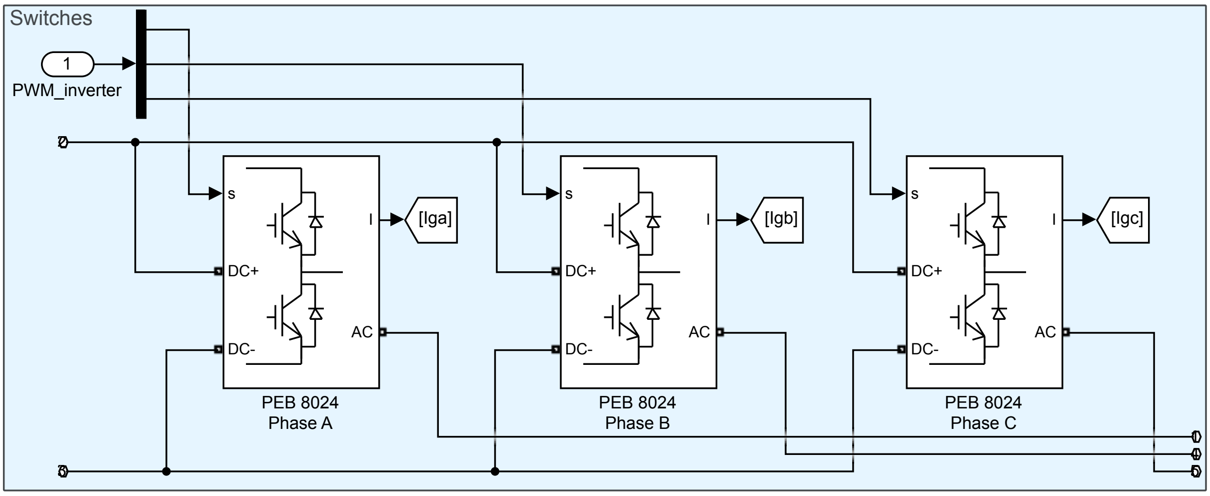

Figure 4.7: Detailed Imperix model of the semiconductor switches in Simulink®

4.1.4 Converter Filter Model

The filter is represented with three phase symmetrical impedances. The serial part consists of a resistor and a inductance and the parallel part of a resistor and a capacitance with a grounded neutral point shown in Figure 4.8.

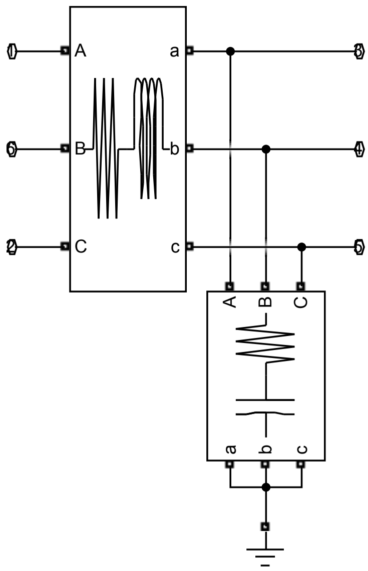

Figure 4.8: Model of Converter filter for the model in Simulink®

4.1.5 Additional Components

After the filter the next part in line is the breaker which connects and disconnects the converter to the grid. Lastly a set of measurements is taken here for both the voltage and the current. The measurement is after the switch so that even if the switch is open the conditions at the POC can be measured as depicted in Figure 4.9

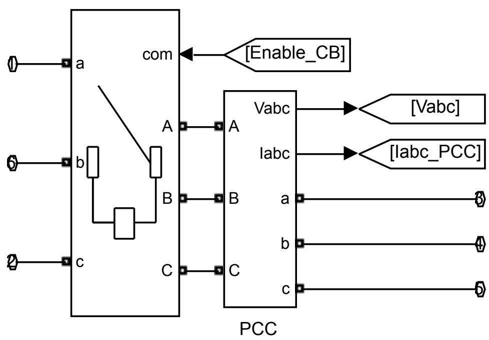

Figure 4.9: Models of additional components for the converter in Simulink®

4.2 Controller Models

A controller is the main component of a converter and responsible for controlling most of its behaviour. The controller therefore determines for example whether the converter operates in a GFL or GFM mode or in a different form altogether. It defines how the converter interacts with the grid, responds to disturbances and manages other operational states.

To achieve this, the controller processes measured data, uses predefined parameters and differentiates between different states. This altogether is used to generate an output signal. The output signal is the PWM signal that directly controls the switching of the semiconductors which are between the DC and AC side.

4.2.1 Simulating a discrete controller

An important aspect of simulating controllers is recognising that, the behaviour of physical systems is continuous, whereas most controllers are digital. Digital controllers operate with signals that are both discrete in time and value. This means they process data at discrete intervals and handle a limited set of amplitudes due to quantisation. In addition, there is a delay in digital controllers due to the time required to compute the output response and transmit it through a interface (digital or analogue). These delays have to be taken into account when simulating the controllers to ensure a reasonable approximation of system behaviour and performance.

The difference between a time-discrete and value-discrete signal is displayed in Figure 4.10. In a time-discrete signal, the values are sampled at specific time intervals, meaning that the signal is only defined at distinct time points . While the amplitude can still represent a continuous range of values. On the other hand, a value-discrete signal, has a continuous time dimension but the amplitude of the signal is restricted to a finite set of discrete values. In many practical systems and all systems used in this thesis, both the time and value of a signal are discretised. The resulting signal is fully digital. Which means time and amplitude are represented by discrete sets of points.

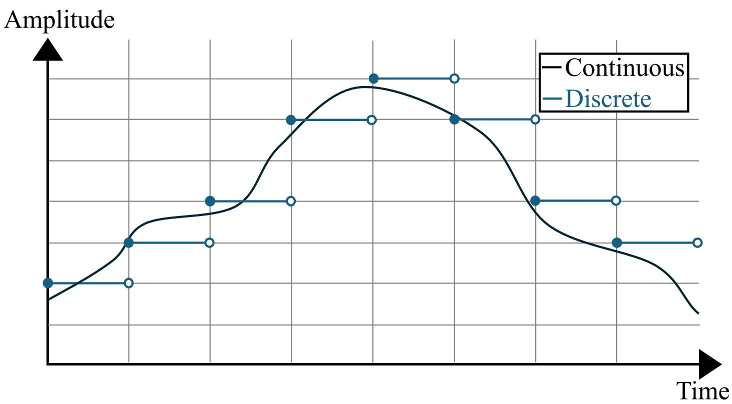

Figure 4.10: Continuous and discrete signals, Illustration

This discretisation process introduces both errors and delays in the signal. As depicted in Figure 4.10, the signal is sampled at discrete time intervals. Where each measurement is held until the next sample is taken. This then means that any changes in the signal between sampling points are not captured. Additionally, the amplitude is constrained to a fixed set of discrete levels, causing a quantisation error. This is where the actual value of the signal deviates from its closest discrete level. Furthermore, delays may be introduced by the time required for sampling and quantisation processes, as these operations take time to execute.

To now simulate these errors and behaviours accurately, the simulation frequency is 1 MHz, corresponding to a time step size of 1 μs. The controller is simulated at 20 kHz, which gives a time step size of 50 μs, the same as in the hardware implementation later. The implementation is shown in Figure 4.11 where the whole simulation runs discrete with a step size of 1 μs. The controller is a separately triggered block inside of this simulation, with latched inputs and triggered every 50 μs. These steps result in a time step ratio of 50 between the simulated hardware and controller. A ratio of 50 to 100 is generally considered sufficient to simulate hardware, which is inherently continuous. This ensures that the discrete nature of the controller is accurately represented.

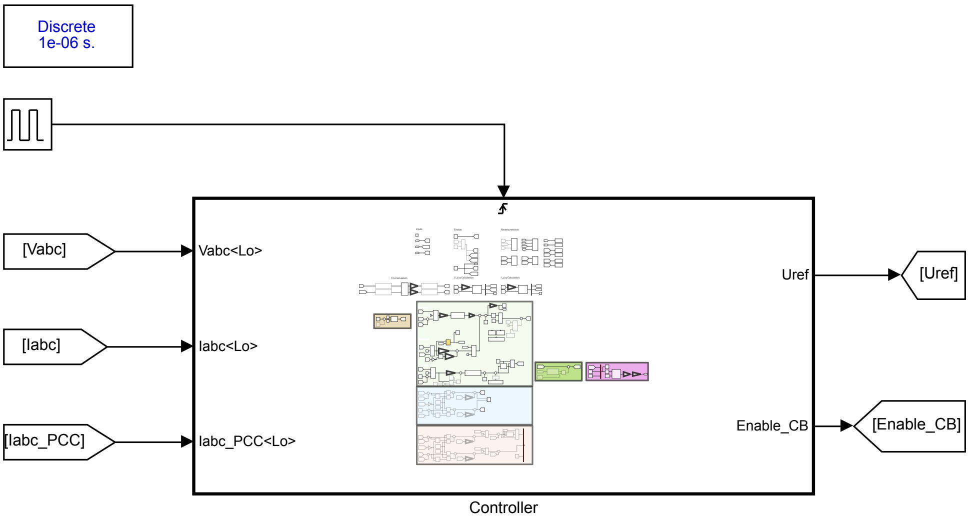

Figure 4.11: Model of a controller in Simulink®

4.2.2 Per Unit System

The per unit (p.u.) system is a method used to normalise values of voltage, current, power and impedance [32]. In the p.u. system, all quantities are expressed as parts of a defined base unit. This simplifies calculations and reduces the complexity of working with varying system ratings. This approach facilitates the analysis of systems of various sizes and power levels. By providing a common framework for all components and it helps to compare, test and simulate potential systems more effectively. The physical relationships between units remain consistent, meaning that if the base units for three-phase apparent power and phase-to-phase voltage as a root mean square (RMS) value are are given and the base values are defined as:

$$U_{\text{Base}} = \frac{U_{\text{r}} \cdot \sqrt{2}}{\sqrt{3}} \tag{4.1}$$

$$S_{\text{Base}} = S_{\text{r}} \tag{4.2}$$

The voltage base unit in Equation 4.1, is defined as the peak value, such that a sine wave with an amplitude of one corresponds to the RMS value of the rated voltage. With these definition the base unit for the current and the impedance can be calculated as:

$$I_{\text{Base}} = \frac{2}{3} \cdot \frac{S_{\text{Base}}}{U_{\text{Base}}} \tag{4.3}$$

$$Z_{\text{Base}} = \frac{U_{\text{Base}}}{I_{\text{Base}}} \tag{4.4}$$

If the base voltage is applied across the base impedance in a three-phase system, the base current will flow as a result, generating the base apparent power. This can tremendously help to asses the systems status quickly and effectively. For example, if the system's power is at 5 p.u., it indicates a disturbance or at least a significant overload. Another significant advantage of using the p.u. system is that when a controller is programmed within this framework, the only parameters that need adjustment when switching to a different voltage or power level are the base voltage and/or base power values. Without the per unit system, all the gains for PID controllers and other control parameters would need to be recalibrated for each new set of system values. This flexibility makes the per unit system ideal for designing controllers, independent of the power and voltage levels, which is why it is employed for all controllers in this thesis.

4.2.3 Grid-following

The basic principle of a GFL controller was discussed in section 3.3. In this section, the tuning of controller parameters, the startup and synchronisation process of a GFL converter and other essential steps necessary to achieve a fully operational controller will be explored. Figure 4.12 depicts the full implemented controller in Simulink®. Measurements which were taken for debugging and analysis are omitted in this figure to increase the clarity.

The process begins with the input of the three phase voltages and currents at the top of Figure 4.12. Initially these voltages and currents are normalised to the p.u. system as explained in subsection 4.2.2. Subsequently they are transformed to the dq0 system with the equations 3.1 and 3.2.

As outlined in subsection 3.1.4 the angle of the grid voltage is still needed to complete this transformation. To obtain this information a PLL as depicted in Figure 3.7(b) is employed. Gain factors for the PLL, $K_{\text{p,PLL}}$ and $K_{\text{i,PLL}}$ are calculated using Equation 3.4 and Equation 3.5 respectively with the parameters from Table 4.2, where T_{s} and U_{Base} are determined by system properties. While $f_{\text{cut,PLL}}$ is tuned inherently. The computed results are presented in Table 4.3.

Following the PLL the next step is a current loop which regulates the current injected into the grid. The gain factors for this current loop, which is again a PI-controller, are $K_{\text{p,CC}}$ and $K_{\text{i,CC}}$. They are calculated using the Equation 3.8 and Equation 3.9 provided in subsection 3.3.2. The values of the parameters are again listed in Table 4.2. L_{f} and R_{Lf} are the values from the filter components in p.u., while $f_{\text{cut,CC}}$ is again tuned manually for the desired system response. The computed gain values are shown in Table 4.3.

Table 4.2: Parameters for the calculation of the Control Parameters of the PLL and Current Control

Parameters					
$f_{\text{cut,PLL}}$	T_{s}	U_{Base}	$f_{\text{cut,CC}}$	L_{f}	R_{Lf}
10 Hz	$5 \cdot 10^{-5}$ s	1 p.u.	1 kHz	$2.3 \cdot 10^{-4}$ p.u.	$4 \cdot 10^{-3}$ p.u.

Table 4.3: Control Parameters of the PLL and Current Control

Control Parameters			
$K_{\mathrm{p,PLL}}$	$K_{\mathrm{i,PLL}}$	$K_{\mathrm{p,CC}}$	$K_{\mathrm{i,CC}}$
62.83	12.40.	1.60	27.78

A challenging aspect of the control system is managing the integrators, as they retain their stored values even when the input is set to zero. This leads to undesired behaviour, where deviations from the desired levels accumulate in the integrators, even before the controller is actively engaged. Consequently, the integrator values persist, rather than resetting, affecting system performance. To ensure proper controller operation and prevent such issues, a reset mechanism is crucial. This is implemented through an enable signal that activates or deactivates both the PLL and current control loops. On deactivation it additionally sets the inputs to the loops to zero. This enables the activation and resetting of the controls when necessary. For example during the startup and shutdown processes or if a control for a variety of reasons gets unstable.

The output of the current control now represents the voltage that the converter should deliver. To prevent damage during subsequent hardware testing, this output is first passed through a saturation block, limiting it to a maximum of 1.5 p.u.. Following this, the voltage is transformed back into the abc system using phase information from the PLL. Afterwards, the output is scaled from the per-unit system. This is done by first multiplying the voltage by the base voltage and then adjusting it to take the DC source voltage into account. The final result is the three-phase reference voltage signal which serves as the controller output.

A basic process to start the controller can be seen in Figure 4.12 on the bottom right. The sequence begins by switching on the PLL. Once the PLL successfully locks onto the grid voltage, the current loop gets activated. At this point the reference currents, given in dq coordinates, can be injected into the grid. The converter is now operating. In more advanced controllers, this sequence can be managed more effectively by using a state machine. This state machine then handles not only the transitions between these stages, but also error, fault-ride through and a host of other possible scenarios.

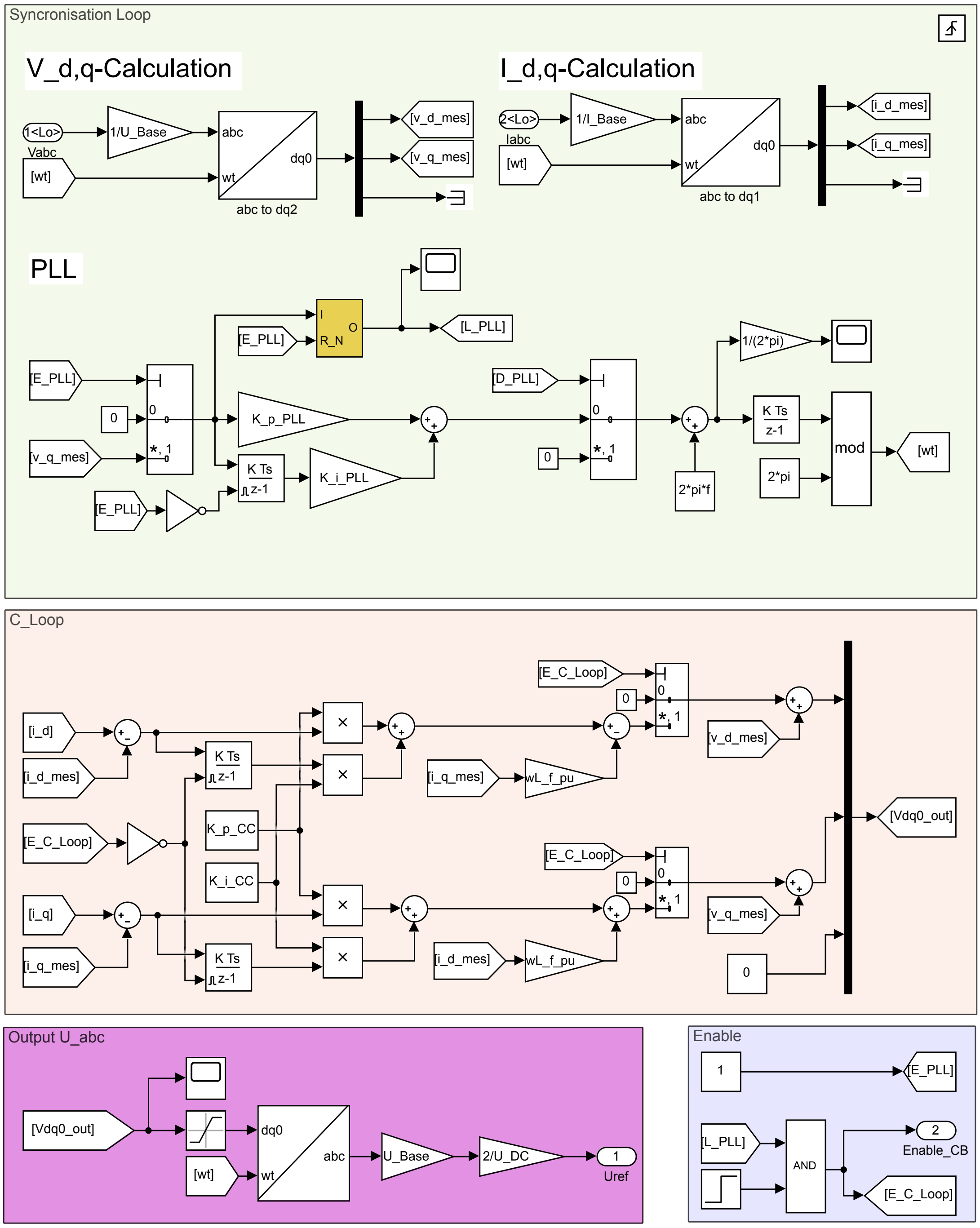

Figure 4.12: Implementation of grid feeding control in Simulink®

4.2.4 Droop

The droop control discussed in section 3.4 is the first GFM control implemented in the simulations. In comparison to the theory, to develop a fully functional controller, numerous practical considerations also have to be addressed. These include tuning the control parameters and synchronising the controller to the external grid on startup.

To synchronise the GFM control with the grid during startup, a PLL is used. This PLL is identical to the one used for the GFL control, detailed in subsection 4.2.3. Once the PLL achieves synchronisation between the controller and the grid, it is deactivated. The phase angle loop within the GFM control now takes over the task of maintaining the synchronisation between the controller and the grid.

The phase angle loop, as shown in Figure 3.9, is the synchronising component of the droop control. To function, this control requires the active power to be calculated accurately and instantaneous. In this setup, the power is computed using the Simulink® three-phase instantaneous power block. However, a key limitation of this instantaneous conversion is that the voltages and currents must be strictly sinusoidal for it to work flawlessly. In practice, this is not the case for converters, as the PWM output introduces harmonics. Despite the presence of harmonic content, the 50 Hz component remains dominant. The influence of higher harmonics is minimal enough to be considered negligible.

It's also important to note that, unlike voltages and currents, the power must be normalised after the calculation. Instead of using normalised voltages and currents directly. This is due to the fact that, the normalisation process for voltages and currents is based on their peak values. Therefore, first the power is calculated and after that, the normalisation is performed using the apparent power.

The phase angle loop functions by controlling the ratio between the change in the converter's active power and the change in frequency at the POC. This ratio is represented by the gain K_P in the control system. The amount of active power injected into the grid is dictated by the frequency of the controller and the grid frequency, as illustrated in Equation 3.10. During normal operation, this mechanism is used to inject the desired active power into the grid. Grid operators typically impose limits on this relationship; however, within these constraints, the parameter can be adjusted for optimal performance. This tuning was conducted empirically for this thesis, with the base value for K_P shown in Table 4.4.

In the phase magnitude control shown in Figure 3.9, the gain K_Q acts as a proportional part of the controller. As illustrated in Equation 3.11, the reactive power is regulated by adjusting the voltage amplitude based on the difference between the desired and actual reactive power. The gain K_Q was not derived through mathematical analysis but instead tuned empirically based on practical experience. The chosen base value is listed in Table 4.4. However, using only proportional control leads to a permanent steady-state error. To overcome this, a small offset can be added to Q^*, allowing the system to compensate.

Table 4.4: Control Parameters of the Droop control

Control Parameters	
K_P	K_Q
0.03	1.00

The GFM controllers used in this thesis do not utilise inner loops and are therefore direct control, as mentioned earlier in subsection 3.4.5. The startup and testing sequence for all GFM controls is described in section 4.3. The controllers use a dq0 reference system.

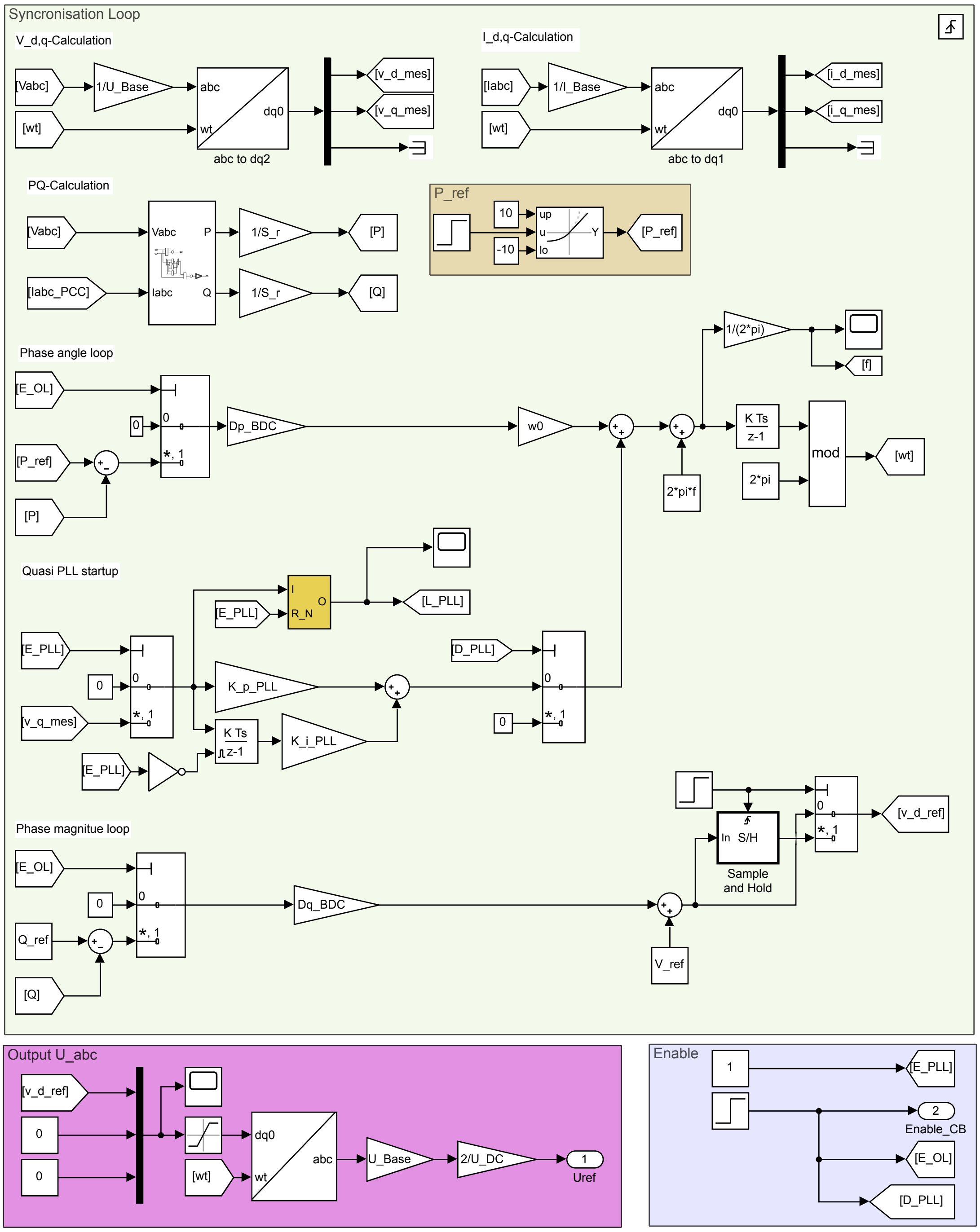

Figure 4.13: Implementation of basic droop control in Simulink®

4.2.5 Droop with LPF

Droop control with a LPF is the second GFM controller presented in this thesis. The only difference from the standard droop control is the addition of the LPF, as the name suggests. All other aspects of the control remain unchanged. This includes the parameters K_P and K_Q as displayed in Table 4.5.

Consequently, in Figure 4.14, only the modified sections are illustrated. As can be observed, the two low-pass filters are introduced after the P and PI controllers in the synchronisation and phase magnitude controls, respectively.

The cut off frequency of the low-pass filter in the phase angle loop f_p, plays a crucial role in balancing the converter's responsiveness to active power changes and stability. It is chosen based on the operating conditions. While lower frequencies favour stability and noise rejection, higher frequencies enable faster system responses. Therefore reducing the stress on the physical components, or even ensuring that they stay within their limits. Generally, the cut-off frequency is set between 1-10 Hz [33] to ensure a appropriate balance, between the two trade offs. The base value chosen for the cut off frequency of the phase angle loop f_p is noted in Table 4.5.

In the phase magnitude control, the cut-off frequency of the LPF balances the voltage stability and responsiveness to reactive power changes. A lower cut-off frequency ensures smooth and stable voltage control by filtering out fast transients, which is crucial in weak grids. Conversely, a higher cut-off frequency allows for quicker voltage regulation but may risk voltage instability due to fast reactive power variations. Again typically the cut-off frequency is selected between 1-10 Hz [33]. The base value chosen for the cut off frequency of the phase magnitude control f_q is noted in Table 4.5.

Table 4.5: Control Parameters of the Droop control with LPF

Control Parameters			
K_P	f_p	K_Q	f_q
0.03	5 Hz	1.00	1 Hz

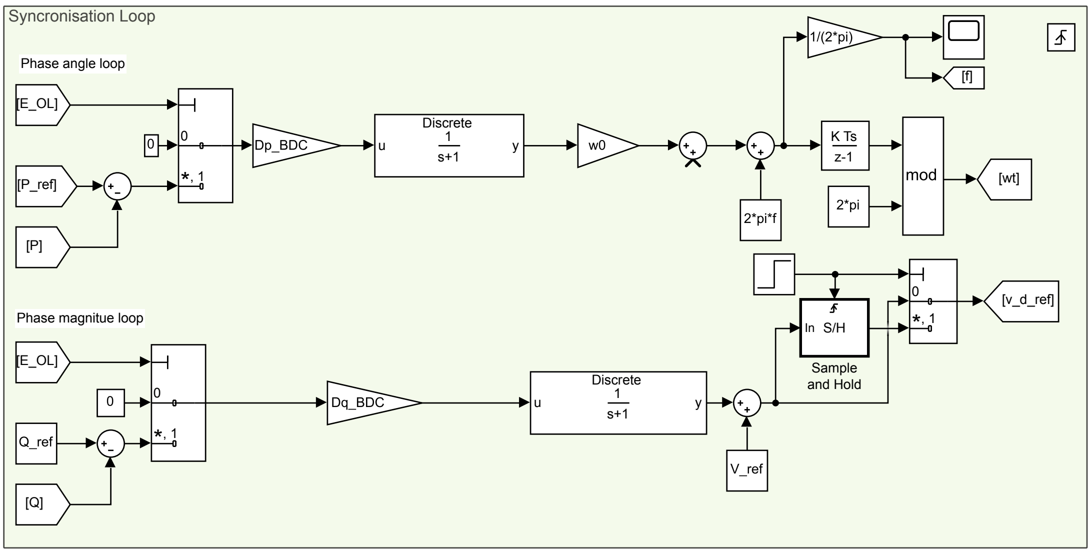

Figure 4.14: Implementation of basic droop control with LPF in Simulink®

4.2.6 VSM

The VSM control, as discussed in section 3.4, represents the final control strategy implemented in the simulations. Since the VSM is derived from the swing equation, its structure differs significantly from the other two GFM control methods presented in this thesis: droop control and droop control with a LPF. But as shown in subsection 3.4.4 it can be tuned to be equivalent to the droop control with a LPF.

Several aspects of the implementation remain consistent across all GFM control strategies as shown in Figure 4.15. These include the measurement and normalisation of voltages, currents and both active and reactive power. Additionally, the transformation of the output signal into abc components remains unchanged. Lastly, the startup process follows the same procedure as before.

For the VSM key distinction lies in the output of the PLL. As the VSM features an internal control loop that must synchronise with the grid frequency before connecting to the grid, in contrast to the droop controls. As a result, the PLL is now placed before the feedback gain and after the base frequency feedforward, as illustrated in Figure 4.15. This configuration enables the PLL to ramp up the VSM to match the external grid frequency.

In subsection subsection 3.4.4, the mathematical equivalence between the VSM and droop control is demonstrated. To validate this equivalence through simulation, the base parameters of the VSM model are tuned to match the droop control with a LPF. This is achieved by using Equation 3.21 and Equation 3.23. The results of these calculations are detailed in Table 4.6.

Table 4.6: Control Parameters of the VSM

Control Parameters			
D_{P}	H	D_{Q}	τ
0.1061	0.0017 s	1.0000	0.1592 s

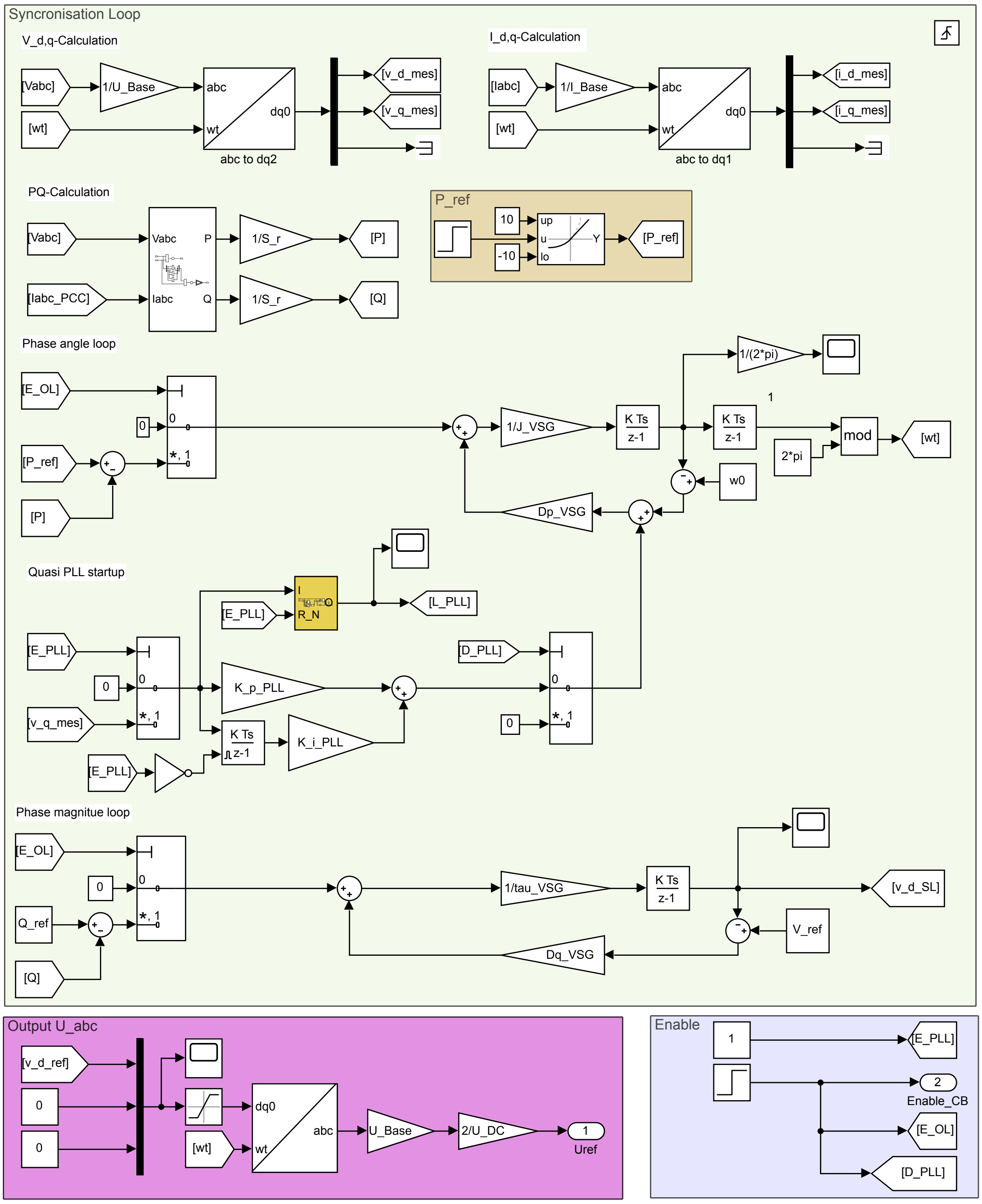

Figure 4.15: Implementation of virtual synchronous machine in Simulink®

4.3 GFM Synchronization and Test

GFL controlled converters rely on the grid's existing voltage and frequency to operate. Their phase-locked loop adjusts the q-axis component of the voltage, in the dq0 system to zero, to synchronize with the grid voltage. Once locked onto the grid, they are ready to inject power in accordance with the grid's voltage and frequency. In contrast GFM controlled converters operate similarly to synchronous machines by generating their own internal reference for frequency and voltage amplitude. Like a synchronous machine, these converters maintain a voltage and frequency, which must be synchronised with the external grid before connection. Once synchronised, the circuit breaker between the converter and the grid can be safely closed, allowing power exchange.

The process of starting, connecting and finally testing the GFM controllers, in this thesis, is illustrated step by step in the flow diagram, Figure 4.16. At the beginning of the simulation, grid voltage is applied at the POC, simultaneously the PLL of the GFM control is enabled. Once the PLL locks onto the external grid, the converter's voltage is held at the grid voltage level, with a feed forward structure. At this point, the voltages of both the grid and the converter are synchronised, allowing the switch to be closed.

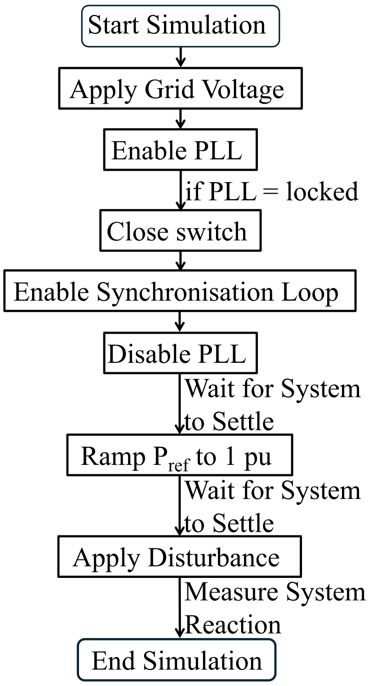

Figure 4.16: Flow chart of the simulation process

As soon as the switch is closed, the phase angle and phase magnitude controls are activated, while the PLL is disabled. The converter is now connected to the grid and operating in GFM mode. Initially, due to potential discrepancies in voltage measurements and a small voltage drop across the filters, oscillations may occur. During this oscillatory phase, the reference power is maintained at zero to avoid any unwanted power flow.

Once the oscillations subside and the system stabilises, the reference power is gradually ramped up from zero to the desired setpoint. This ramping process is done smoothly to prevent sudden jolts, which could cause control overshoot or damage the system due to its rapidness. When the system stabilises at the target active and reactive power levels, testing begins by introducing a disturbance.

The disturbance applied is one of the three types described in subsection 2.3.1, introduced at the grid voltage source. The converter's response to this disturbance at the POC is measured throughout the event. Once all resulting oscillations have fully decayed, the simulation is concluded. The data collected during the simulation is then saved for further analysis.

4.4 Simulation Results

This section presents a exploration of a few key simulation results. The results in this section focus on specific properties of the simulations. A complete run-through of a typical simulation, is explained step-by-step. For simulations a comparison between modelled semiconductor switches including PWM and a averaged model based VSC is made. Additionally, the simulations show the equivalence of the VSM and droop control with a LPF, in a simulated environment. In the final part, an analysis of the impact of grid resistance and inductance on converter performance is conducted. Where their influence on the overall system behaviour is analysed.

4.4.1 Full Simulation Run

A complete run of a simulation as described in section 4.3 is detailed in Figure 4.17, Figure 4.18 and Figure 4.19. The applied disturbance consists of a phase jump of $-5°$ at $t = 0$. At $t = 700$ ms, the phase returns to its original state, resulting in a phase jump of $+5°$. The simulation begins 1.25 seconds prior to the disturbance. This pre-disturbance period allows the converter to synchronise and in succession the power to ramp up to 1p.u.. After that the entire system is allowed to stabilise into a steady state before the test begins. The simulation concludes 1.25 seconds after the second phase jump, once the response has sufficiently decayed and the system is again in a steady state.

In Figure 4.17 the active power P and the reactive power Q at the POC with the internal frequency f are pictured throughout the simulation process. As the switch connecting the converter to the grid is open for the first 200 ms, P and Q are zero as no current can flow between the grid and the converter. In contrast, the internal frequency f of the converter is regulated by the PLL to ensure that the voltage angles of both the grid and the converter are synchronised. At $t = -1050$ ms the switch is closed. The small discrepancy between grid and converter voltage, due to the filter of the converter, results in a small disruption in the system. Subsequently at $t = -750$ ms the reference power is ramped up linearly from 0 to 1 p.u. within 100 ms. During this transition, the converter adjusts its internal frequency to inject the desired active power into the grid. As it is controlled by a proportional control it overshoots slightly. After a few hundred milliseconds, the system settles. The reactive power Q also fluctuates during this process. At $t = 0$ the disturbance occurs. From this point on the next 300 ms are the most important part of the reaction and the time-frame which will used for further analysis. While the recorded jump of $+5°$ is recorded for completeness, it will not be analysed in depth.

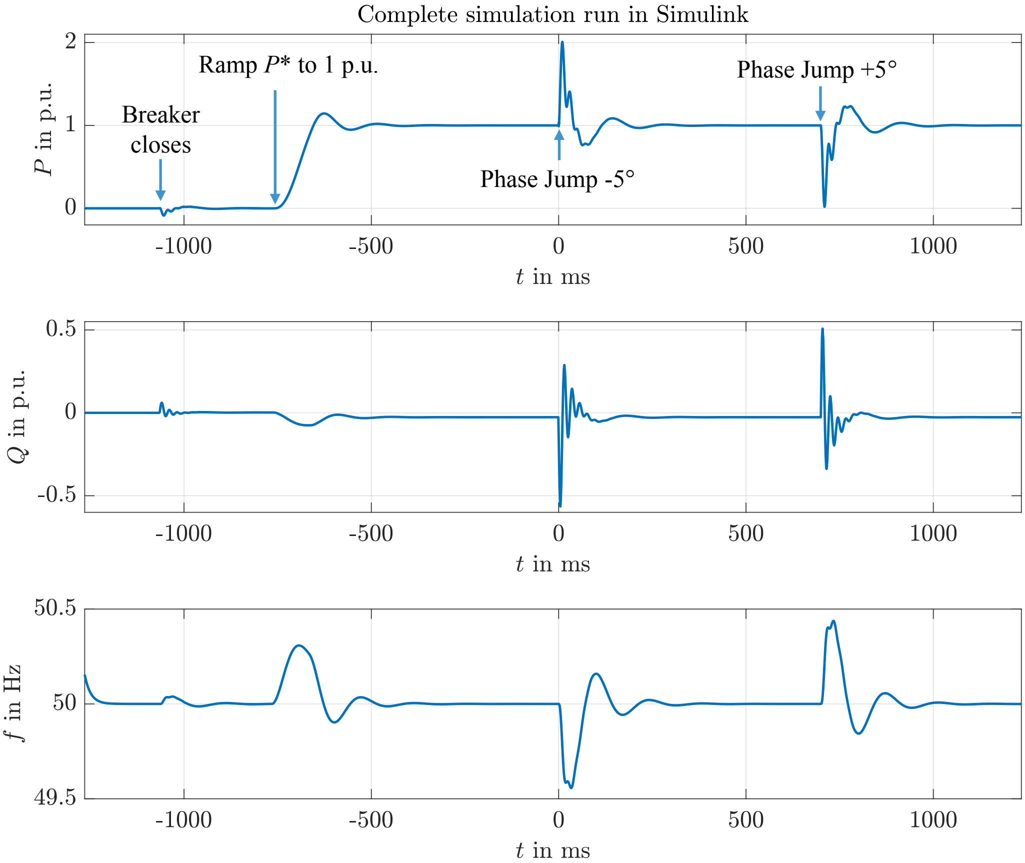

Figure 4.17: Complete simulation run trough in Simulink®, P, Q and f.

The voltages v_d and v_q, in Figure 4.18, are measured in the dq0 system at the POC within the converter. Initially, a small deviation from 1 p.u. for v_d and from zero for v_q can be seen as the PLL adjusts the frequency until v_q is zero, thereby aligning the grid voltage with that of the converter. When the active power is adjusted, minor fluctuations in the voltages occur due to the grid impedance, which introduces a voltage as current begins to flow. At the moment of the disturbance, the voltages exhibit a swing but quickly return to their previous levels as the converter compensates for the disturbance.

The currents i_d and i_q, shown in Figure 4.19, are measured in the dq0 system within the converter's reference frame. Unlike the voltages, these currents are not measured at the POC but rather after the inductive part of the filter and before the filter capacitor. This allows for the measurement of the exact current flowing through the semiconductor switches. At the start of the simulation, the charging of the filter capacitor is visible due to this measurement location. The current peaks are quite high during this process and cannot be overlooked. To mitigate this issue in the PHIL implementation, the feed forward voltage is raised slowly. In the simulations there is no risk to any hardware and therefore no mitigation has to take place. After the capacitor is loaded, a small steady-state current between the voltage source of the converter and the filter can be seen, before the switch is closed. As the switch closes, a minor disturbance is observed in the currents, similar to the behaviour seen in other measurements. When

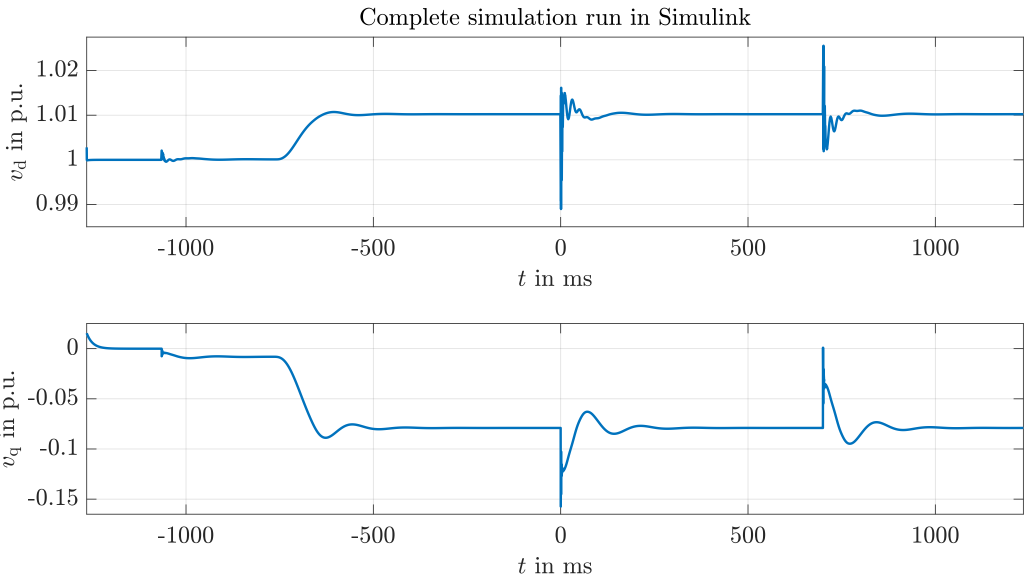

Figure 4.18: Complete simulation run trough in Simulink®, v_d and v_q.

the active power is increased, the current i_d increases, as the voltage remains almost constant. The current i_q only shifts slightly. At the moment of the disturbance, the currents exhibit a swing but, again quickly return to their previous levels as the converter compensates for the disturbance.

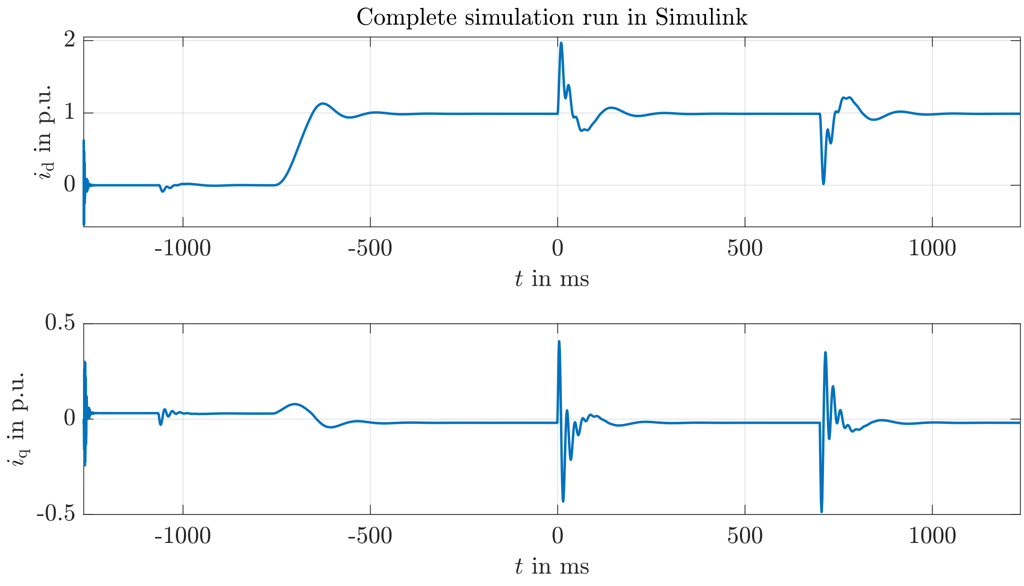

Figure 4.19: Complete simulation run trough in Simulink®, i_d and i_q.

4.4.2 Averaged vs. Detailed Switch Model

For the simulations, two distinct models of the semiconductor switches were introduced. The first is the voltage-averaged model provided by Simulink®, which is controlled via a reference voltage signal. The second is the Imperix model, representing the Metal-Oxide-Semiconductor Field-Effect Transistors (MOSFETs) used in the PEB8024 power module, controlled by a PWM signal that is generated from the reference voltage.

A comparison between the two models is detailed in Figure 4.20. The first model is referred to as the averaged model, while the second is called the detailed model. The detailed model is so called, as it depicts the hardware more accurately. Since the detailed signal lacks filtering and is very noisy, a third signal called filtered is added. This filtered signal is generated by applying the detailed signal to a third-order Butterworth low-pass filter with a cutoff frequency of 80 Hz. This is followed by a 4 ms forward shift along the time axis to correct for phase delay.

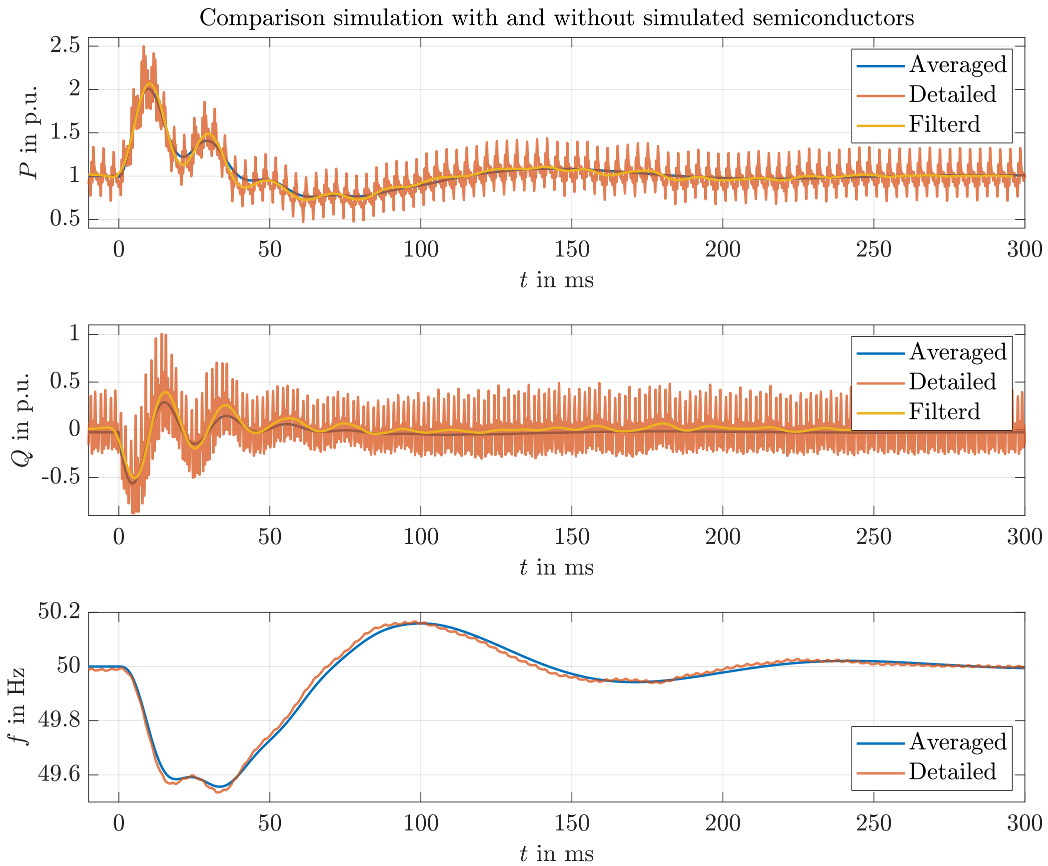

Figure 4.20: Comparison with and without simulated semiconductors

As illustrated in Figure 4.20, the detailed model provides greater granularity. For the disturbances considered in this thesis although the difference between the two models is very small. This becomes particularly evident when the averaged model is compared to the filtered signal. They are nearly indistinguishable, with the two curves almost perfectly superimposed. The detailed model however introduces substantial computational overhead, making it inefficient for longer or repeated simulations. In contrast, the voltage-averaged model delivers a nearly identical representation of the relevant system's dynamics without imposing a heavy computational load. Consequently, the voltage-averaged model is preferred for further simulations, as it strikes a better balance between precision and efficiency.

4.4.3 Equality of VSM and Droop with LPF

In mathematical analysis, from subsection 3.4.4, the VSM and droop control with a LPF are proven to exhibit identical behaviour under equivalent conditions. This equivalence is further corroborated here by simulation data. As shown in Figure 4.21, the system responses to a phase jump of $-5°$ are identical. The two curves in the plot overlap perfectly. This makes it impossible to tell them apart. To highlight this, the VSM curve was plotted dashed.

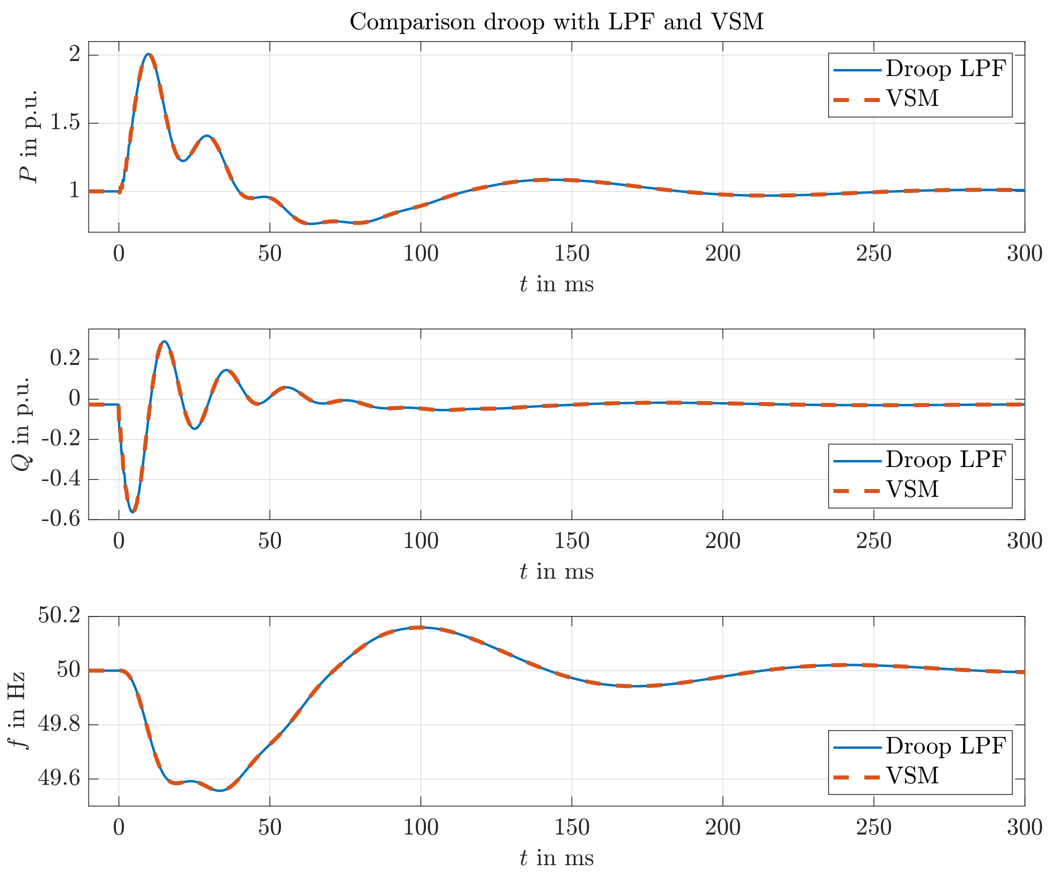

Figure 4.21: Comparison droop with LPF and VSM

These findings demonstrate that, despite differing design approaches, the VSM and droop control with LPF can be regarded as equivalent from a dynamic performance perspective. Consequently, the implementation of the VSM in PHIL tests is considered impractical due to the substantial effort required for integration and the negligible knowledge gain. Consequently the VSM is not implemented in chapter 5.

4.4.4 Influence of Grid Impedance

The grid impedance significantly influences the behaviour of GFM converters. As the grid and the converter act as voltage sources it governs the interaction between the two. To analyse these interactions effectively, the two components of grid impedance the grid resistance and the grid inductive were modulated individually, while keeping the other component constant. This approach allows a clearer understanding of how each aspect of the impedance affects the converter's dynamics and stability. The converter used for these experiments is the droop with LPF as described and parametrised in subsection 4.2.5. As the disturbance a phase jump of $-5°$ was applied at $t = 0$.

Figure 4.22 shows the converter's response to variations in the grid resistance, R_g. A clear inverse relationship between the grid resistance and system oscillations can be observed. As the resistance decreases, the damping effect follows, leading to increased oscillations when a disturbance occurs. This is to be expected as the resistance converts electrical energy to heat taking it out of the system and damping the oscillations. Conversely, as the resistance increases, the oscillations become slower and more prolonged. This behaviour is observed in both active and reactive power responses.

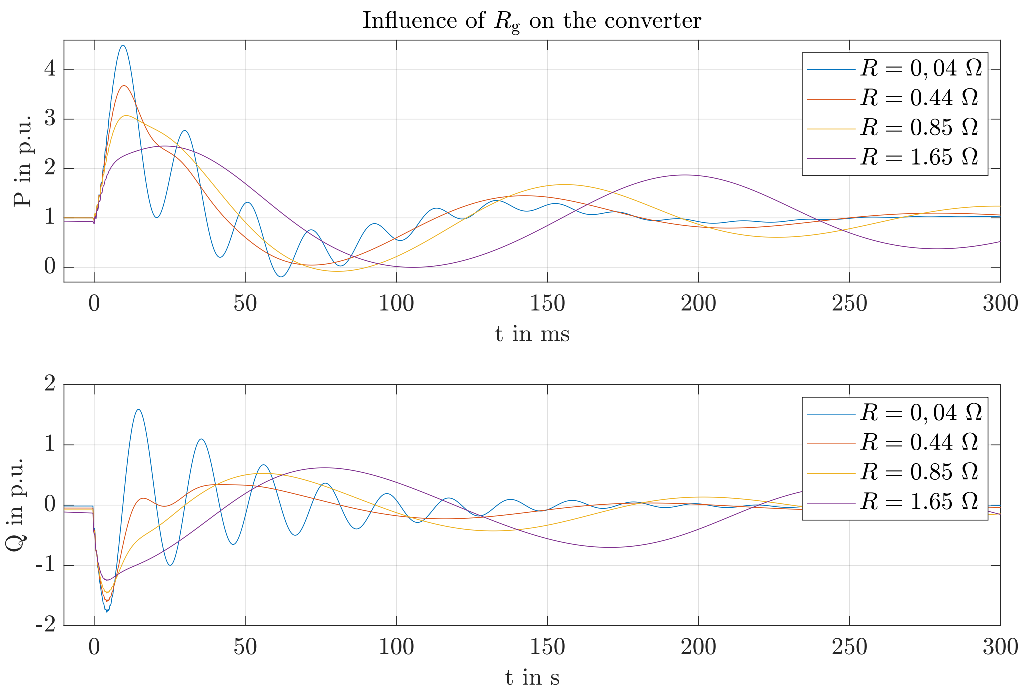

Figure 4.22: Influence of R_g on the converter behaviour

The peak magnitudes of the response also demonstrate an inverse relationship with grid resistance. Lower resistance values lead to higher peaks. This is as anticipated. Additionally, it is noteworthy, that the difference in peak magnitudes is more pronounced for active power compared to reactive power.

Figure 4.23 now illustrates the converter's response to variations in grid inductance, L_g. Unlike the grid resistance, changes in inductance do not significantly affect the oscillation frequency of the power between the grid and the converter, in response to a disturbance. Despite the variation in impedance, the oscillation frequency remains almost constant.

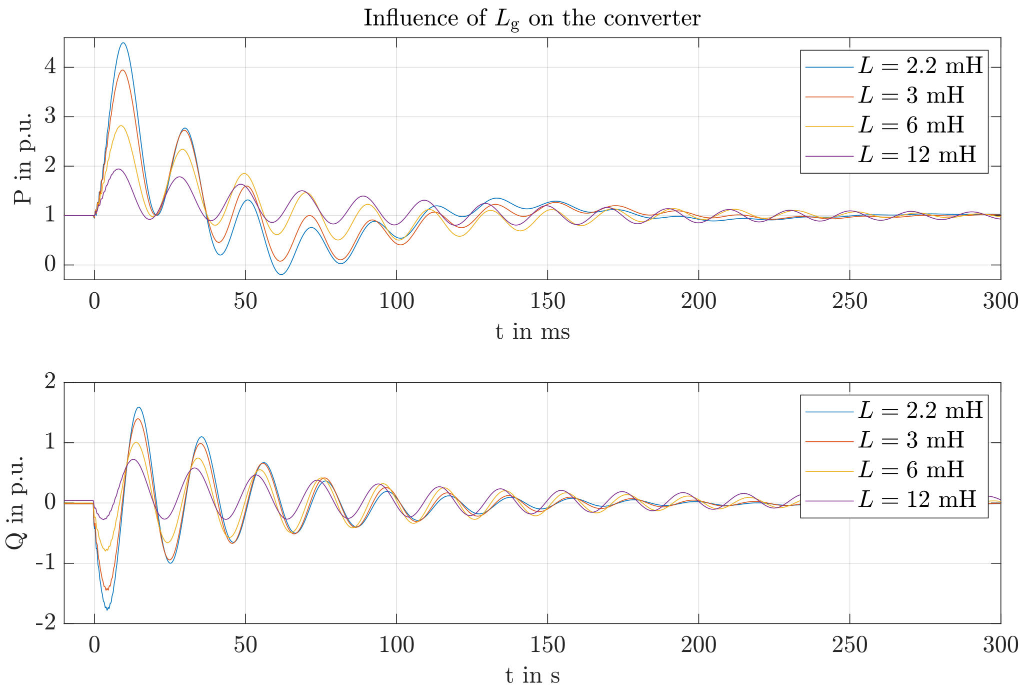

Figure 4.23: Influence of L_g on the converter behaviour

However, the amplitude of the oscillations is greatly influenced by the inductance. Similar to the resistance, changes in inductance also significantly impact both active and reactive power. As expected, a smaller inductance results in lower peak values for both powers.

These effect can analysed further with the equations for the power transfer between two points in mind [34]:

$$P \approx \frac{U_{\mathrm{Conv}} U_{\mathrm{g}}}{Z} \sin(\theta) \tag{4.5}$$

$$Q \approx \frac{U_{\mathrm{Conv}}^2}{Z} - \frac{U_{\mathrm{Conv}} U_{\mathrm{g}}}{Z} \cos(\theta) \tag{4.6}$$

With the impedance between the two voltages:

$$Z \approx |R_{\mathrm{Lf}} + \mathrm{j}\omega \cdot L_{\mathrm{f}} + R_{\mathrm{g}} + \mathrm{j}\omega \cdot L_{\mathrm{g}}| \tag{4.7}$$

The impact of the impedance Z can be clearly seen in Equation 4.5 and Equation 4.6 for both active and reactive power. This explains the perceived coupling of the reactive and the active power in Figure 4.22 as well as Figure 4.23 as the impedance clearly influences both equations.

5 Power-Hardware in the Loop (PHIL) Implementation

PHIL testing has emerged as a crucial method for evaluating various systems under realistic operating conditions. Especially for converters testing is possible without a physical connection to an operational grid. While simulations and other tools provide valuable insights, PHIL testing stands out by allowing real-time experimentation with various parameters. Additionally, PHIL testing enables the exploration of dynamic responses to grid disturbances, including voltage phase jumps, voltage amplitude jumps and RoCoF events. The PHIL testing method therefore is vital for understanding and optimising converter behaviour in complex grid scenarios, bridging the gap between theoretical models and practical implementation.

5.1 Power-Hardware in the Loop (PHIL) Setup

The PHIL setup used for experimental testing, featuring a freely programmable converter, is illustrated in Figure 5.1. In this configuration, three Imperix PEB8024 half-bridge modules are controlled by the Imperix B-Box RCP, which manages the power electronic switches via PWM signals. The filter structure, as discussed in subsection 3.1.3, is housed within one section of the Imperix passive filter box, with identical components mirrored in the remaining section. The primary energy supply is provided by an ITECH IT-M3900C 800-24 DC source.

To emulate the power grid, a combination of a real time system, a power amplifier and a hardware impedance is employed. The hardware impedance is provided by the second section of the Imperix passive filter box. The power amplifier, is controlled by the real-time system. It regulates the grid voltage and can simulate various grid disturbances to assess the converter's performance. Depending on experimental requirements, an additional grid impedance may be emulated, as described in section 5.2, to achieve the desired short-circuit impedance of the grid, without the need for additional Hardware.

The PHIL implementation mirrors the simulation setup, with the distinction that the specialised power blocks for the simulation are now actual hardware components. Additionally, the software used now must operate in real-time to interface with the hardware elements. The physical parameters of the PHIL setup dictate the simulation parameters, ensuring consistency across both scenarios. These parameters, listed in Table 4.1, therefore remain identical for both cases.

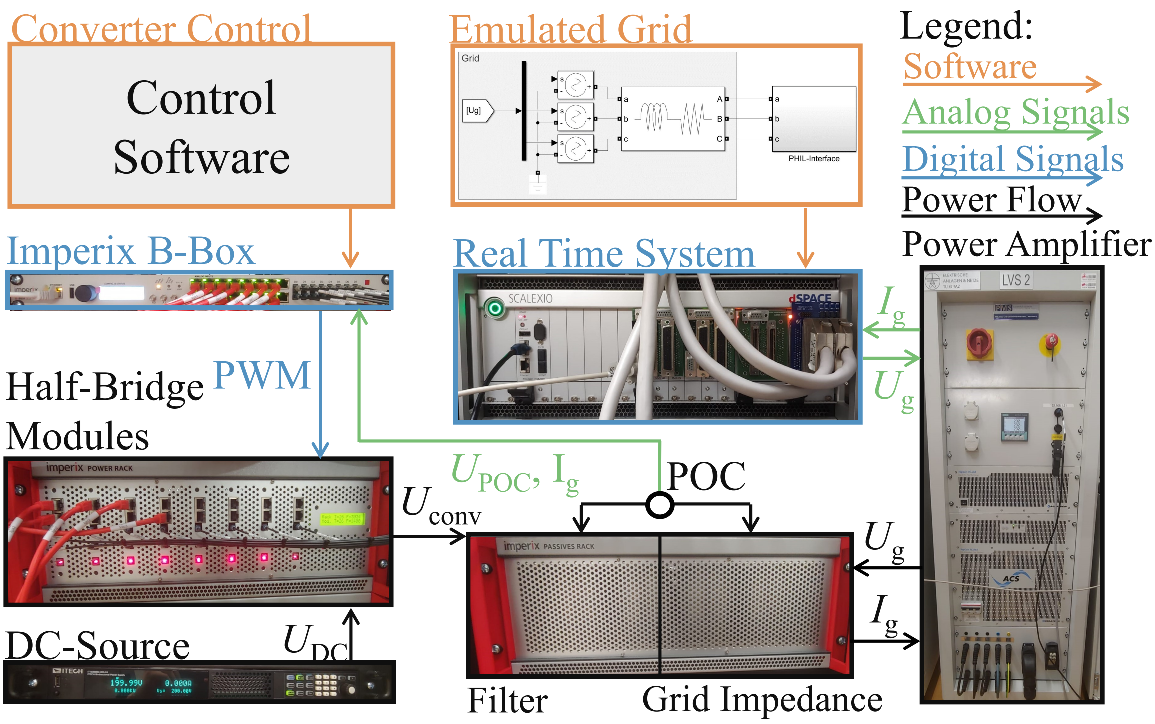

Figure 5.1: Overview of the PHIL lab set up

5.1.1 DC-Source

Figure 5.1 shows the ITECH IT-M3900C 800-24 in the bottom left corner. The IT-M3900C 800-24 is a regenerative, bidirectional programmable DC power supply, enabling both power sourcing and absorption. Its bidirectional capability allows for both sourcing and absorbing power, making it ideal for converter testing as power feedback into the DC-Source can be absorbed. The integrated safety features, including overvoltage, overcurrent and overtemperature protections, ensure safe and reliable operation throughout the testing process.

5.1.2 Imperix Converter

Imperix provides a complete hardware environment for the control prototyping of power electronic systems. This thesis uses it specifically for converters. In this setup, the B-Box RCP is employed to execute control software and manage the necessary I/O operations. The unit features a dual-core 1 GHz ARM processor coupled with a Kintex-grade FPGA. This enables closed-loop control frequencies of up to 250 kHz. The B-Box RCP supports as many as 134 user Inputs/Outputs per unit and incorporates PWM capabilities with a switching frequency range of 3.72 to 1 MHz.

The PWM signals generated by the B-Box RCP drive the Imperix PEB8024 half-bridge modules, which are equipped with two SiC MOSFETs. These modules support switching frequencies of up to 200 kHz and include onboard sensors. These provide isolated measurements of DC voltage and AC output current. Additionally, the PEB8024 modules come with built-in protections against over-current, over-voltage and over-temperature conditions.

The final component of the Imperix hardware is the Passive Filters Box. Which contains two sets of three 2.2 mH/32 A power inductors, as well as two three-phase EMC filters with star-connected capacitors. Together, the B-Box, half-bridge modules and passive filter, represent the complete hardware configuration of the converter, as discussed in chapter 3 and section 4.1. The parameters of the Hardware are listed in Table 4.1. The hardware operates well below its rated values to ensure a sufficient safety margin during testing.

The converter software models for the GFM and GFL controls, as described in section 4.2, remain functionally consistent. However, to operate with the Imperix B-Box RCP, adjustments are necessary. Specifically in the mapping of the controller's inputs and outputs. To match the physical ports on the B-Box RCP. Additionally, the PWM signals are now generated using the internal PWM generators of the B-Box RCP. The mapping process is illustrated in Figure 5.2.

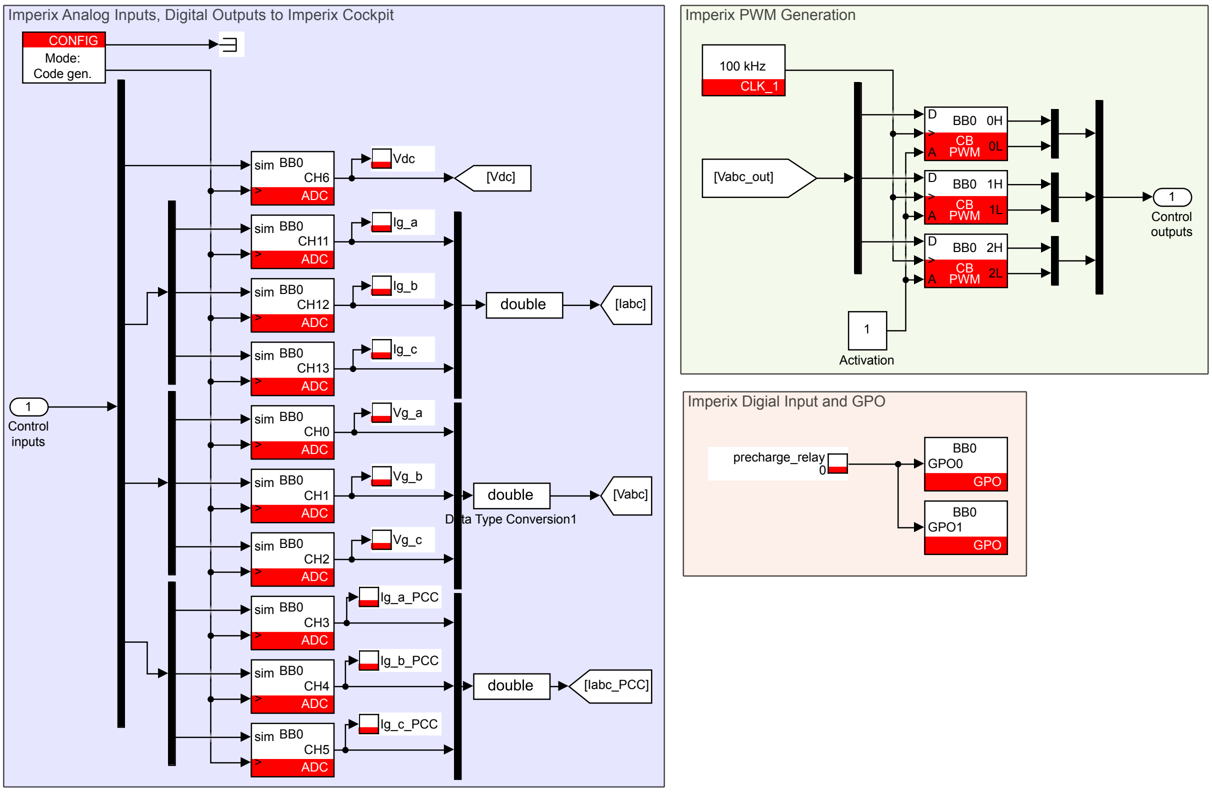

Figure 5.2: Input/Output mapping for the B-Box RCP

The Configuration Block in the top-left corner of Figure 5.2 contains essential data, including the initialisation parameters file and control frequency settings. Lined up below, the analog inputs of current and voltage measurements are mapped to the physical input channels of the B-Box RCP. For each input, offsets and gain adjustments can be made. These inputs are then output digitally to the Imperix Cockpit, which runs on a separate computer and is connected via a network. This allows for real-time data recording during testing. The collected data is used for the analysis of the PHIL experiments. After capturing, the data is multiplexed for more efficient handling and typecast to double precision for compatibility with the controllers designed in section 4.2.

On the top right of Figure 5.2, the PWM generation process is shown. The output voltage, represented in the abc reference frame, is fed into the PWM generator. Along with it, the clock signal for PWM timing. An activation signal provides control over enabling or disabling the output of the PWM generators. The PWM blocks facilitate mapping to the appropriate channels. As well as offering adjustments for carrier waveform shape, duty cycle and phase.

In the bottom right of Figure 5.2, a general-purpose input from the Imperix Cockpit is connected to two general-purpose outputs. This enables the user to manually control the connection between the converter and the external grid. This setup provides a simple mechanism for managing the grid connection during testing.

5.1.3 Grid Real-Time System

The dSPACE SCALEXIO LabBox, along with its corresponding configuration and Control Desk, is used to simulate and control the grid voltage source as depicted in Figures Figure 4.3 and Figure 4.4. The Simulink®model is adapted for compatibility with the real-time system, then compiled to run on this platform. Afterwards, the model's mapping is completed using the dSPACE Configuration Desk, ensuring proper interaction between the software and hardware the template for this can be seen in Figure 5.3.

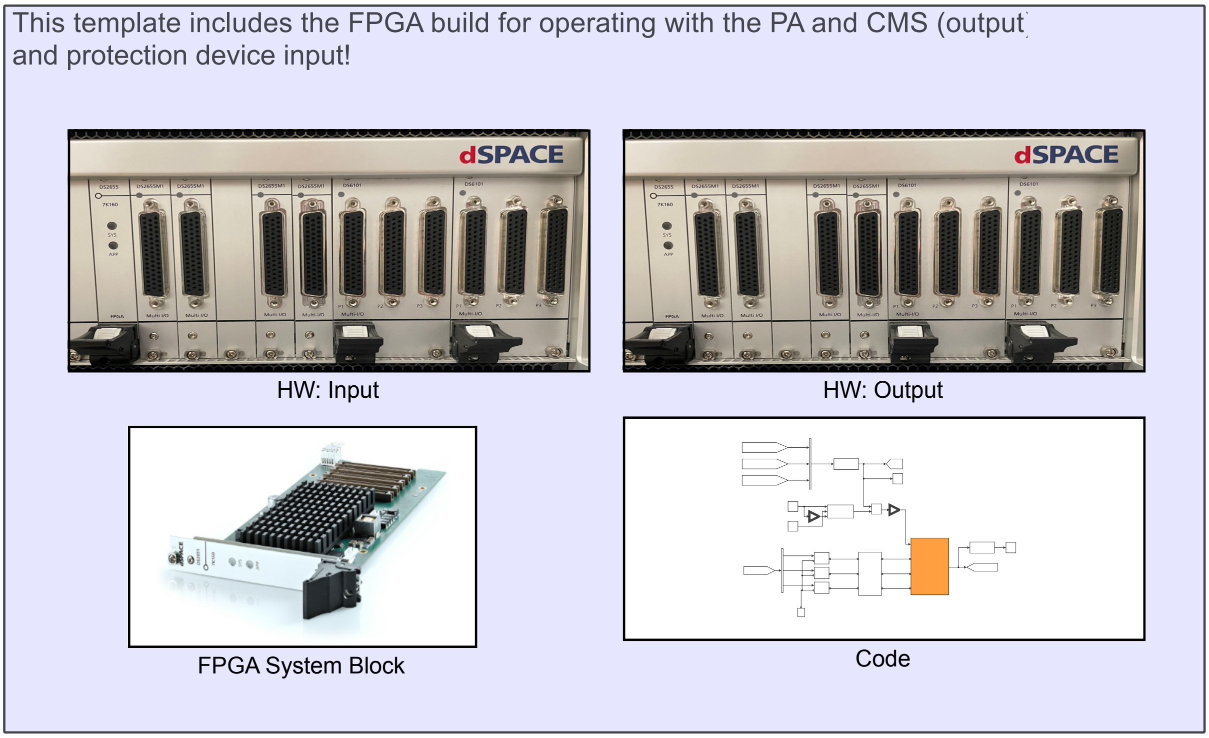

Figure 5.3: Input/Output mapping and Software for the dSpace SCALEXIO LabBox

The control system, embedded in the code portion, enables the user to trigger three different disturbance scenarios on demand. These disturbances are synchronised to occur precisely at the voltage peak, ensuring comparable initial conditions across tests. Additionally, a signal is transmitted to the

Imperix B-Box RCP at the moment of the disturbance, facilitating disturbance localisation and data synchronisation for seamless comparison during analysis.

The dSPACE SCALEXIO LabBox provides analog outputs that are used to deliver the voltage signals. However, these outputs are limited to a maximum of ten volts and only a few hundred milliamps of current. To achieve the necessary power levels, an ACS Top Con-LAE power amplifier is employed as a linear amplifier, boosting the dSPACE real-time system's output to the required levels. Proper configuration of the gain and offset in both the power amplifier and the real-time system is crucial to attaining the desired output. The analoge inputs which are fed back from the converter enable a feedback loop. This can be used for example to emulate a impedance as shown in section 5.2.

Finally, the system's hardware grid impedance is supplied by the inductive component of the Imperix Passive Filters Box. For this application, only the inductive elements of the filter box are utilised, ensuring accurate representation of grid impedance in the test setup.

5.1.4 Commercially Available Converters

To test a commercially available GFL converter, adjustments were made to the setup, as shown in Figure 5.4. Several components remain unchanged, including the grid emulator, which continues to function as before. The only modifications here involve adjusting power and voltage parameters to suit the tested converter. The DC source that feeds the converter also remains functionally the same, with only a power setting adjustment required.The In- and output parameters of the commercially available converter are noted in Table 5.1.

Table 5.1: Rated values of the commercially available converter

Rated Values				
U_{g}	S_{r}	f_{r}	U_{DC}	P_{DC}
400 V	0-10 kVA	50/60 Hz	80-1000 V	0-10,3 kW

The Imperix B-Box RCP is still connected to the system, but its role is now limited to that of a measurement unit rather than controlling the converter. The PLL locks onto the voltage at the POC, ensuring that the measurement process is consistent with the one used for the self-developed converter.

Following the grid impedance, the commercial converter is connected. The second half of the Passive Filters Box is not utilised in this setup, as the commercial converter already contains all the necessary filtering components within its design. With the setup complete, the system is ready for testing. The startup sequence and any required configurations are now managed entirely by the converter itself. Once the converter reaches the desired power level, the test can proceed, disturbance conditions and disturbances are able to be triggered as needed.

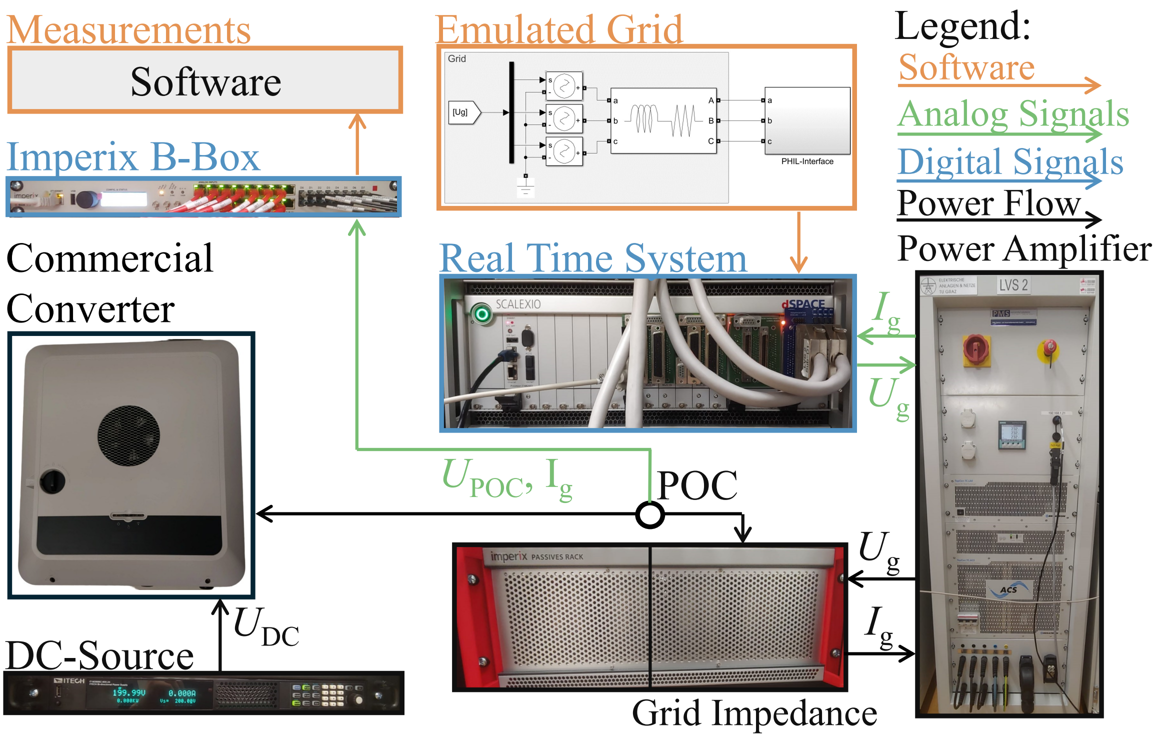

Figure 5.4: Overview of the PHIL lab set up with a Commercial Converter

This converter must comply with current grid codes that were developed primarily for grid-following controls. These codes specify the required responses to various grid disturbances and faults, including fault-ride through behaviours. However, the requirements for fault-ride through can vary significantly from one region to another. In this thesis, the voltage phase and amplitude disturbances applied, do not trigger the fault-ride through behaviours, as they are not substantial enough. In contrast, the RoCoF tests did activate the fault-ride through behaviour. The manufacturer's settings designed to meet Austrian grid codes were selected for these cases. Additionally only half of the total available power was utilized, with a soft limit applied to ensure additional headroom for the converter during testing. Leading to the parameters in Table 5.2 for testing.

Table 5.2: Used values of the commercially available converter

Used Values				
U_g	S_r	f_r	U_{DC}	P_{DC}
400 V	5 kVA	50 Hz	800 V	5,5 kW

5.2 Emulation of Grid Impedance

The power grid is modelled using a three-phase voltage source along with a corresponding grid impedance. When testing converters under varying grid conditions, it becomes necessary to adjust this grid impedance. One approach is to use physical hardware components to represent the impedances. Hardware impedances, particularly in this power range, tend to be large, heavy and costly. Moreover, they are difficult to swap out and cannot be adjusted continuously. To overcome these limitations, a more versatile and adaptable solution is to emulate the impedance using a real-time system. This approach enables seamless and fast adjustments of grid conditions. Thereby providing greater flexibility and control during testing, allowing for easier adaption between different scenarios.

5.2.1 Modelling

To emulate impedance after the voltage source, the real-time system utilises the measured current as feedback to simulate the voltage drop across the emulated impedance. As illustrated in Figure 5.5, several additional factors must be considered to ensure the model functions effectively. Since the system forms a feedback loop, it has the potential to become unstable. To mitigate this risk, a low-pass filter is applied at the input of the current sensors, preventing the formation of a high-frequency positive feedback loop that could destabilise the system.

Moreover, to gradually introduce the effect of the virtual impedance, an adjustable gain, with a limiter, is incorporated into the current measurement. This feature allows the user to smoothly ramp up or down the influence of the virtual impedance on the system. This gradual adjustment is crucial, as a sudden change in impedance has the same impact as a fault condition on the system. Causing significant shifts in phase and voltage angle. By carefully managing the transition, the system can avoid abrupt disruptions.

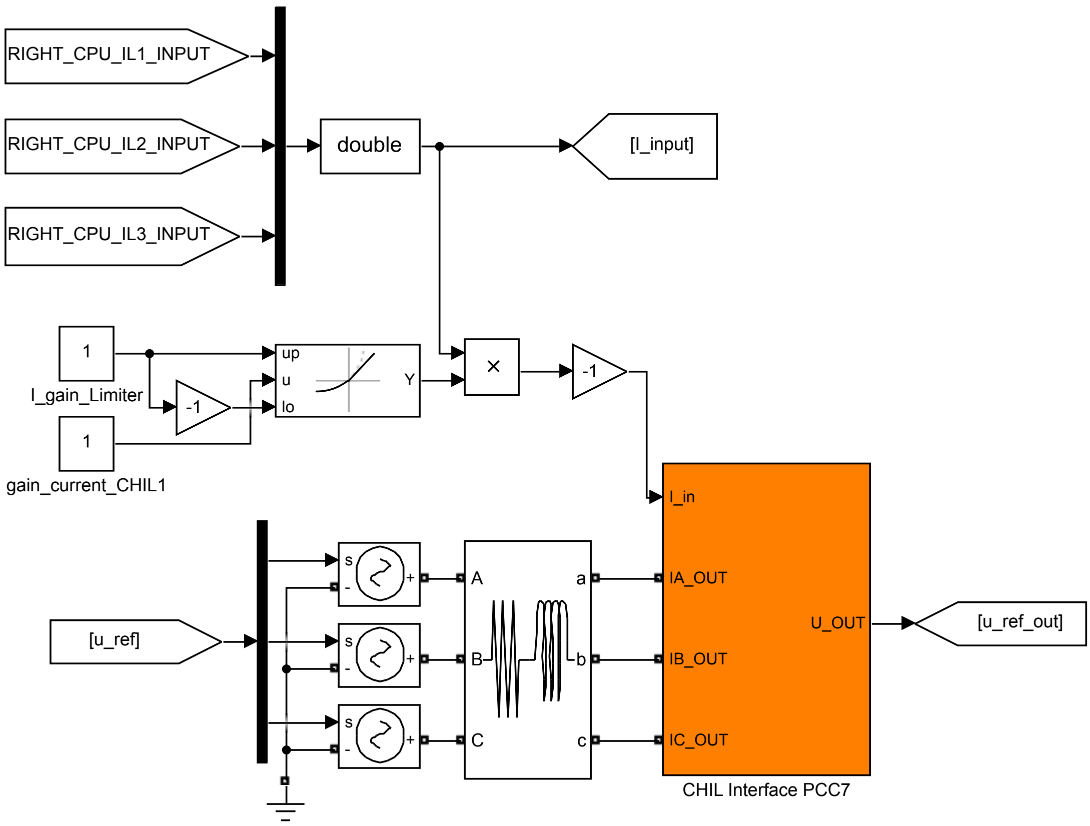

Figure 5.5: Overview of the impedance emulation

In the bottom part of Figure 5.5 the voltage sources and the impedance are simulated with components from the specialised power systems library of Simulink®. To interface those with the outputs of the real time converter the custom CHIL Interface block is used. This block enables the feedback of the currents via the I_{in} path. Then the resulting voltage in this simulation is measured and used to generate the output voltage which is then feed back to the power amplifier. This constitutes the loop.

In the lower section of Figure 5.5, the voltage sources and impedance are modelled using components from Simulink®'s Specialized Power Systems library. To interface these elements with the outputs of the real-time converter, a custom Controller Hardware-in-the-Loop Interface block is employed. This block facilitates the feedback of currents through the I_{in} path. The simulated voltage generated as a result is measured and utilized to generate the output voltage, which is subsequently fed back into the power amplifier. This creates a closed feedback loop, ensuring that the simulated behaviour accurately replicates the real-time response of the corresponding impedance in the physical system.

5.3 PHIL Results

This section provides an exploration of several key PHIL results. Each scenario presented in this chapter has been tested across all disturbance cases. However, for clarity and conciseness, only the most representative results are selected and discussed in this thesis. There are four distinct control strategies analysed:

- A Grid-following commercial of the shelf converter (GFL_{COTS})
- Grid-feeding control with current control (GFL_{CC})
- Grid-forming droop control ($\text{GFM}_{\text{Droop}}$)
- Grid-forming droop control with a low-pass filter (GFM_{LPF})

All PHIL tests shown in this thesis with chosen control structures and disturbances are shown in Table 5.3.

Table 5.3: Overview PHIL tests

PHIL tests			
section	description	controls	disturbances
5.3.1	simulation, hardware and PHIL	GFM_{LPF}	Phase: $-5°$
5.3.2	different controls, same conditions	GFL_{COTS}, GFL_{CC}, $\text{GFM}_{\text{Droop}}$, GFM_{LPF}	Phase: $-5°$ Amplitude: 0.9 p.u.
5.3.3	same controls, different SCRs	GFL_{COTS}, $\text{GFM}_{\text{Droop}}$	Phase: $-5°$ Amplitude: 0.9 p.u. RoCoF: 2 Hz/s
5.3.4	same controls, different disturbances	GFL_{COTS}	Phase: $-5, -10, -15°$ RoCoF: 1, 2 Hz/s
5.3.5	same controls, different parameters	GFM_{LPF}	RoCoF: 2 Hz/s

5.3.1 Comparison of Simulation, Hardware and PHIL

To validate the proposed approach of section 5.2 using an emulated grid impedance, an experimental comparison was performed between setups. Both emulated and real hardware impedances where utilised in the experiments. A phase jump of -5° was applied to the grid voltage source at time zero, serving as the test disturbance. The converter model employed was that of the droop control with a LPF (GFM_{Droop}) described in section 4.2. The procedure was executed under identical converter control configurations for both grid setups.

Figure 5.6 presents the active and reactive power at the POC. The red curves represent the outcomes when using a real hardware impedance, while the orange curves correspond to those with the emulated impedance. The Figure 5.6 indicates that the emulation of the grid impedance mimics the behaviour of the real hardware. However, a noticeable deviation between the two cases occurs at the peak during the initial moments of the disturbance. This discrepancy stems from a slight delay in the current measurements and their feedback into the real-time system. As a result, during fast transients, the real-time system requires more time to compute its response. While on the other hand the hardware reacts inherently and instantaneously. While this deviation is relatively minor, it can be further minimised by combining a portion of the hardware impedance with the real-time system emulation of the remaining grid impedance, to get to a desired SCR-Ratio. This hybrid approach, blending hardware and emulation, is employed in all subsequent testing when adjusting the SCR of the grid.

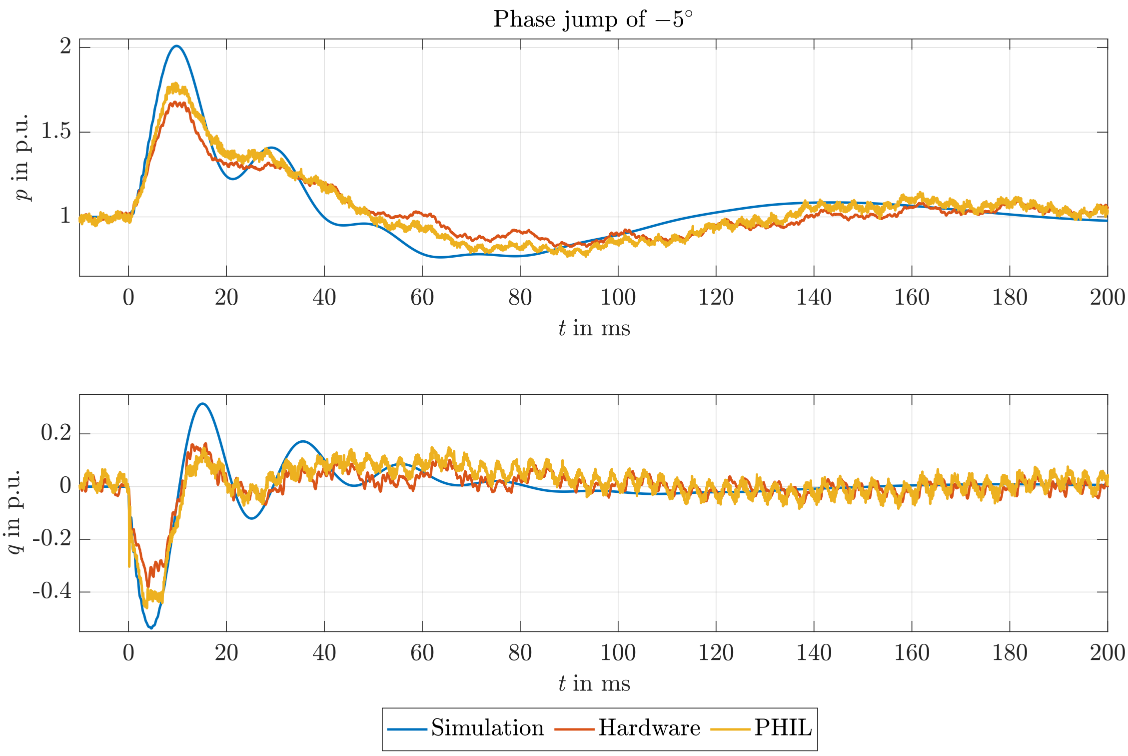

Figure 5.6: Phase jump of grid voltage of -5°

In addition to the PHIL experiments, simulations were carried out using the models presented in chapter 4. The simulations where conducted under the same converter configuration and with the nominal values of the devices. As shown in Figure 5.6, the simulations exhibit a significant deviation from the actual system behaviour observed in the experiments. To investigate this further, the resistive and inductive behaviour of the Imperix filters used in the experiments was measured. The results are illustrated in Figure 5.7. The measurements reveal a pronounced frequency dependency, particularly in the resistance. This variation in resistance depending on frequency is expected to significantly affect the transient behaviour of the system. Especially for transients. However, this frequency-dependent behaviour is not captured in the simulation models, which rely solely on nominal values for the device parameters.

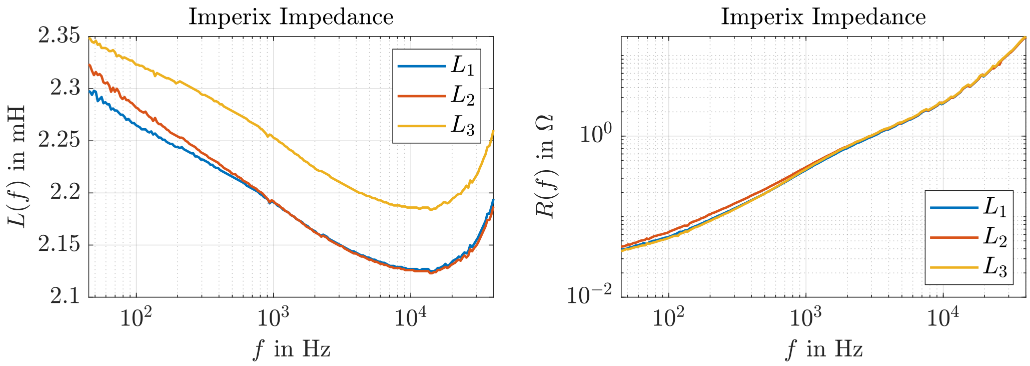

Figure 5.7: Measurement of R and L of the used Grid Impedance

In conclusion, while the grid impedance emulation proves to be sufficiently accurate for practical testing, the minor deviations underscore the need for careful consideration of measurement delays and the role of real hardware in ensuring more reliable and realistic system behaviour, particularly in the presence of dynamic disturbances. The findings also underscore the limitations of relying purely on simulations for dynamic analysis. They highlight the importance of performing real hardware experiments, to accurately capture the system behaviour especially in dynamic situations.

5.3.2 Comparison of different Controls

Figure 5.8 and Figure 5.9 compare the different control structures in response to two different disturbances. For the converters designed in this thesis the parameters from section 4.2 where used. The commercial of the shelf converter uses the parameters detailed in Table 5.2.

In Figure 5.8, the effects of a $-5°$ phase jump are shown. In the event of a sudden shift in grid voltage phase, grid-forming requirements mandate the injection of active power within 5 milliseconds to stabilise the frequency, as outlined in [7]. Both GFL controls do not increase their active power output in response to the disturbance. The GFL_{COTS} converter, as described in subsection 5.1.4, and the GFL_{CC} control developed for this thesis, exhibit virtually identical behaviour. With the primary distinction being the higher noise floor of the GFL_{COTS}, likely due to its lower switching frequency. Both GFL converters fail to meet grid-forming requirements, which is expected. For the GFL_{COTS}, this performance aligns with the current grid codes it is required to fulfil. In contrast, both GFM controls ($\text{GFM}_{\text{Droop}}$ and GFM_{LPF}) inherently increase their active power output. During the return to the reference power, it is noteworthy that the $\mathrm{GFM_{Droop}}$ control stabilises without overshooting. While the $\mathrm{GFM_{LPF}}$ control exhibits a tendency to overshoot. Reactive power behaviour shows that both GFM controls exhibit slight jumps but quickly stabilise back to zero, with the $\mathrm{GFL_{CC}}$ showing a smaller amplitude jump followed by a rapid return to stability.

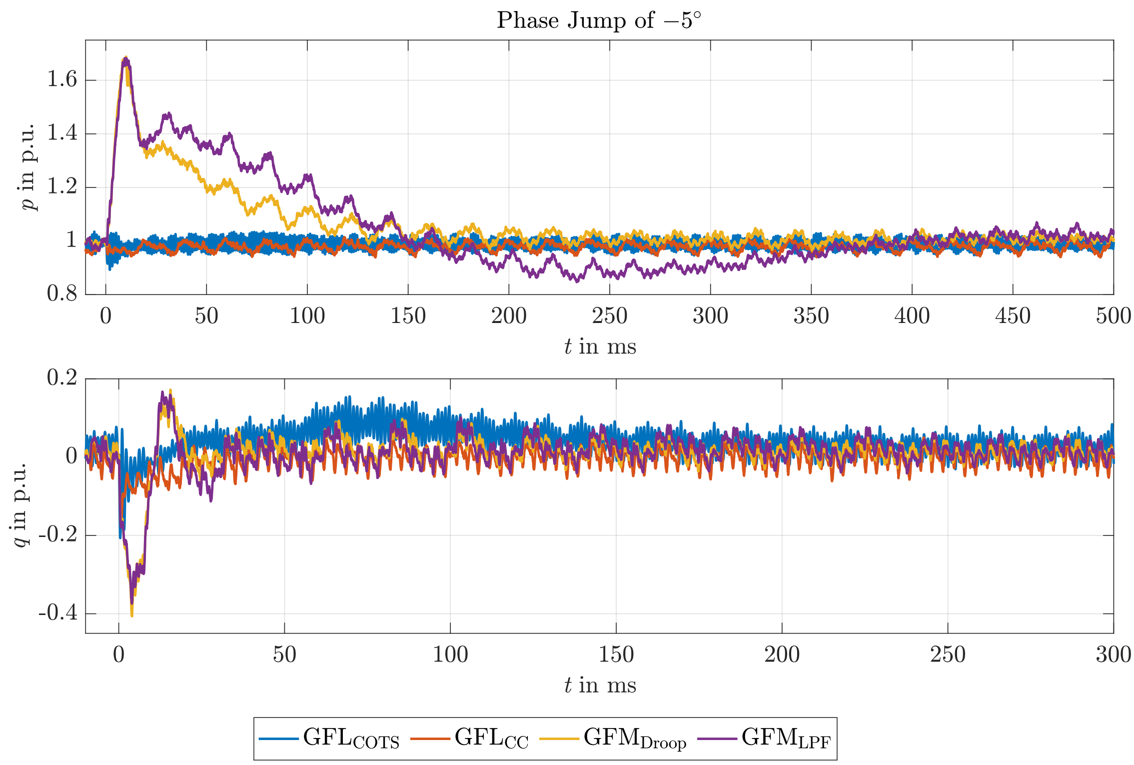

Figure 5.8: Comparison of different controller models with PHIL, Phase Jump

In Figure 5.9, the analysis shifts to an amplitude jump. Compliance with grid forming capabilities according to [7], mandates that reactive power be injected within 5 milliseconds to aid voltage stability. Again, the GFL controls do not increase their output. While GFM controls respond with an increase in reactive power, thereby contributing to voltage stabilization. The behavior of the active power during a voltage drop highlights a clear distinction among the $\mathrm{GFL_{COTS}}$, $\mathrm{GFL_{CC}}$, and GFM controls. The $\mathrm{GFL_{COTS}}$ clearly has a control with a output power target and returns to its full output of 1 p.u. the quickest. In contrast, the $\mathrm{GFL_{CC}}$ maintains a constant current injection, resulting in a decrease in active power output, due to the reduced voltage. Similarly to the $\mathrm{GFL_{COTS}}$, the GFM converters actively regulate their output power to the desired level and aim to return to their pre-disturbance active power output. However, GFM converters are significantly slower in their recovery compared to the $\mathrm{GFL_{COTS}}$ converters.

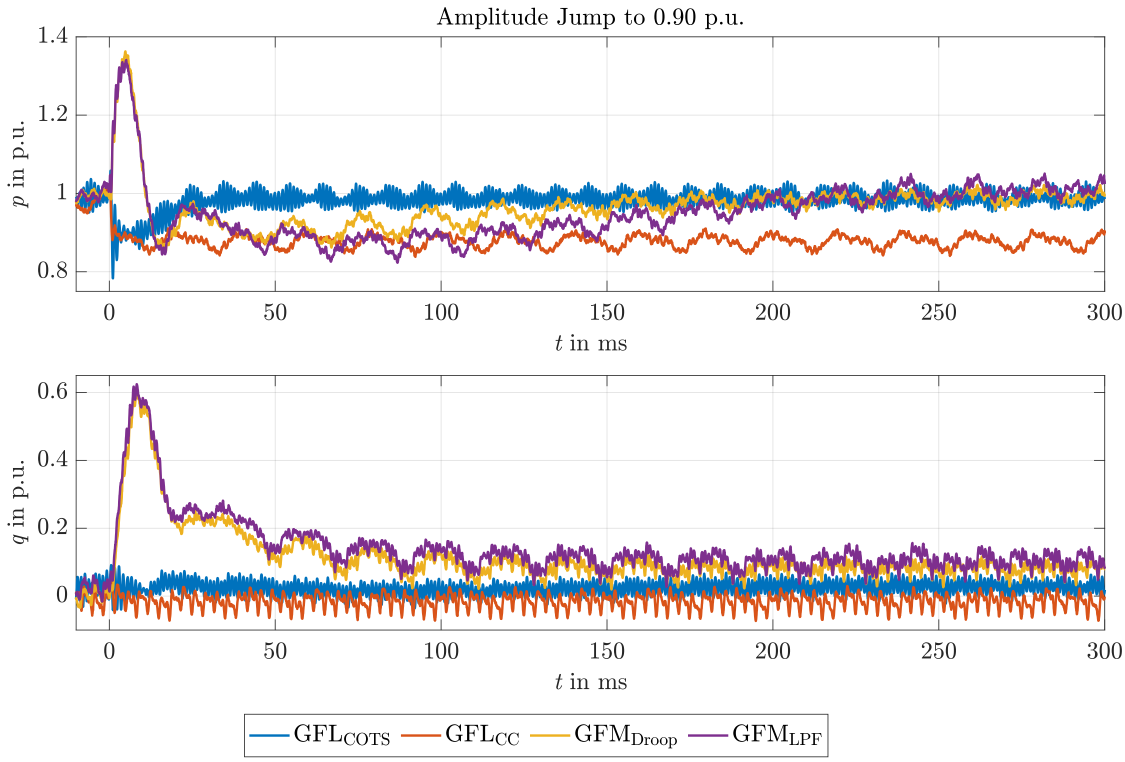

Figure 5.9: Comparison of different controller models with PHIL, Amplitude Jump

In conclusion, the analysis confirms that the conceptualised GFM converters effectively fulfil their expected behaviour in responding to these grid disturbances. Thereby validating their classification as grid-forming systems. The GFL converters also function as intended, this means they cannot meet the GFL requirements as they where not designed to do so. Additionally the applied disturbances where not drastic enought to trigger FRT behaviour from the GFL$_{COTS}$ converter. While reactive power can be supplied by the converter without requiring an additional energy source, active power, essential for stabilizing the grid during phase jumps, must be sourced or stored somewhere. In synchronous machines, this energy is stored in the rotating mass of the machine. For converters aiming to provide GFM capabilities, an alternative energy source must also be available. One solution involves operating the system below its maximum capacity. Therefore reserving energy for stabilization. However, this approach leads to underutilization of the available power. Another option is integrating rapid-response energy storage on the DC side. For example capacitors or fast-access batteries. These can supply the required energy instantly when needed.

5.3.3 Influence of Grid Strength

Grid-following commercial of the shelf

The impact of the SCR for the GFL_{COTS} is shown in Figure 5.10. It is apperent, that the SCR does not significantly affect the converter's response. The only observable effect of a lower SCR is an increase in the noise floor, with the signal becoming noisier as the SCR decreases.

SCRs of 7 and 5 were also tested, but under these conditions, the converter became unstable. The weak grid condition, characterized by low SCR values, made it difficult for the converter to lock onto the grid frequency, with it's PLL. Ultimately, this loss of synchronism led to unstable operation.

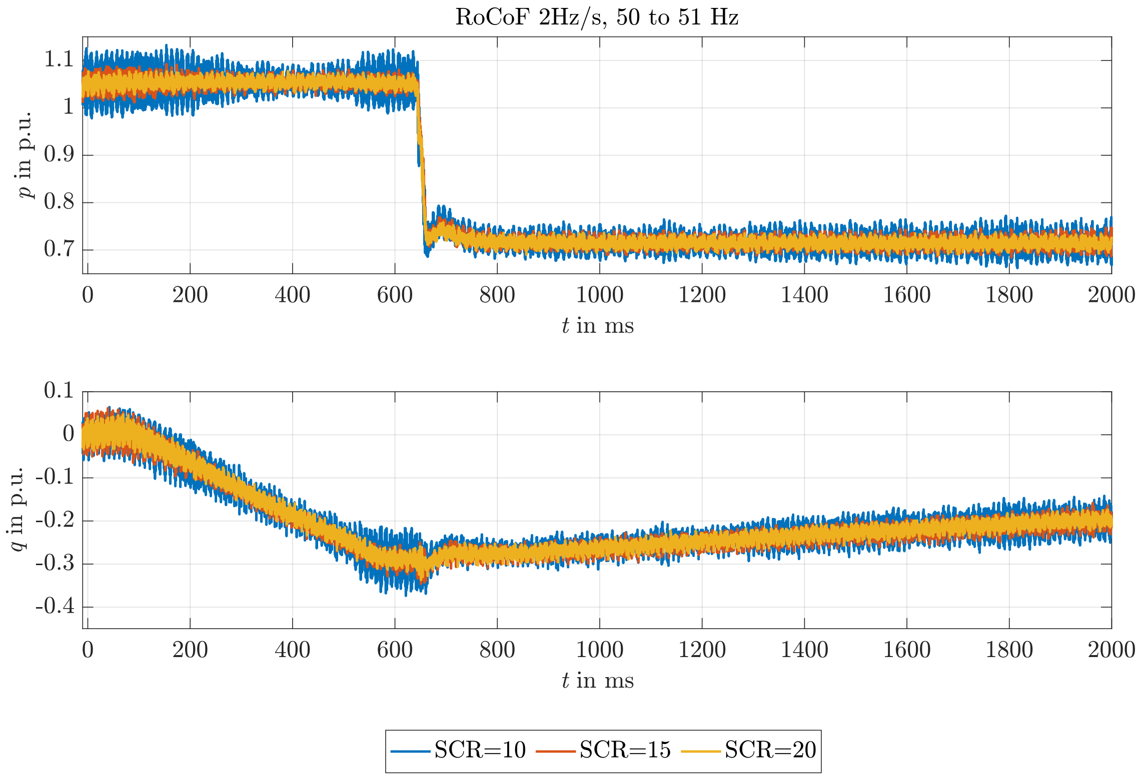

Figure 5.10: Influence of SCR on GFL_{COTS}, RoCof 2 Hz/s to 49 Hz

This underscores the critical role of grid strength for GFL converters. As they rely on an external grid to maintain stable operation. In contrast, GFM converters are capable of generating their own reference signal, allowing them to operate independently of an external grid. As a result, GFM converters can maintain stability and continue functioning even in weak grid conditions or in the absence of a external grid altogether.

Grid-forming droop with LPF

To analyse the impact of the SCR on the performance of the GFM_{LPF} converter the SCR was varied while keeping all other parameters consistent. In these experiments, voltage phase- and amplitude jumps were applied to assess the effects of the SCR on converter performance. The control method utilised in this analysis is the droop control, as speced in section 4.2, with the tuning parameters detailed in Table 4.4.

Figure 5.11 presents the influence of the SCR on the control performance during a phase jump of $-5°$. As it is a phase jump, the primary focus in this scenario is the change in active power. The results clearly demonstrate a significant dependency of the phase jump response on the grid strength. Notably, as the grid becomes stronger, the peak of the active power response to the phase jump increases significantly. The reactive power flow is also disturbed by the phase jump but returns close to zero within around 20 ms or one 50 Hz cycle.

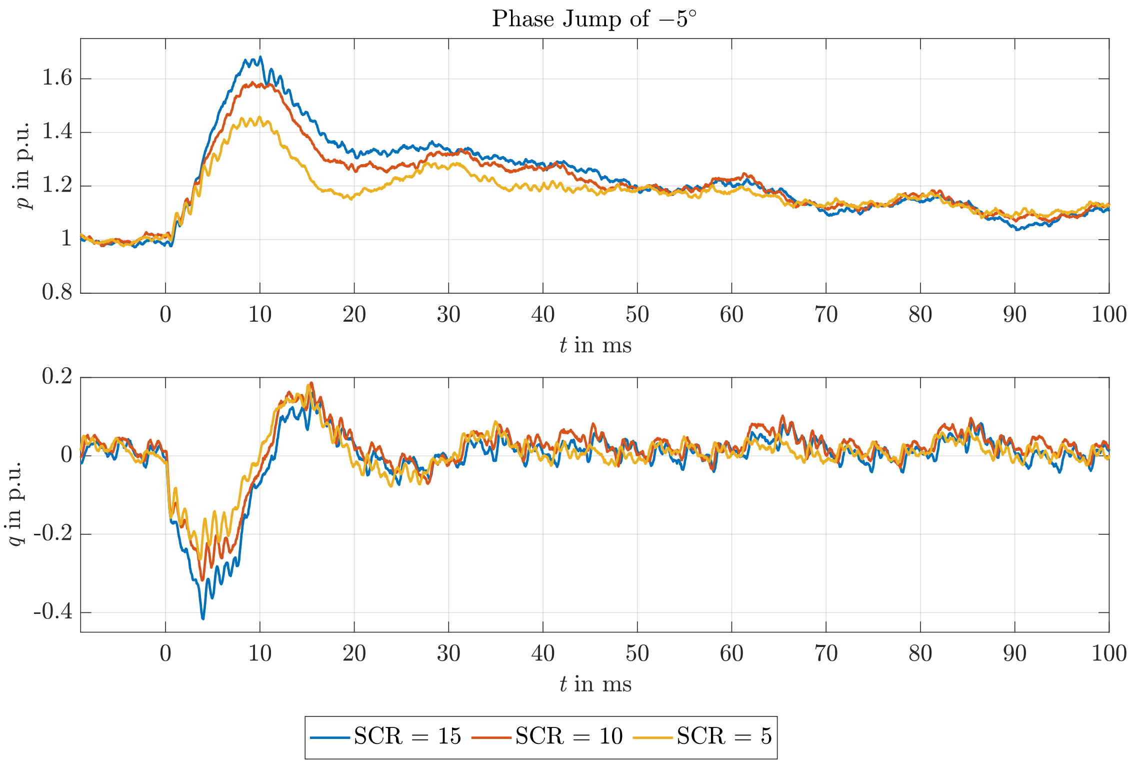

Figure 5.11: Influence of SCR on GFM_{Droop}, phase jump of $-5°$

In Figure 5.12, the influence of the SCR on the converter's reaction to a voltage amplitude jump from 1 to 0.9 p.u. is illustrated. In this case, reactive power is the critical parameter. The plot reveals that the oscillation patterns during the amplitude jump are largely consistent across all SCR values. However, it is important to note that the SCR does impact the magnitude of the reactive power response. Specifically, the first peak of the response is influenced by the SCR. It is showing a decrease in amplitude as the SCR decreases. Similarly to before the secondary power in this case now the active power flow is also disturbed by the phase jump and returns almost to 1 p.u. within around 20 ms or one 50 Hz cycle, but in this case with a bigger offset. After around 150 ms it will be as close to 1 p.u. as before the fault.

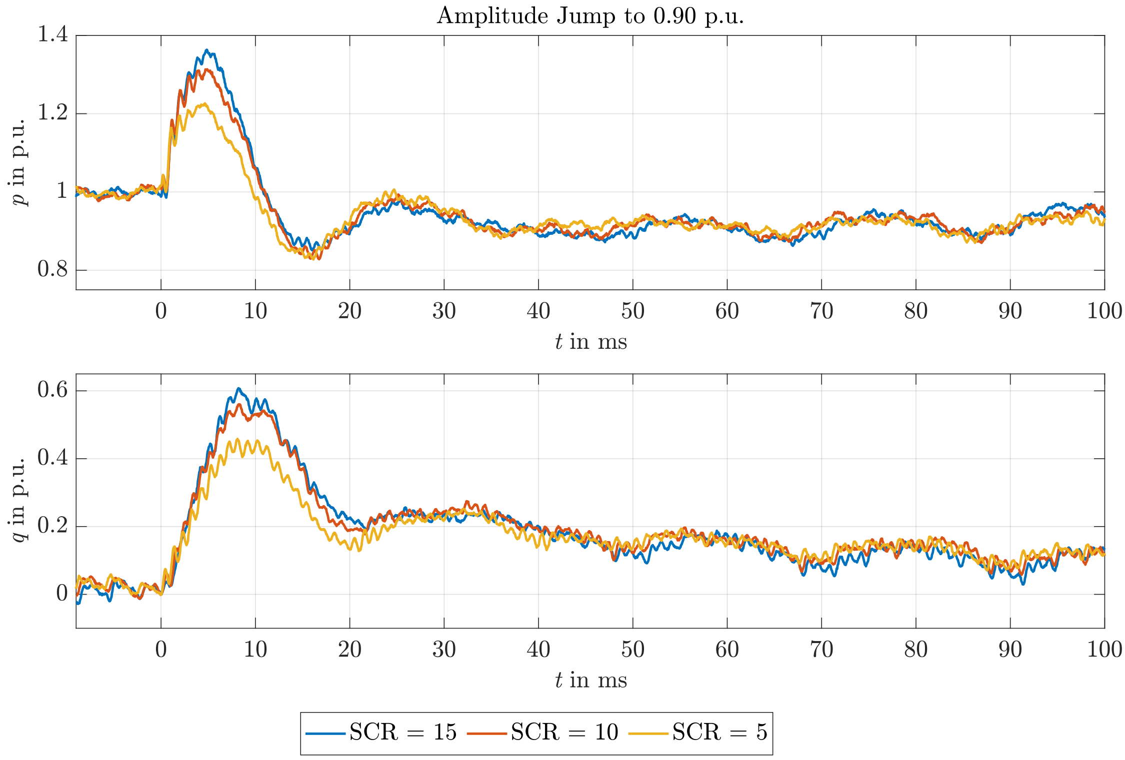

Figure 5.12: Influence of SCR on $\text{GFM}_{\text{Droop}}$, amplitude jump to $0.0 p.u.$

Overall, these findings indicate that the coupling between the grid and the GFM converter, both functioning as voltage sources, significantly influences their behaviour. Especially during dynamic situations. As anticipated, a weaker grid with higher grid impedance results in increased damping. Thereby reducing the peak response. The analytical validation can be found with Equation 4.5 for active and Equation 4.6 for reactive power.

5.3.4 Influence of Disturbance Strength

Grid-following commercial of the shelf

In Figure 5.13, phase jumps of varying magnitudes were applied to observe their impact on the system. However, none of the disturbances were substantial enough to trigger the fault ride-through routines. Therefore the phase jump disturbance primarily affects the system's response in the first few milliseconds. During which a direct correlation is observed between the phase jump amplitude and the initial reaction. The active power response remains symmetrical around 1 p.u., whereas the reactive power response predominantly stays below zero.

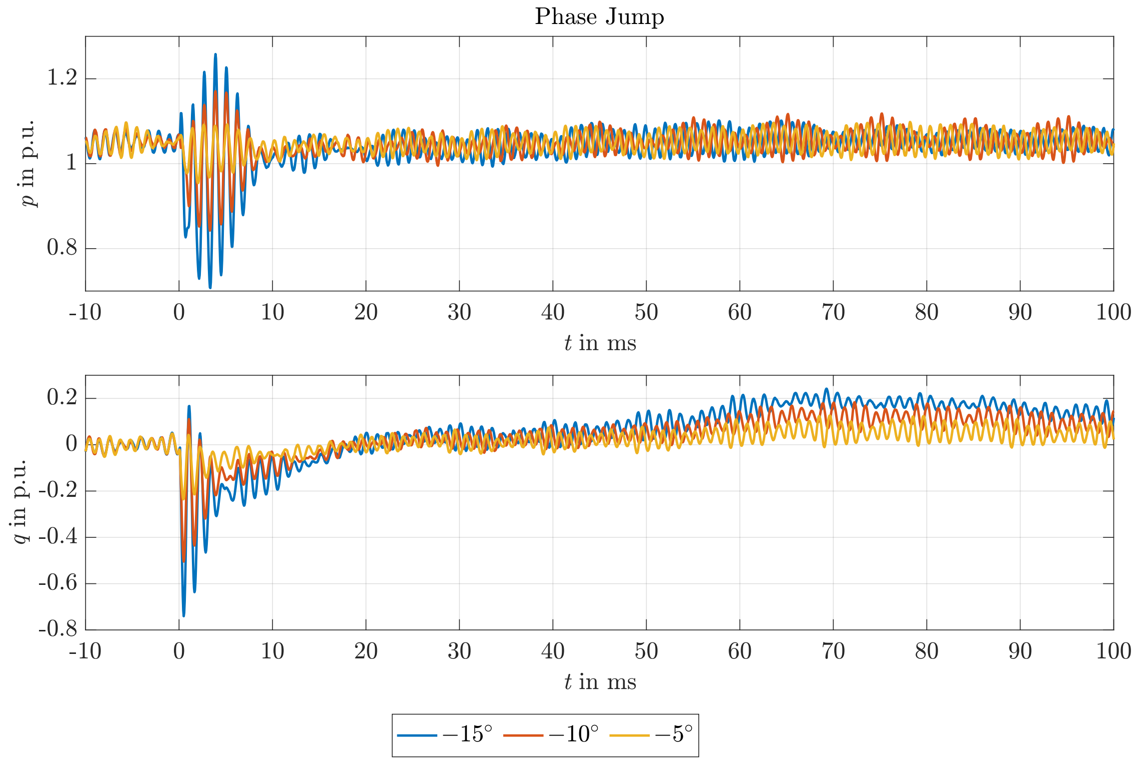

Figure 5.13: Influence of disturbance strength on GFL_{COTS}, phase jumps

Figure 5.14 illustrates the response of the grid-following converter to two different RoCoF events. Since the converter's output power is capped at 1 p.u., it cannot provide additional power in the event of a frequency drop. However, the inverse is also possible. When the frequency increases, the converter should ideally reduce its active power output proportionally. In this experiment, the frequency was increased from 50 Hz to 51 Hz to observe the converter's reaction. Ideally, the converter should promptly reduce its active power in response to rising frequency. However, as shown in Figure 5.14, the converter reacts very slowly to the RoCoF disturbance. The active power reduction begins only after approximately 650 to 750 milliseconds, or around 35 cycles, which is quite delayed. This slow response could exacerbate the effects of a RoCoF event, potentially destabilizing the system further.

The RoCoF speed is varied and it is evident that the converter's response time increases as the RoCoF rate decreases. However, the delay in response is not directly proportional to the RoCoF speed. The reaction time increases only slightly with slower RoCoF rates. Additionally, the reactive power decreases as the frequency rises.

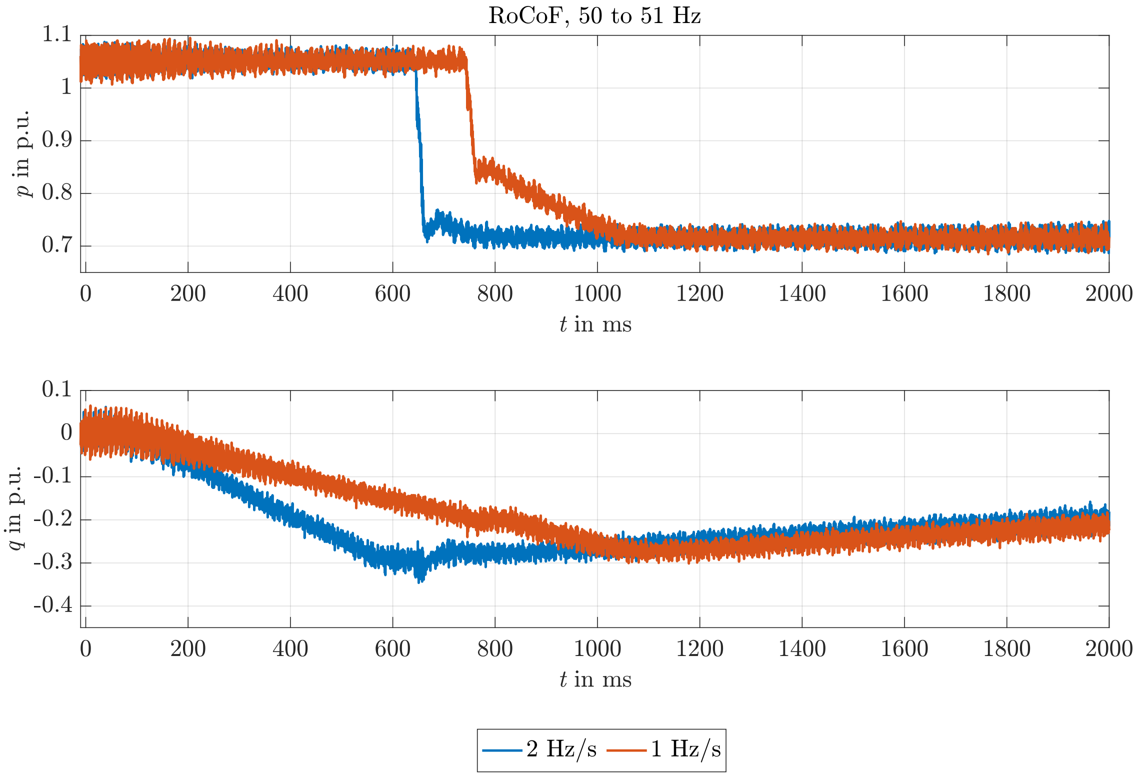

Figure 5.14: Influence of disturbance strength on GFL_{COTS}, RoCofs

5.3.5 Variation of control parameters

Grid-forming droop with LPF

For the sensitivity analysis of the GFM control parameters, a frequency ramp is applied. The GFM_{Droop} control, as specified in section 4.2, is utilised, with the results plotted in Figure 5.15. The frequency starts at 50 Hz and decreases to 49 Hz with a RoCoF of 2 Hz/s. Frequency serves as an indicator of the balance between generation and load in the power grid, with any imbalance causing a frequency increase or decrease. RoCoF measures the rate these frequency changes. In [7], the converter must withstand a RoCoF of 2 Hz/s, tolerating frequencies up to 52 Hz and down to 47 Hz.

The cut-off frequency of the LPF f_p is inversely proportional to the system's inertia. The higher the cut-off frequency, the lower the inertia. This can clearly be seen in Figure 5.15 on the left, where the proportional gain K_P is kept steady while f_p is varied. With $f_p = 2$ Hz the system has a higher overshoot and oscillates more than with higher cut-off frequencies. This is consistent with the mathematical analysis and verifies Equation 3.21, where it is shown that a lower f_p results in a higher virtual-inertia constant.

The parameter K_P influences mainly the additional active power feed in, during a frequency decrease, as seen in Figure 5.15 on the right. It influences not only the peak but also the final value at which the active power settles in response to the frequency change. The smaller the parameter KP, the greater the response. As seen in Equation 3.21 KP influences both the inertia constant as well as the damping inversely. This can also be verified in the results as not only the magnitude of the active power but also the overshoot increases, with the magnitude being influenced more than the oscillation.

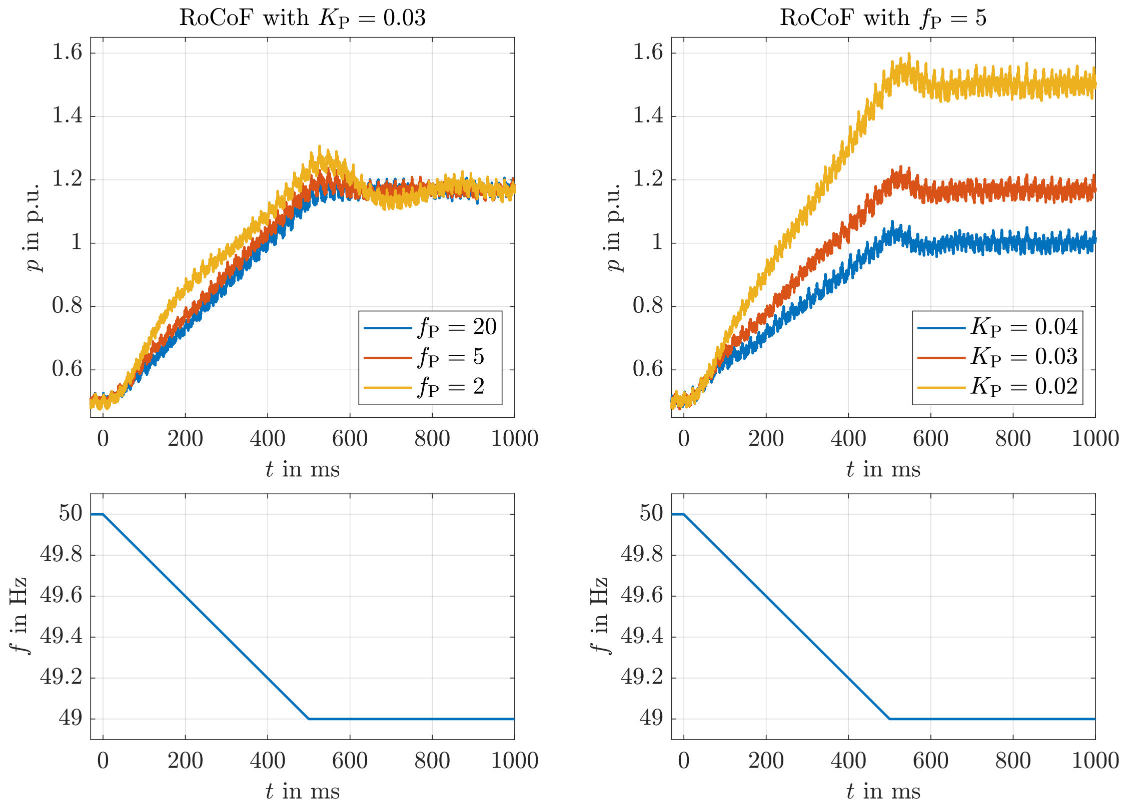

Figure 5.15: Influence of the variation of the control parameters

6 Conclusion and Future Work

This thesis aims to provide insights into the dynamics and control strategies of GFM converters in modern power systems. With a analysis and focus on current and anticipated future grid codes. The development and verification of various test setups, in simulation, with hardware components and using PHIL approaches, makes it possible to analyse the performance and stability of GFM converters. Especially under varying grid and control parameter settings. In this chapter, the key findings are summarised and potential directions for future research are discussed.

6.1 Summary of Contributions

The main goals of this thesis are stated in section 1.2. This chapter now reflects on these goals and aims to validate and quantify how and to which degree of success the goals have been reached.

- Comparison of Grid Codes:
  Different grid codes are compared and the GBGF [7] code is chosen as a basis for the testing in this thesis. Especially due to its well defined requirements and guidelines for testing.
- Development of Assessment Tools:
  Different grid-following and grid-forming controls where discussed theoretically and subsequently implemented in simulations and in hardware. A grid model with adjustable disturbances and grid parameters, was also designed. It was subsequently used for the assessment of the before mentioned controls with the addition a commercially available grid-following converter.
- Simulation:
  - A averaged VSC model for the semiconductor switches was compared to a more detailed model considering every switch. The results show that the averaged model is accurate enough for the tested cases.
  - The equality of the virtual synchronous machine with the droop with LPF was first shown mathematically and then verified within a simulation.
  - The influence of grid parameters was analysed showing that both the resistive and inductive part of the grid impedance influence both active and reactive power.
  - One area where the simulations fell short of expectations was in accuracy, as the simulation results differed significantly from the hardware test outcomes. A potential reason identified was the frequency dependency of the impedances. However, due to time constraints, no modelling of this effect has been conducted. As a result, it is unclear whether this is the sole reason for the discrepancies or if additional factors would also have to be considered.

- PHIL Methodology:
  A comparison was conducted between a hardware grid impedance and an emulated grid impedance emulated using Power Hardware-in-the-Loop. The emulated impedance results deviated slightly from the actual hardware impedance. To address this discrepancy, a combined approach was recommended, where a portion of the grid impedance is represented by real hardware and the remainder is emulated. This allows for straightforward adjustments of the grid impedance.
- Comparative Analysis of Control Structures:
  - The findings demonstrate that, GFL converters do not inherently respond to the test disturbances used. Therefore they are not able to contribute to stabilizing the grid inhernetly unless a fault-ride through mechanism is triggered. This leads to delayed responses, since the disturbance must first be detected, before the converter can take action.
  - In contrast, GFM converters exhibit more favourable behaviours, as they inherently react to disturbances. Which enables them to respond more quickly and to smaller deviations. This inherent response allows GFM converters to enhance grid stability without the need for disturbance detection delays and specialised fault-ride through mechanisms.
- Examine Grid Strength Influence:
  - For grid-following control, the impact of grid strength was minimal, with the control response remaining very similar across varying SCRs. However, once the SCR dropped below a critical threshold the converter's PLL could no longer maintain synchronization with the grid, resulting in instability.
  - In contrast, grid-forming controls demonstrate a clear dependency on grid strength. Since both the converter and the grid function as voltage sources, their interaction is shown to be primarily influenced by the phase angle difference between these voltage sources and the impedance separating them. The grid-forming controls did not become unstable even with low SCRs.
- Examine Disturbance Strength Influence:
  The strength of disturbances was analysed and found to predictably affect the intensity of the system's response. Since these disturbances were applied without any current-limiting actions, the system reactions remained proportionally consistent. This indicates that, as long as FRT or similar behaviour is not triggered, the influence of disturbance strength remains relatively directly proportional.
- Sensitivity Analysis of Control Parameters:
  In this testing, a grid-forming droop control with a low-pass filter was utilized. It is demonstrated that the LPF is able to provide a inertial response. With its cut-off frequency inversely affecting inertia. While the control's proportional gain exhibits an inverse relationship with both inertia and damping.

6.2 Future work

There are several promising avenues for future research, many of which focus on addressing existing limitations of the converter design as well as the simulation and test setups. Key areas include but are not limited to:

- Improving Simulation Setup:
  Developing a more accurate and representative simulation. Particularly to modelling the frequency dependency of the impedances could reduce the deviations of the simulations significantly. Providing a more realistic basis for simulated testing.
- Distinguishing Between GFL and GFM Methods:
  A methodology is needed to differentiate between grid-forming (GFM) and grid-following (GFL) controls, including the potential to identify wich control is used via black box testing. To take this one step further a possible analysis of converter control parameters based solely on black box tests could be developed.
- Expanding Fault Scenarios Analysis:
  Investigating a broader range of fault scenarios, especially those that introduce asymmetrical conditions, will help to reveal additional aspects of converter behaviour and stability.
- Developing a Comprehensive Converter Design:
  Designing a converter that fully meets operational requirements, with optimal GFM capabilities. Including a more dedicated tuning of the control loop parameters and different inner controls structures could also be a crucial research direction.

Bibliography

[1] A. Monti, “Low inertia grids: Towards a power electronics-based power system,” in *2019 21st European Conference on Power Electronics and Applications (EPE’19 ECCE Europe)*, IEEE, 2019, pp. 1–1.

[2] Y. Gu and T. C. Green, “Power system stability with a high penetration of inverter-based resources,” *Proceedings of the IEEE*, vol. 111, no. 7, pp. 832–853, 2022.

[3] U. Markovic, O. Stanojev, P. Aristidou, E. Vrettos, D. Callaway, and G. Hug, “Understanding small-signal stability of low-inertia systems,” *IEEE Transactions on Power Systems*, vol. 36, no. 5, pp. 3997–4017, 2021.

[4] R. Rosso, X. Wang, M. Liserre, X. Lu, and S. Engelken, “Grid-forming converters: An overview of control approaches and future trends,” in *2020 IEEE Energy Conversion Congress and Exposition (ECCE)*, IEEE, 2020, pp. 4292–4299.

[5] S. Ghimire, G. M. Guerreiro, K. Vatta Kkuni, *et al.*, “Functional specifications and testing requirements of grid-forming offshore wind power plants,” *Wind Energy Science Discussions*, vol. 2024, pp. 1–21, 2024.

[6] P. Christensen, G. Andersen, M. Seidel, *et al.*, *High Penetration of Power Electronic Interfaced Power Sources and the Potential Contribution of Grid Forming Converters*. European Network of Transmission System Operators for Electricity, Jan. 2020.

[7] A. Johnson, “Minimum specification required for provision of gb grid forming (gbgf) capability (formerly virtual synchronous machine/vsm capability),” *Nat. Grid ESO, Warwick, UK, Final Modification Rep. GC*, vol. 137, 2021.

[8] D. Pan, X. Wang, F. Liu, and R. Shi, “Transient stability of voltage-source converters with grid-forming control: A design-oriented study,” *IEEE Journal of Emerging and Selected Topics in Power Electronics*, vol. 8, no. 2, pp. 1019–1033, 2019.

[9] X. Meng, J. Liu, and Z. Liu, “A generalized droop control for grid-supporting inverter based on comparison between traditional droop control and virtual synchronous generator control,” *IEEE Transactions on Power Electronics*, vol. 34, no. 6, pp. 5416–5438, 2018.

[10] R. Rosso, J. Cassoli, G. Buticchi, S. Engelken, and M. Liserre, “Robust stability analysis of lcl filter based synchronverter under different grid conditions,” *IEEE Transactions on Power Electronics*, vol. 34, no. 6, pp. 5842–5853, 2018.

[11] M. Liserre, R. Teodorescu, and F. Blaabjerg, “Stability of photovoltaic and wind turbine grid-connected inverters for a large set of grid impedance values,” *IEEE transactions on power electronics*, vol. 21, no. 1, pp. 263–272, 2006.

[12] S. L. Harrison, “Advancements in converter-based frequency stability: Recommendations for industrial applications,” *University of Strathclyde*, 2023.

[13] Z. Zhang, R. Schürhuber, L. Fickert, X. Liu, Q. Chen, and Y. Zhang, "Hardware-in-the-loop based grid compatibility test for power electronics interface," in *2019 20th International Scientific Conference on Electric Power Engineering (EPE)*, IEEE, 2019, pp. 1–6.

[14] A. Hoke, S. Chakraborty, and T. Basso, "A power hardware-in-the-loop framework for advanced grid-interactive inverter testing," in *2015 IEEE Power & Energy Society Innovative Smart Grid Technologies Conference (ISGT)*, IEEE, 2015, pp. 1–5.

[15] P. Hackl, C. Lehmal, Z. Zhang, and R. Schuerhuber, "A novel modular combinable hardware-in-the-loop platform for stability investigations of converter-driven power grids," *21st Wind & Solar Integration Workshop (WIW)*, 2022.

[16] G. Schoepf, P. Hackl, Z. Zhang, and R. Schuerhuber, "Evaluating grid-forming converter performance: Insights from power hardware-in-the-loop testing," *IEEE Power and Energy Student Summit (PESS)*, 2024.

[17] F. Kalverkamp, B. Schowe-von der Brelie, T.-D. Nguyen, T. Mertens, and M. Meuser, "Comparative analysis of european grid codes and compliance standards for distributed power generation plants with respect to future requirements of," in *International ETG Congress 2015; Die Energiewende-Blueprints for the new energy age*, VDE, 2015, pp. 1–6.

[18] J. Bialek, "What does the gb power outage on 9 august 2019 tell us about the current state of decarbonised power systems?" *Energy Policy*, vol. 146, p. 111 821, 2020.

[19] P. Imgart, M. Beza, M. Bongiorno, and J. R. Svensson, "An overview of grid-connection requirements for converters and their impact on grid-forming control," in *2022 24th European Conference on Power Electronics and Applications (EPE'22 ECCE Europe)*, IEEE, 2022, pp. 1–10.

[20] V. V. d. E. E. Informationstechnik, *„vde-ar-n 4131: Technische regeln für den anschluss von hgü-systemen und über hgü-systeme angeschlossene erzeugungsanlagen (tar hgü),"* 2019.

[21] C. T. PAGE, R. VERSION–NOT, and F. T. CLEAN, "P2800™/d6. 2 (october 2021) draft standard for interconnection and interoperability of inverter-based resources interconnecting with associated transmission systems," *IEEE*, 2021.

[22] Z. Zhang, R. Schuerhuber, L. Fickert, and G. Chen, "Investigating the effects of current thresholds on phase jump limits and withstand capabilities in grid-forming converters," *IET Generation, Transmission & Distribution*, 2024.

[23] O. E. Oni, I. E. Davidson, and K. N. Mbangula, "A review of lcc-hvdc and vsc-hvdc technologies and applications," in *2016 IEEE 16th International Conference on Environment and Electrical Engineering (EEEIC)*, IEEE, 2016, pp. 1–7.

[24] H. Latorre and M. Ghandhari, "Improvement of power system stability by using a vsc-hvdc," *International Journal of Electrical Power & Energy Systems*, vol. 33, no. 2, pp. 332–339, 2011.

[25] E. Clarke, *Circuit analysis of AC power systems: symmetrical and related components*. Wiley, 1943, vol. 1.

[26] R. H. Park, "Two-reaction theory of synchronous machines generalized method of analysis-part i," *Transactions of the American Institute of Electrical Engineers*, vol. 48, no. 3, pp. 716–727, 1929.

[27] S.-S. Shin, J.-S. Oh, S.-H. Jang, J.-H. Cha, and J.-E. Kim, "Active and reactive power control of ess in distribution system for improvement of power smoothing control," *Journal of Electrical Engineering and Technology*, vol. 12, no. 3, pp. 1007–1015, 2017.

[28] I. Subotić and D. Groß, “Power-balancing dual-port grid-forming power converter control for renewable integration and hybrid ac/dc power systems,” *IEEE Transactions on Control of Network Systems*, vol. 9, no. 4, pp. 1949–1961, 2022.

[29] F. Milano, F. Dörfler, G. Hug, D. J. Hill, and G. Verbič, “Foundations and challenges of low-inertia systems,” in *2018 power systems computation conference (PSCC)*, IEEE, 2018, pp. 1–25.

[30] Z. Zhang, *Control parameter tuning method of grid-connected inverter*, Accessed: 2024-1-10, 2020.

[31] Q.-C. Zhong, G. C. Konstantopoulos, B. Ren, and M. Krstic, “Improved synchronverters with bounded frequency and voltage for smart grid integration,” *IEEE Transactions on Smart Grid*, vol. 9, no. 2, pp. 786–796, 2016.

[32] W. D. Stevenson *et al.*, *Elements of power system analysis*. McGraw-Hill New York, 1982, vol. 4.

[33] J. Chen, H. Bai, J. Chen, W. Ao, and X. Chen, “Parameters design and optimization for droop-controlled inverters considering impedance characteristics and power stability,” *Energy Reports*, vol. 9, pp. 3369–3379, 2023.

[34] P. Kundur, “Power system stability,” *Power system stability and control*, vol. 10, pp. 221–226, 2007.

List of Figures

List of Tables